The Dissertation Committee for Michael Boone Muhlestein
certifies that this is the approved version of the following dissertation:

Willis Coupling in Acoustic and Elastic Metamaterials

Committee:

Preston S. Wilson, Supervisor

Michael R. Haberman, Co-Supervisor

Andrea Alù

Mark F. Hamilton

Loukas F. Kallivokas

Willis Coupling in Acoustic and Elastic Metamaterials

by

Michael Boone Muhlestein, B.S., M.S.

DISSERTATION

Presented to the Faculty of the Graduate School of

The University of Texas at Austin

in Partial Fulfillment

of the Requirements

for the Degree of

DOCTOR OF PHILOSOPHY

THE UNIVERSITY OF TEXAS AT AUSTIN

December 2016

Dedicated to my wife Natalie, with whom I am eternally coupled.

Acknowledgments

It has been said that no man is an island, and it is certainly true of me. First and foremost I am grateful to my Heavenly Father, who has buoyed me up countless times and inspired me to solutions I could not see on my own. I am grateful to my wife, Natalie, for her unwavering love and support of me throughout my education, and for leading out on our real (and more difficult) work of raising a family. I am grateful for our two boys, Adam and Samuel, for their joy and love. And I am grateful for my parents for their constant faith in me and encouragement of excellence in all aspects of my life.

In addition to my family, I must acknowledge the invaluable guidance and assistance of my advisers, Michael Haberman and Preston Wilson. I can't count all the times I have walked into Dr. Haberman's office and been able to chat freely about any aspect of our research, from trivial mathematical problems to administrative issues. I have learned much from these conversations and have increased my self confidence as well. I am also grateful to Dr. Wilson for always encouraging me and giving me opportunities to teach.

I also wish to thank my advisers from my masters program at Brigham Young University. In particular, I want to thank Kent Gee for teaching me the importance of publishing early in a program, and I want to thank Timothy Leishman for helping me learn how to run an impedance tube. This

information was extremely useful to me for my research in Texas.

Lastly, I would like to express appreciation to my graduate committee for being willing to review my work and give suggestions, and to my fellow graduate students for very helpful discussions. In particular, I am grateful to Caleb Sieck for wonderfully helpful discussions and advise.

Willis Coupling in Acoustic and Elastic Metamaterials

Publication No. _____

Michael Boone Muhlestein, Ph.D.
The University of Texas at Austin, 2016

Supervisors: Michael R. Haberman
Preston S. Wilson

An acoustic metamaterial is a mechanical or material system with a subwavelength structure designed to generate specific effective material properties in the homogenization limit. Most acoustic metamaterials are assumed to be properly and fully described using two material properties: mass density and stiffness. However, Willis showed that for general elastodynamic homogenization theory another material property emerges [Willis, *Wave Motion* **3** (1981)]. This additional material property is necessary to describe what have come to be known as Willis materials, and couples the stress and momentum equations in a phenomenon called Willis coupling. The purpose of this dissertation is to expand the understanding of Willis coupling.

First, a derivation of the restrictions on the range of elastic Willis material properties imposed by assuming reciprocity, passivity, and causality is presented. Reciprocity is found to impose symmetry conditions on the Willis coupling coefficients and passivity is found to impose bounds on the range of

the real part of the Willis coupling coefficients, for Willis constitutive relations in the standard form. Causality is used to suggest an alternative, more physically meaningful, formulation of a Willis material's constitutive equations.

A physical interpretation of local Willis coupling is then presented in the context of one-dimensional systems. Local Willis coupling is shown to arise from systems with inherently asymmetric microstructures, which leads to a misalignment of the centroid of an effective material element and its center of mass. These examples also present a new theoretical method for determining the effective material properties of such systems, which is then compared with experimentally determined effective material properties and found to be in good agreement.

A method for determining macroscopic effective material properties of a three-dimensional elastic matrix material with small, randomly distributed inclusions is then derived. While approximate, this homogenization method is very general, accounting for Willis coupling among other phenomena. This homogenization method demonstrates that subwavelength elements exhibiting Willis coupling may lead to macroscopic Willis coupling, and it provides a means to quantify this effect. Finally, a summary of the results of this research is presented, and topics related to Willis coupling that should receive further research are discussed.

Table of Contents

List of Tables

List of Figures

Chapter 1

Introduction

The field of "metamaterials" has received a lot of attention in the past couple of decades, starting in the electromagnetism community in the early 1990s and picked up by the elasticity and acoustics communities in the 2000s. However, despite the popularity of its name and applications, most notably cloaks, the field of metamaterials remains a rather esoteric field of research. Since the topic of this dissertation broadens the understanding of a particular class of metamaterials, it is necessary to include a brief introduction to the concepts of metamaterials.

1.1 What is a Metamaterial?

When one speaks of a material, one is usually referring to a solid, such as steel, wood, or granite, or a fluid, such as water, air, or oil. However, each of these examples is actually a complicated system of interacting atoms. The notion of a "material" comes from the idea that one does not need to know all of the details of a system at all length- and time-scales in order to be able to make meaningful and efficient predictions about the system's behavior [1].

For example, consider common liquid water in drinking glass (see Fig. 1.1).

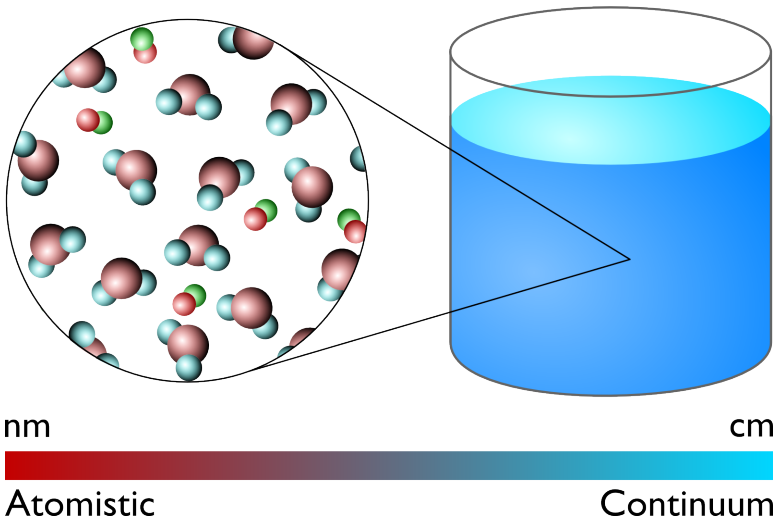

Figure 1.1: Schematic explanation of the material or continuum approximation. On the scale of nanometers or below (left) the system is atomistic and may not be accurately considered a material. On the scale of centimeters or above (right) the details of the atoms become irrelevant and the system may be accurately called a material.

Water that comes from the tap is generally comprised of water molecules, along with dissolved minerals and other chemicals. Modeling water as individual molecules and atoms requires one to account for the position, velocity, net forces, and chemical reactions of a very large numbers of objects, on the order of 10^{26} molecules ($\sim$ 1 mole). Storing the positions of the molecules in this system in a computer, let alone studying its dynamics, is completely impractical. Fortunately, the vast majority of the details of such a system are not significant to engineering applications. For example, in determining the net force exerted by water molecules on the wall of the liquid's container it doesn't matter whether the force was exerted by molecule A or molecule B, just that *some* molecule exerted the force. Furthermore, it is far more

efficient (and probably reliable) to simply treat the water as a homogeneous, continuous fluid and use experimental methods to estimate a pressure. The reason why this approximate method is valid is that the size of the water's container is much larger than the length scales associated with the molecular interactions. On the other hand, an estimate of the behavior of the system may also be obtained by modeling a portion of the molecular behavior (i.e., molecular dynamics), and then generalize the molecular behavior to larger and larger collections of molecules.

Using the idea of related length scales, we may posit a definition of a material:

> A material is any system where the length scales associated with the components and collections of components comprising the system are much less than any length scale of interest.

Using this definition, air at standard atmospheric conditions may be considered a material if the smallest length scale of interest is on the order of microns, but not if the length scale of interest is on the order of nanometers, because the characteristic length scale of the molecular dynamics, the mean free molecular path, is on the scale of nanometers. Notice that the discrete nature of a system must be accounted for if either the limiting length scale is increased, such as for rarefied gases [2], or if the length scale of interest decreases, such as for nanoelectromechanical systems (NEMS) [3]. Table 1.1 gives some more examples of systems and at what length scales of interest they may be considered a material.

Table 1.1: A list of physical systems and the length scales at which they are considered materials. The × symbol indicates that the system on the left may not be considered a material for the length scale listed above, and the ✓ symbol indicates the system may be considered a material. The limiting length scale is listed on the right.

On the scale of:	nm	μm	mm	m	km	Limiting length scale
Air	×	✓	✓	✓	✓	Molecular mean free path
Steel	×	×	✓	✓	✓	Grain size
Asphalt	×	×	×	✓	✓	Gravel size
Fish school	×	×	×	×	✓	Inter-fish separation

While a system may be considered a material for a given length scale of interest, it is common for the microstructure of the material (the details that are masked by considering it a material) to affect the macroscopic behavior (behavior associated with the length scales of interest). A classic case from acoustics is molecular relaxation in fluids. Essentially, as an acoustic wave passes over a portion of fluid, the molecules within the fluid are excited and may begin to vibrate. Some of this vibrational energy is then lost to the acoustic wave in the form of heat, the net result being an attenuation of the passing acoustic wave [4, 5]. The details of which molecules are vibrating and how are irrelevant to the acoustic wave, but the fact that some portion of the molecules *can* and *do* vibrate is important. The possibility of molecular vibration is an example of a hidden degree of freedom, "hidden" in that it is masked by the approximation that the system is a material. This simple example captures the essence of the thrust of acoustic metamaterials (AMM) research.

A "metamaterial" is a material that has a microstructure which has

been engineered to yield specific, usually dynamic, material properties. Often, hidden degrees of freedom are designed to yield unusual or exotic properties. While humans have been designing new materials for millennia (e.g., steel and its alloys), recent advances in fabrication technology have given designers unprecedented access to and control of the microstructure of materials with smaller and smaller length scales of interest [6, 7]. While there are a vast number of examples in the literature, three notable and simple examples are presented below. In particular, a mass-in-mass system is shown to exhibit negative dynamic mass density near resonance, an array of Helmholtz resonators in a waveguide is shown to behave as a material with negative stiffness, and labyrinthine structures may be used to create non-resonant "metasurfaces" to steer and focus transmitted or reflected acoustic waves. Then, some examples of applications of metamaterials are provided.

1.1.1 Negative Dynamic Mass

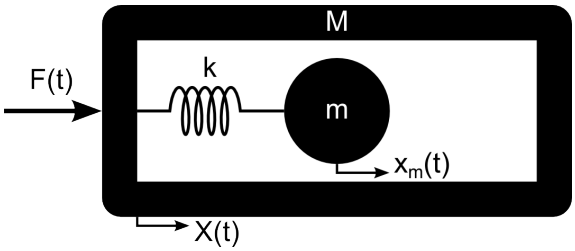

Figure 1.2: Schematic depiction of a mass inside another mass, connected by a spring.

Perhaps the simplest way that negative dynamic mass may be understood is by considering a mass inside another mass connected by a spring,

as shown in Fig. 1.2. This problem has been worked out many times; for example, see Refs. [8] and [9]. Given an external harmonic forcing function $F(t) = \Re\{f_\omega e^{-i\omega t}\}$ the resulting motion of the external mass M is written $X(t) = \Re\{x_\omega e^{-i\omega t}\}$. Solving Newton's second law for the external mass results in the equation

$$f_\omega = -\left(M - \frac{m\omega_0^2}{\omega^2 - \omega_0^2}\right)\omega^2 x_\omega, \tag{1.1}$$

where m is the internal mass and $\omega_0 = \sqrt{k/m}$ is the natural resonance of the internal mass-spring system. At this point the interpretation of the system becomes important. In one respect, Eq. (1.1) is the response function of the two-mass system. However, since the inner mass may be hidden from observation, measurement of the mass of the system can only be made by relating the external (observable) force $F(t)$ with the motion of the external structure. In this perspective, the external mass must take on different values at different frequencies to account for the motion of the inner mass. This *effective mass* is then given by

$$M_{\text{eff}} \equiv \frac{f_\omega}{-\omega^2 x_\omega} = M + \frac{m}{1 - \omega^2/\omega_0^2}. \tag{1.2}$$

Notice that the effective mass may be negative if

$$\omega_0 > \omega > \omega_0\sqrt{1 + \frac{m}{M}}. \tag{1.3}$$

Thus, for frequencies between the natural frequency of the inner mass ω_0 and $\omega_0\sqrt{1 + m/M}$ the system behaves as though it consisted of a single mass with a negative value. Since this is a dynamic effect, the effective mass is often

called the dynamic mass. The first known experimental evidence of negative dynamic mass was reported by Liu, *et al.* in 2000 using a mass-in-mass method, though they refer to this behavior as negative stiffness [10]. Their structure consisted of an array of lead spheres, coated in silicone rubber, and embedded in an epoxy matrix (see Fig. 1.3 for a picture of the structure).

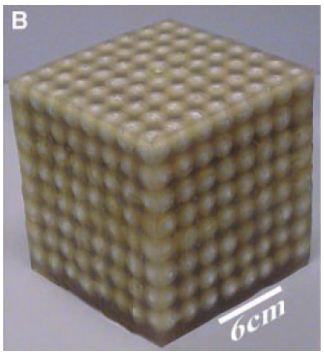

Figure 1.3: Picture of a negative dynamic mass structure from Liu, *et al.* [10]. The structure consists of lead balls, coated in rubber, and emmbedded in epoxy. Figure adapted from Ref. [10].

1.1.2 Negative Stiffness

Negative dynamic stiffness has been observed in a periodic array of Helmholtz resonators in a waveguide, such as the one schematized in Fig. 1.4 [11, 12]. In the long-wavelength limit, the resonators may be modeled as compliance elements located at infinitesimal points on the walls. If the waveguide is then interpreted as a one-dimensional structure, the resonators represent a hidden degree of freedom and modify the effective wall stiffness, which in turn modifies the effective stiffness of the system. The effective stiffness of the

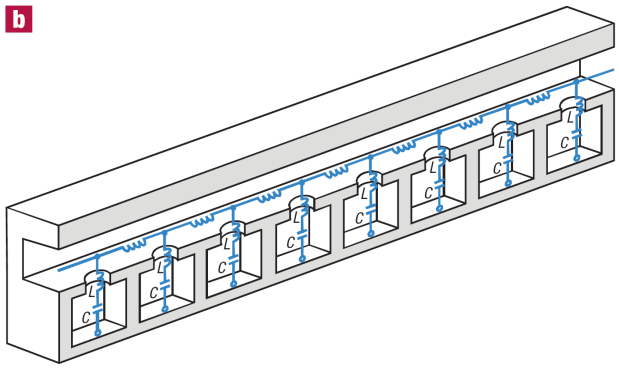

Figure 1.4: Schematic of a waveguide that exhibits negative stiffness from Fang, *et al.* [11]. Figure adapted from Ref. [11].

entire waveguide may be written as

$$\kappa_{\text{eff}} = \kappa_0 \left[1 - \frac{F\omega_0^2}{\omega^2 - \omega_0^2 + i\Gamma\omega} \right]^{-1}, \tag{1.4}$$

where κ_0 is the stiffness of the medium in the waveguide, F is a positive geometric factor, ω_0 is the resonance frequency of each Helmholtz resonator, and Γ is a dissipation factor [11]. As with the dynamic mass in the previous case, the effective stiffness is only negative for a finite bandwidth. For example, in the lossless case $\Gamma = 0$, the stiffness is negative for $1 < \omega/\omega_0 < \sqrt{F+1}$.

1.1.3 Non-Resonant Metasurfaces

The negative dynamic mass and negative dynamic stiffness examples described above rely on hidden resonant elements for their exotic properties. The negative dynamic mass element included a mass-spring system which possess a resonance, and the negative dynamic stiffness system included Helmholtz resonators, which also resonate. While resonant elements are an important

tool in the design of metamaterials, there are additional means to obtain internal degrees of freedom. An example is the labyrinthine metasurface, where propagation distance becomes the hidden degree of freedom.

A "metasurface" may be thought of as a metamaterial that is significantly smaller in one of its multiple dimensions than an effective wavelength around the structure. One notable class of metasurface consists of an array of labyrinthine structures of varying lengths [13]. Examples of labyrinthine metasurfaces from the work of Li, *et al.* [14] and Xie, *et al.* [15] are shown in Fig. 1.5, as well as analytically predicted and experimentally measured focusing acoustic fields generated using the structure from Ref. [14]. The apparent phase speed in a material element (the labyrinthine structure) may be tuned by modifying the length of the labyrinth, so the additional propagation distance inside the material element may be considered a hidden degree of freedom. This effect is limited to zero-order modes within the labyrinthine structure, and is therefore a long-wavelength effect. Since the propagation distance does not depend on the frequency, the unique properties of the labyrinthine metasurface do not arise from resonances, and the effect is broadband in the absence of structural resonances and below cut-on frequencies of higher-order modes in the metamaterial elements.

1.1.4 Applications of Metamaterials

The driving motivation behind the study of acoustic metamaterials is the variety of desirable applications which require exotic material properties.

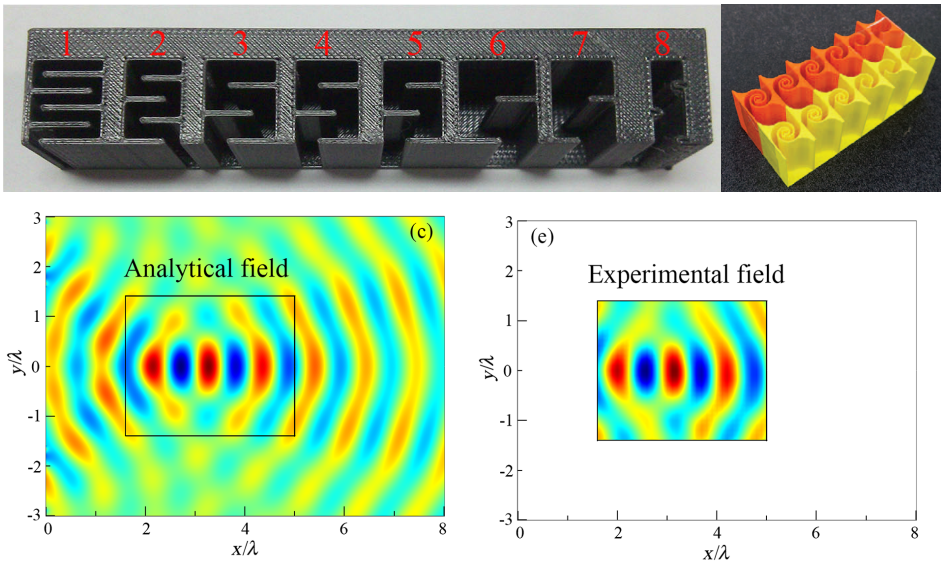

Figure 1.5: Examples of labyrinthine metasurfaces adapted from Ref. [14] (top left) and [15] (top right). Analytically predicted and experimentally measured focusing of an acoustic pressure field due to the labyrinth described in and adapted from Ref. [14] (positioned to the left of the axes) are shown in the bottom left and right, respectively.

Some notable applications, namely transformation acoustics-based applications such as acoustic cloaks, superlenses, and beam-steering metasurfaces, are discussed below.

Many of the applications of acoustic metamaterials stem from the concept of transformation acoustics. First described in optics [16], transformation acoustics comes from the fact that the acoustic wave equation is invariant under coordinate transformation [17]. If a given geometry of an acoustic system were deformed and the resultant coefficients were interpreted as material properties, the deformed geometry would behave the same as though it were

undeformed with the original material properties. Perhaps the most popular example of transformation acoustics is the concept of acoustic cloaking devices [17]. An acoustic cloak is a domain that surrounds an object of finite size that is engineered to minimize scattered acoustic fields. As with many applications of metamaterials, the concept of a cloak was first established and demonstrated for electromagnetic waves [18, 19, 20]. While transformation acoustics may be the most popular method, alternative approaches to acoustic cloaking also exist, such as scattering cancellation methods [21]. All of these methods require specific and sometimes nearly unrealizable materials [17], which illustrates the reason for the interest in metamaterials.

Another application of transformation acoustics that requires metamaterials is an acoustic super lens. Typical lenses are limited by aperture diffraction, but if the lens were made of some material with, for example, a negative index of refraction, the diffraction limit may be surpassed [22, 23]. Since the index of refraction is a ratio of sound speeds, a negative index of refraction implies one of the sound speeds is negative. This scenario occurs when both the effective bulk modulus and effective dynamic mass density of the lens material are negative; that is, the lens is made of a double negative material [23]. Since double negative materials have not been found in nature, superlens materials can only be fabricated from metamaterials. An alternative approach is to use strong anisotropy in the effective mass density [22]. Figure 1.6 shows an example of yet another type of two-dimensional acoustic metasurface lens from the work of Zigoneanu, *et al.* [24]. This lens is based on the principle

of gradient-index materials, where the effective index of refraction of the lens varies smoothly as a function of position.

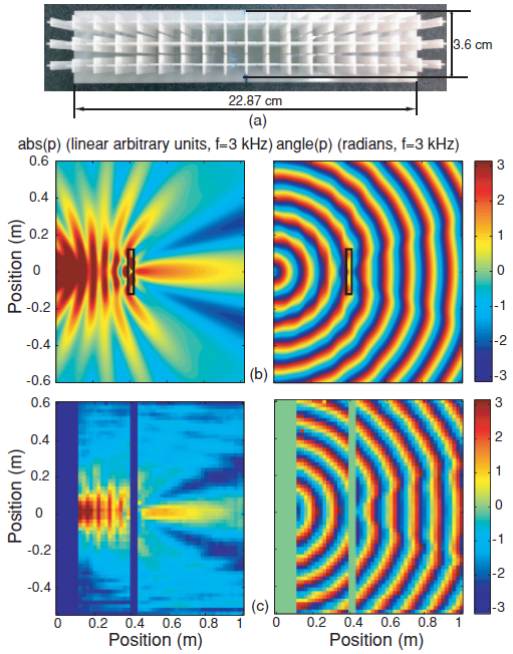

Figure 1.6: Example of a two-dimensional acoustic lens adapted from Ref. [24]. A picture of the lens made by stereolithography is given on the top, and simulated (middle) and measured (bottom) acoustic pressure magnitude (left) and phase (right) are shown for an incident Gaussian beam.

The final application of acoustic metamaterials discussed here is that of a metasurface beam steering device. It is sometimes desirable to change the propagation direction of a sound beam with a thin layer of some material [25, 26]. This may be done by varying the sound speed of the layer as a function of position. The labyrinthine metasurface represents one productive method to accomplish this functionality. As an example, Xie, *et al.* demonstrated that extraordinary beam steering may be obtained using a metasurface such as that

shown in Fig. 1.5 [15].

1.2 Homogenization Theory

A theoretical model describing the effective material properties of a system with a particular microstructure is a fundamentally important tool in the design of metamaterials. Since metamaterials have inhomogeneous microstructures but are treated as homogeneous materials with effective material properties, the process of applying a descriptive model to a metamaterial to determine effective material properties that consider subwavelength geometry and properties is called homogenization. There are many diverse methods to homogenize a system to describe the overall response of a heterogeneous elastodynamic material, such as using statistical mechanics (e.g., kinetic theory of gases [27] and linear/nonlinear sigma models [28]). Two of the major classes of homogenization methods in acoustics and solid mechanics, single scattering-based methods and multiple scattering-based methods, are relevant to this work and are therefore presented in this introduction.

1.2.1 Single Scattering

Perhaps the simplest non-trivial system to homogenize is one that is nearly homogeneous at the outset, known as the single scattering problem. The basic assumption of single scattering models is that a system is accurately represented as a homogeneous matrix material with well separated inhomogeneities, where well separated means interactions between inhomogeneities

are negligible. The first scattering problems were solved by Rayleigh, who considered the scattering of waves by rigid and fluid spheres [29]. These scattering solutions prepared the way for many effective medium models. For example, Sewell predicted the effect of fog on the index of refraction of air [30]. Another notable advancement was made by Ying and Truell, who extended single scattering theory account for the scattering of elastic waves from an elastic sphere, and briefly mentioned the derivation of absorption coefficients through suspensions [31].

In a seminal work for single scattering-based homogenization, Chaban predicted effective elastic moduli and mass density of a homogeneous elastic matrix with embedded inhomogeneities [32]. Chaban's predictions were based on two fundamental assumptions. The first assumption was that the inhomogeneities did not interact with each other, which is the essence of single scattering-based homogenization. The second assumption was that the scattered field from a control volume V_0 of the inhomogeneous medium was the same in the far-field as for the scattered field from the volume V_0 with the effective material properties. These assumptions restricted Chaban's predictions to systems with dilute concentrations of inhomogeneities that were small relative to a wavelength. However, methods have since been developed to extend these methods to greater concentrations of inhomogeneities. For example, Norris presented an extension to higher volume fractions called differential effective medium theory [33]. This homogenization method will be explained in greater detail in Chapter 5, but the main idea is that the effective

material properties for a large volume fraction of inhomogeneities may be determined by embedding a dilute quantity of inhomogeneities into the matrix, homogenizing, and using the resultant effective material as the matrix for another dilute quantity of inhomogeneities. This process would continue until the desired volume fraction of inhomogeneities is achieved.

While not strictly a "scattering" method since it is only valid for purely static problems, another important homogenization method that relies on non-interacting inhomogeneities is the Eshelby method [34]. The Eshelby method considers an ellipsoidal inhomogeneity embedded in an infinite medium under a uniform stress (or strain) load. Using what is now called the Eshelby tensor, the load at infinity is directly related to the stress and strain fields within the inhomogeneity, as well as the resultant strain (or stress) field due to the presence of the inhomogeneity. Then the volume averaged field quantities may be derived entirely in terms of the imposed fields, and the coefficients relating the volume averaged fields may be identified as the effective material properties [35]. While Eshelby originally considered a static problem, these methods have been extended to dynamic systems [36]. While the Eshelby method is restricted to dilute cases, it may also be extended to higher volume fractions using differential methods, such as that mentioned above, or a self-consistent method, where the matrix properties are assumed to be the unknown effective properties and one then numerically solves the resultant implicit equations for homogenization [37].

1.2.2 Multiple Scattering

When the interactions between inhomogeneities may not be neglected, as is the case of higher volume fractions of inhomogeneities and for high frequency systems, single scattering-based homogenization methods cease to be valid and multiple scattering-based homogenization methods should be used instead. The essence of multiple scattering-based approaches is that the scattered fields from each inhomogeneity scatter again from the neighboring inhomogeneities. The first work on notable multiple-scattering is that of Foldy, who used configurational averaging to derive a dispersion relation for scalar waves propagating through a medium with isotropic inhomogeneities [38]. Lax subsequently extended the work of Foldy to account for anisotropic inhomogeneities [39], and Waterman and Truell incorporated the effects of far-field back-scattering [40].

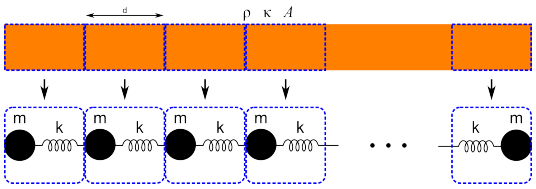

Figure 1.7: Discretization of a rod into a spring-mass lattice.

A special class of materials that is particularly well suited to multiple scattering-based analyses is periodic media. Newton used periodic media to describe propagation of sound in air by discretization (e.g., see Fig. 1.7) [41], and Rayleigh studied acoustic vibrations in continuous periodic structures [42]. Using Bloch-Floquet theory, the exact multiple-scattering problem of a peri-

odic medium may be solved by solving the dynamics of a single unit-cell with periodic boundary conditions [43, 44]. One of the most influential works on homogenization of periodic structures was by Brillouin, who studied a wide variety of topics associated with periodic media [45].

Of particular interest to the present dissertation are homogenization theories that may result in effective Willis materials. Willis materials are described below. While Willis derived a homogenization scheme which accounts for arbitrarily inhomogeneous elastic media, the resulting equations are intractable due to the presence of convolutions in the time domain and so the homogenization scheme is impractical [46, 47]. Srivastava and Nemat-Nasser used the restricted case of periodic media to develop an exact numerical homogenization scheme that accounts for Willis coupling in one dimension [48] and two and three dimensions [49]. The homogenization methods of Srivastava and Nemat-Nasser were developed assuming the existence of some background material. Norris, *et al.*, on the other hand, developed an alternative numerical homogenization method that accounts for Willis coupling in periodic media that does not require a background material [50]. Both Srivastava and Nemat-Nasser and Norris, *et al.* relied on Bloch-Floquet theory for their analyses, which yields exact results but does not differentiate between local and nonlocal effects. This ambiguity makes physical interpretation of Willis coupling from their homogenization schemes difficult. Sieck, *et al.* derived a homogenization scheme for periodic one-dimensional acoustic matrix with inhomogeneities small enough relative to an effective wavelength that the scat-

tered fields may be accurately modeled using only their monopole and dipole modes [51]. These assumptions lead to infinite convergent summations, rather than Bloch-wave analyses, to determine the Willis material properties, and may be used to distinguish local and nonlocal sources of Willis coupling. This method is based on a homogenization scheme developed for electromagnetic systems by Alù [52], as is the homogenization method developed by Koo, *et al.* [26]. Recently, another homogenization scheme for potentially-piezoelectric, one-dimensional, periodic elastic media that also accounts for Willis coupling was developed using a lumped-element approach [53]. Of particular importance, it is notable that all of the published homogenization techniques that account for Willis coupling are restricted to periodic media.

1.3 Constitutive Equations and Willis Materials

The equations resulting from imposing conservation of mass, momentum, and energy are not sufficient to fully describe the motion of a material, and must be supplemented by constitutive equations. Since the conservation laws apply to all materials equally, it is only in the constitutive equations that one material is mathematically distinguished from another, and all material properties are embedded within at least one constitutive equation. The form of the constitutive equations, which determines the material type, is often assumed based on experimentally observed behaviors. The most common constitutive equations used in describing linear elastic materials is the common

definition of momentum density and Hooke's law:

$$\vec{\mu} = \rho\dot{\vec{u}}, \tag{1.5}$$

$$\boldsymbol{\sigma} = \mathsf{C} : \boldsymbol{\varepsilon}, \tag{1.6}$$

where the momentum per unit volume $\vec{\mu}$, particle displacement $\vec{u}$, stress tensor $\boldsymbol{\sigma}$, and strain tensor $\boldsymbol{\varepsilon} = [\nabla\vec{u} + (\nabla\vec{u})^T]/2$ are the field quantities and the mass density ρ and stiffness tensor C are the material properties. In these relations, the over-dot denotes a time-derivative, the colon denotes a double inner product, the ∇ operator denotes a gradient, and the superscript T denotes a matrix transpose. These constitutive equations are then generally combined using the the dynamic equation (or Newton's second law for elastic materials) [54]:

$$\nabla \cdot \boldsymbol{\sigma} = \dot{\vec{\mu}}, \tag{1.7}$$

where $\nabla \cdot \boldsymbol{\sigma}$ is the divergence of the stress tensor.

While Eqs. (1.5) and (1.6) are sophisticated enough to describe the vast majority of materials that are commonly encountered, including solids, liquids, and gases, they do not describe all possible behavior that has been observed. For example, additional terms in Hooke's law are required to describe the handed nature of chiral materials [55] and to describe the electromechanical coupling of piezoelectric materials [56]. (Examples of other possible constitutive equations may be found in Ref. [57], and experimental evidence for some unique constitutive equations may be found in Ref. [58].) In fact, the inclusion

of the appropriate material properties in the simplest form of an accurate constitutive equation may be considered the definition of a class of material. For example, one could say that a piezoelectric material is a material that requires electromechanical coupling terms in its constitutive equations.

With this perspective of constitutive equations, the definition of a linear "Willis material" is a material which is most accurately described by the following constitutive equations:

$$\vec{\mu} = \boldsymbol{\rho} \cdot \dot{\vec{u}} + \tilde{\mathcal{S}} : \boldsymbol{\varepsilon}, \tag{1.8}$$

$$\boldsymbol{\sigma} = \mathcal{S} \cdot \dot{\vec{u}} + \mathsf{C} : \boldsymbol{\varepsilon}, \tag{1.9}$$

where $\boldsymbol{\rho}$ is the effective mass density tensor and $\mathcal{S}$ and $\tilde{\mathcal{S}}$ are called the Willis coupling tensors (or coefficients). Because J. R. Willis was the first to derive these relations for heterogeneous elastodynamic media [46], Eqs. (1.8) and (1.9) are called the Willis equations or Willis constitutive equations. The Willis coupling tensors couple the definition of momentum density with Hooke's law through a mechanism called Willis coupling.

Materials which are modeled by the constitutive equations (1.8) and (1.9) were first described by Willis in 1981 [46], and then later formalized into the above form [47, 59]. Willis was interested in the effective properties of a generally inhomogeneous elastic system, and developed Eqs. (1.8) and (1.9) using asymptotic expansions of field variables and taking the highest-order terms. This general approach resulted in mathematically intractable expressions for the material properties [47]. Since it was first described, approximations and

simplifications to the general approach of Willis have been published to estimate the values of the Willis material properties. A common element between these methods is the assumption of a periodic microstructure. Nemat-Nasser and Srivastava used Fourier transforms of the micromechanical material properties to determine the effective material properties for one-dimensional periodic media [48], and Srivastava and Nemat-Nasser later extended this method to three dimensions [49]. Norris, *et al.* used a plane-wave expansion method to determine the effective material properties in one, two, or three dimensions, and demonstrated this technique for a one-dimensional case [50]. Sieck, *et al.* used a multiple-scattering approach to determine the effective material properties for one-dimensional inclusions in a background material [51], and Kutsenko, *et al.* used a transfer matrix approach to extract Willis properties from a one-dimensional periodic system of potentially piezoelectric slabs [53].

1.3.1 Applications of Willis Materials

Despite being a relatively newly discovered class of materials, Willis materials promise to be useful in a variety of applications. Three potential applications are presented briefly in this section.

Nonreciprocal Media

A nonreciprocal acoustic (or elastic) medium is one where the rate of energy transfer depends on the direction of propagation [60]. While a comprehensive review of nonreciprocal behavior is beyond the scope of this dis-

sertation (see Fleury, *et al.* for an introductory review [61]), one method by which reciprocity may be broken is by imposing a momentum bias on the system. This was the driving mechanism behind the acoustic circulator reported in 2014, where the momentum bias was provided by a flowing medium [62]. Since a Willis material couples the momentum density to Hooke's law, it is possible that by imposing a significant stress on the material's boundaries a momentum bias may be generated within the medium that is sufficiently strong to render wave propagation within the medium to be non-reciprocal. This approach to nonreciprocity may be useful for applications where a flow is not practical, such as solid panels.

Impedance Matching

An important quantity in acoustical design is the specific acoustic impedance, or impedance. Large impedance mismatches at material interfaces results in significant reflection of acoustic energy, while impedance matched interfaces minimizes the reflected acoustic energy [5]. Often significant reflections are undesirable and an impedance matching material is used to mediate the natural impedance mismatch. The impedance of a Willis material depends not only on the mass density and stiffness but also on the Willis coupling coefficient (see Chapter 4), through which the impedance is dependent on the direction of propagation. Thus, Willis materials may be designed to create highly efficient impedance matching slab between two disparate materials.

Enhanced Absorption

The goal of many applications is to convert vibrational energy into another form of energy, such as heat, in as short a space as possible [63]. Examples of such applications are protective armor and helmets, noise control devices, and mechanical stabilizers. In a given vibration control device the dominant mode of energy absorption may depend on the particle velocity or the pressure in the material, but not necessarily both, such as a friction-based absorber. Since Willis materials couple Hooke's law with the momentum density, these materials may be designed to place pressure and particle velocity nodes at optimal locations to improve energy absorption.

1.4 Dissertation Summary

The purpose of this dissertation is to establish a physical and mathematical understanding of one of the sources of Willis coupling in elastic materials, structural asymmetry, using considerations of the microstructure and homogenization methods.

In order to begin the discussion of Willis materials on a firm foundation of physical principles, restrictions on the range of realizable material properties assuming a reciprocal, passive, and causal material are derived in Chapter 2. It is shown that reciprocity imposes symmetry conditions on the Willis material properties and passivity (with reciprocity) requires the imaginary part of the stiffness and mass density to be less than or equal to zero and greater than or equal to zero, respectively. Considerations of causality suggest that while

the Willis equations presented in Eqs. (1.8) and (1.9) may be accurate in the frequency domain, an alternative form may be more physically meaningful and important in time domain analyses.

Three simple models are presented in Chapter 3 which develop a physical understanding of microstructural asymmetry as a source of Willis coupling. The first model is a one-dimensional model of a fluid element which consists of two unequal masses connected by a spring, and the second model generalizes this using a transmission-line formalism. These models demonstrate that Willis coupling arises from interpreting the geometric center of a volume element as the center of mass when the true center of mass is offset. The third model is an arbitrary one-dimensional heterogeneous system that is interpreted as a material element. Expanding the momentum density and the average strain of the element about the geometric center is shown to lead to Willis coupling. This final model is important in that it constitutes a method by which finite element analyses may extract material properties.

Chapter 4 presents experimental evidence of the existence of Willis coupling for a one-dimensional system and the associated measurement setup. Comparison of the experimentally extracted material properties with theoretically predicted values shows very good agreement and strongly suggests the existence of Willis coupling in the material sample measured.

While Chapters 3 and 4 focus on Willis coupling on the mesoscale (e.g., a single element of a large system), Chapter 5 demonstrates a method by which knowledge of the mesoscale material properties may be used to de-

termine macroscopic material properties. The problem of determining the effective material properties of randomly distributed inhomogeneities embedded in a matrix material, both of which may be themselves effective materials possibly exhibiting Willis coupling, is considered. By assuming quasi-static loading and weakly-interacting inhomogeneities, the effective material properties for a very broad class of materials and geometries may be predicted. In particular, arbitrarily anisotropic, dynamic, and Willis coupled materials may be used for the matrix and inhomogeneities, and the inhomogeneities may be arbitrarily ellipsoidal in shape. Using established iterative methods, these predictions may be extended to arbitrary filling fractions of inhomogeneities and any number of inhomogeneity types and orientations may be accounted for.

Some final thoughts on Willis coupling are given in Chapter 6 along with some ideas of possible future work to further understand this interesting phenomenon.

1.5 A Note on Notation

Extensive use of zeroth, first, second, third, and fourth order tensors is found in this dissertation, and a uniform notation system must be used to clearly convey the mathematics described with it. Two systems will be used, as each system has its benefits and drawbacks. The two systems are the standard index notation and a tensorial notation, and are summarized in Table 1.2. The tensorial notation is useful in that there are fewer characters used, which

Table 1.2: Summary of the two notation systems used to describe tensorial algebra throughout the dissertation. (Because all of the results throughout this dissertation are obtained assuming a Cartesian coordinate system, the concepts of the first and second order tensors are equivalent to a vector and matrix, respectively.)

Symbolic	Index	Meaning
a	a	0^{th} order tensor/scalar
$\vec{x}$	x_i	1^{st} order tensor/vector
$\boldsymbol{\sigma}$	σ_{ij}	2^{nd} order tensor/matrix
$\mathcal{S}$	S_{ijk}	3^{rd} order tensor
C	C_{ijkl}	4^{th} order tensor
$\boldsymbol{A} \cdot \vec{x}$	$A_{ij}x_j$	Inner product
$\mathsf{C} : \boldsymbol{\sigma}$	$C_{ijkl}\sigma_{kl}$	Double inner product
$\vec{x} \otimes \vec{y}$	$x_i y_j$	Outer product
$\nabla \vec{u}$	$u_{i,j}$	Gradient
$\nabla \cdot \vec{u}$	$u_{i,i}$	Divergence
$\mathcal{S} = \mathcal{S}^T$	$S_{ijk} = S_{jik}$	Transpose Type 1
$\mathcal{S} = \tilde{\mathcal{S}}^{\mathsf{T}}$	$S_{ijk} = \tilde{S}_{kij}$	Transpose Type 2

facilitates understanding of the broad concepts more clearly. Using the index notation, on the other hand, more clearly expresses symmetry conditions and transposes of the tensors.

Each chapter will make exclusive use a single notation style, unless otherwise specified. Chapter 2 uses index notation due to its emphasis on symmetry conditions. Chapter 3 predominantly uses scalar quantities, for which there is not distinction between the styles, but otherwise uses tensorial notation. Chapter 4 is completely restricted to scalar quantities. Chapter 5 does not make significant use of symmetries and will therefore use tensorial notation.

Chapter 2

Physical Restrictions on Material Properties

In attempting to design materials with extreme properties, such as Willis materials, it is of critical importance to know the constraints placed on the material properties by fundamental physical laws. These constraints provide the scientist with an understanding of what material properties are physically meaningful, yielding a deeper understanding to a material, and provide the engineer with a plausible parameter space for design purposes. Constraints also gives both theoreticians and experimentalists a means to check that predicted or measured effective material properties do not violate underlying physical principles.

Restrictions on the range of material properties are derived from assumptions about the material itself. For example, standard elastic materials are assumed to be passive and causal. If an elastic or acoustic metamaterial is composed of passive materials, the effective material must also be passive and causal. Similarly if all of the constituent materials are reciprocal, reciprocity must also be enforced [60]. The restrictions imposed on general Willis-type material properties due to passivity have been derived by Srivastava and Nemat-Nasser [49] and Srivastava [64]. The restrictions imposed by causal-

ity have been derived for general Willis materials [64], but the implications of these restrictions were not fully explored. The consequences of restrictions placed on Willis coupling parameters due to passivity, reciprocity, and causality are the primary contribution of this chapter. The restrictions derived here provide a physical foundation for the analyses presented in Chapters 3-5.

Reciprocity and passivity in Willis materials are discussed in Section 2.2 and then combined. Reciprocity is shown to impose a symmetry on the material properties corresponding to the major symmetries of the stiffness tensor. Passivity in a reciprocal material is shown to restrict the sign of the imaginary part of the density and stiffness tensors and the real part of the Willis coupling parameters. Then in Section 2.3, the requirements of causality in a local medium are discussed using arbitrary history functions. Considerations of low-order dispersion in light of requirements imposed by causality suggest an alternative representation for Willis coupling which is more appropriate for time-domain analyses. Sections 2.4.1 and 2.4.2 present requirements on dispersion relations in two separate limiting cases, low-loss regions and relaxing media, and Section 2.4.3 specializes the restrictions on the material properties to the acoustic case for application to heterogeneous fluids. Section 2.5 then summarizes the work.

2.1 Constitutive Equations and Minor Symmetries

As discussed in Section 1.3, a linear Willis material is a composite material that, when homogenized, requires the stress-strain and the momentum-

velocity constitutive equations to be coupled. While Eqs. (1.8) and (1.9) are the most common representation of the Willis constitutive equations [47, 50], the most general case replaces the linear strain ε_{ij} with the displacement gradient $u_{i,j}$, where standard index notation has been used. Assuming a time-harmonic motion ($e^{-i\omega t}$ time convention), the generalized Willis constitutive equations take the form [59]

$$\sigma_{ij} = C_{ijkl} u_{k,l} + S_{ijk} v_k, \tag{2.1a}$$

$$\mu_i = \tilde{S}_{ijk} u_{j,k} + \rho_{ij} v_j, \tag{2.1b}$$

where σ_{ij} is the Cauchy stress (hereafter called the stress), C_{ijkl} is the stiffness tensor, $u_{i,j}$ is the displacement gradient, $v_i = \dot{u}_i$ is the particle velocity (hereafter called the velocity) with the over-dot denoting a time derivative, μ_i is the momentum density (hereafter called the momentum), and ρ_{ij} is the mass density tensor. The third-order tensors S_{ijk} and $\tilde{S}_{ijk}$ are the Willis coupling tensors or coefficients. In general, all material properties are temporally and spatially dispersive, i.e., $f(\omega, \vec{k})$.

Written in the form of Eqs. (2.1), Willis coupling encompasses all linear phenomena which generate stress from a net translation and linear momentum from local strain [46, 65]. For example, in reciprocal media this coupling has been demonstrated to arise from asymmetry of a representative volume element [48, 50, 65] and through nonlocal phenomena, such as lattice effects [52, 51]. Willis coupling has also been demonstrated to arise in non-reciprocal media, although not described as such [66]. Additionally, Willis coupling is

mathematically analogous to bianisotropic materials in optics, and so chiral materials may also be considered a subset of general Willis materials [55]. For the sake of simplicity, the derivations and analyses presented in this dissertation will assume that the Willis material is irrotational (so the displacement gradient $u_{i,j}$ may be replaced by the symmetric strain tensor ε_{ij}, and Eqs. (1.8) and (1.9) are recovered) and only accounts for local interactions, unless explicitly stated otherwise.

Under this set of assumptions, various symmetries of the material properties follow from standard elasticity. Assuming no external body forces, the stress tensor is symmetric [67], so the stiffness and the stress-velocity coupling tensor satisfy the symmetry conditions

$$C_{ijkl} = C_{jikl}, \tag{2.2a}$$

$$S_{ijk} = S_{jik}. \tag{2.2b}$$

Likewise, since infinitesimal strains are symmetric by definition [67], the stiffness and the momentum-strain coupling tensor satisfy the symmetry conditions

$$C_{ijkl} = C_{ijlk}, \tag{2.3a}$$

$$\tilde{S}_{ijk} = \tilde{S}_{ikj}. \tag{2.3b}$$

The conditions on the stiffness tensor in Eqs. (2.2a) and (2.3a) are often called the minor symmetries of the stiffness tensor. Therefore, the restrictions placed on the coupling tensors in Eqs. (2.2b) and (2.3b) will be referred to as the minor symmetries of the coupling tensors.

2.2 Reciprocity and Passivity

Reciprocity is qualitatively described as being able to exchange a source and a receiver without experiencing a change in the measured signal, and is a common characteristic of linear elastic and acoustic media [60]. A passive medium cannot generate energy. This is another way of stating that a passive material cannot amplify mechanical disturbances such as elastic waves as they propagate through it. Restrictions on the Willis material properties imposed by assuming that a medium is reciprocal, passive, or both passive and reciprocal will be derived in this section. It is noted that the constraints due to reciprocity and passivity have been derived elsewhere using an alternative approach [49].

2.2.1 Reciprocity

As mentioned above, Willis material properties are a result of the homogenization of inhomogeneous elastic composites. Since linear elastic materials are reciprocal, it follows that the emergent Willis material properties should also exhibit reciprocity [60]. The restrictions placed on the material properties of a linear Willis material by assuming that they are reciprocal materials are derived in this section. The present analysis differs from many analyses associated with reciprocity, in that we assume that the material is reciprocal to derive material symmetries, whereas previous work assumed material symmetries to derive reciprocity [60].

The dynamic equation for a time-harmonic linear elastic system may

be written as the real part of

$$\sigma_{ij,j}e^{-i\omega t} + f_i e^{-i\omega t} = \dot{\mu}_i e^{-i\omega t}, \tag{2.4}$$

where $\vec{f}e^{-i\omega t}$ is a time-harmonic body force density and $\sigma_{ij,j}$ represents the divergence of the stress field. The solution to this equation is the displacement field u_i. The common $e^{-i\omega t}$ may be neglected by noting that the stress, body force and momentum density can be complex-valued and represent the time-averaged fields.

Consider two elastodynamic source distributions in the same material, denoted A and B. These two source distributions are independent of each other, and arbitrary except that they satisfy the dynamic equations

$$\sigma^{\mathrm{A}}_{ij,j} + f^{\mathrm{A}}_i = \dot{\mu}^{\mathrm{A}}_i, \tag{2.5a}$$

$$\sigma^{\mathrm{B}}_{ij,j} + f^{\mathrm{B}}_i = \dot{\mu}^{\mathrm{B}}_i. \tag{2.5b}$$

The solutions to Eqs. (2.5a) and (2.5b) are the displacement fields u^{A}_i and u^{B}_i, respectively, which are not equal to each other in general. In order to determine the restrictions associated with reciprocity, one can employ the reaction principle [68]. For this case, the reaction principle simplifies to multiplying Eq. (2.5a) by the solution to Eq. (2.5b), u^B_i, and Eq. (2.5b) by the solution to Eq. (2.5a), u^{A}_i. The difference between these two relationships yields

$$\left(\sigma^{\mathrm{A}}_{ij,j}u^{\mathrm{B}}_i - \sigma^{\mathrm{B}}_{ij,j}u^{\mathrm{A}}_i\right) + \left(f^{\mathrm{A}}_i u^{\mathrm{B}}_i - f^{\mathrm{B}}_i u^{\mathrm{A}}_i\right) = \left(\dot{\mu}^{\mathrm{A}}_i u^{\mathrm{B}}_i - \dot{\mu}^{\mathrm{B}}_i u^{\mathrm{A}}_i\right). \tag{2.6}$$

For convenience, define $\Delta F \equiv \sigma^{\mathrm{A}}_{ij,j}u^{\mathrm{B}}_i - \sigma^{\mathrm{B}}_{ij,j}u^{\mathrm{A}}_i$, $\Delta B \equiv f^{\mathrm{A}}_i u^{\mathrm{B}}_i - f^{\mathrm{B}}_i u^{\mathrm{A}}_i$, and

$\Delta M \equiv \dot{\mu}_i^{\mathrm{A}} u_i^{\mathrm{B}} - \dot{\mu}_i^{\mathrm{B}} u_i^{\mathrm{A}}$, and so Eq. (2.6) becomes

$$\Delta F + \Delta B = \Delta M. \tag{2.7}$$

Using the relations $\sigma_{ij,j}^{\mathrm{X}} u_i^{\mathrm{Y}} = \left[\sigma_{ij}^{\mathrm{X}} u_i^{\mathrm{Y}}\right]_{,j} - \sigma_{ij}^{\mathrm{X}} u_{i,j}^{\mathrm{Y}} = \left[\sigma_{ij}^{\mathrm{X}} u_i^{\mathrm{Y}}\right]_{,j} - \sigma_{ij}^{\mathrm{X}} \varepsilon_{ij}^{\mathrm{Y}}$, ΔF may be expanded as

$$\Delta F = \left[\sigma_{ij}^{\mathrm{A}} u_i^{\mathrm{B}} - \sigma_{ij}^{\mathrm{B}} u_i^{\mathrm{A}}\right]_{,j} - \left(\sigma_{ij}^{\mathrm{A}} \varepsilon_{ij}^{\mathrm{B}} - \sigma_{ij}^{\mathrm{B}} \varepsilon_{ij}^{\mathrm{A}}\right). \tag{2.8}$$

Further expanding the last term of Eq. (2.8) by assuming the medium in question is a Willis material with constitutive behavior described by Eqs.(2.1) yields

$$\sigma_{ij}^{\mathrm{A}} \varepsilon_{ij}^{\mathrm{B}} - \sigma_{ij}^{\mathrm{B}} \varepsilon_{ij}^{\mathrm{A}} = C_{ijkl} \varepsilon_{ij}^{\mathrm{B}} \varepsilon_{kl}^{\mathrm{A}} - C_{ijkl} \varepsilon_{ij}^{\mathrm{A}} \varepsilon_{kl}^{\mathrm{B}} + S_{ijk} \varepsilon_{ij}^{\mathrm{B}} v_k^{\mathrm{A}} - S_{ijk} \varepsilon_{ij}^{\mathrm{A}} v_k^{\mathrm{B}} \tag{2.9}$$

for the second term on the left-hand side of Eq. (2.7). Similarly, if the medium in question is a Willis material, ΔM may also be expanded as

$$\begin{aligned} \Delta M &= \tilde{S}_{ijk} u_i^{\mathrm{B}} \dot{\varepsilon}_{jk}^{\mathrm{A}} - \tilde{S}_{ijk} u_i^{\mathrm{A}} \dot{\varepsilon}_{jk}^{\mathrm{B}} + \rho_{ij} u_i^{\mathrm{B}} \dot{v}_j^{\mathrm{A}} - \rho_{ij} u_i^{\mathrm{A}} \dot{v}_j^{\mathrm{B}} \\ &= \tilde{S}_{ijk} v_i^{\mathrm{B}} \varepsilon_{jk}^{\mathrm{A}} - \tilde{S}_{ijk} v_i^{\mathrm{A}} \varepsilon_{jk}^{\mathrm{B}} + \rho_{ij} v_i^{\mathrm{B}} v_j^{\mathrm{A}} - \rho_{ij} v_i^{\mathrm{A}} v_j^{\mathrm{B}}, \end{aligned} \tag{2.10}$$

where the time-harmonicity in a linear time-invariant system has been used to move the time derivatives. Combining the results of Eqs. (2.8)–(2.10) with Eq. (2.7), we may write

$$\begin{aligned} \left[\sigma_{ij}^{\mathrm{A}} u_i^{\mathrm{B}} - \sigma_{ij}^{\mathrm{B}} u_i^{\mathrm{A}}\right]_{,j} + \Delta B = &\left(C_{ijkl} \varepsilon_{ij}^{\mathrm{B}} \varepsilon_{kl}^{\mathrm{A}} - C_{ijkl} \varepsilon_{ij}^{\mathrm{A}} \varepsilon_{kl}^{\mathrm{B}}\right) + \left(S_{ijk} \varepsilon_{ij}^{\mathrm{B}} v_k^{\mathrm{A}} - S_{ijk} \varepsilon_{ij}^{\mathrm{A}} v_k^{\mathrm{B}}\right) \\ &+ \left(\tilde{S}_{ijk} v_i^{\mathrm{B}} \varepsilon_{jk}^{\mathrm{A}} - \tilde{S}_{ijk} v_i^{\mathrm{A}} \varepsilon_{jk}^{\mathrm{B}}\right) + \left(\rho_{ij} v_i^{\mathrm{B}} v_j^{\mathrm{A}} - \rho_{ij} v_i^{\mathrm{A}} v_j^{\mathrm{B}}\right), \end{aligned} \tag{2.11}$$

which may be simplified by exchanging dummy indexes to yield

$$[C_{ijkl} - C_{klij}]\,\varepsilon^{\mathrm{B}}_{ij}\varepsilon^{\mathrm{A}}_{kl} + \left[\tilde{S}_{ijk} - S_{jki}\right]\left(v^{\mathrm{B}}_i\varepsilon^{\mathrm{A}}_{jk} - v^{\mathrm{A}}_i\varepsilon^{\mathrm{B}}_{jk}\right) + [\rho_{ij} - \rho_{ji}]\,v^{\mathrm{B}}_i v^{\mathrm{A}}_j = \left[\sigma^{\mathrm{A}}_{ij}u^{\mathrm{B}}_i - \sigma^{\mathrm{B}}_{ij}u^{\mathrm{A}}_i\right]_{,j} + \Delta B.$$

The present analysis makes a point of departure here from previous analyses of reciprocity in generalized elastodynamics. Often, material symmetries are assumed and the reciprocity relations are derived. However, we will assume local reciprocity as derived by Achenbach [60] and then derive material symmetries. For a locally reciprocal, time-invariant material, it has been shown that $\Delta B = -[\sigma^{\mathrm{A}}_{ij}u^{\mathrm{B}}_i - \sigma^{\mathrm{B}}_{ij}u^{\mathrm{A}}_i]_{,j}$, and we conclude

$$[C_{ijkl} - C_{klij}]\,\varepsilon^{\mathrm{B}}_{ij}\varepsilon^{\mathrm{A}}_{kl} + \left[\tilde{S}_{ijk} - S_{jki}\right]\left(v^{\mathrm{B}}_i\varepsilon^{\mathrm{A}}_{jk} - v^{\mathrm{A}}_i\varepsilon^{\mathrm{B}}_{jk}\right) + [\rho_{ij} - \rho_{ji}]\,v^{\mathrm{B}}_i v^{\mathrm{A}}_j = 0. \tag{2.12}$$

Since the choice of force-source distributions was arbitrary, the strain and velocity fields must be considered independent fields. Therefore, the first and third terms in Eq. (2.12) must be individually equal to zero. Consequentially, the second term must also be zero, yielding

$$C_{ijkl} = C_{klij}, \tag{2.13a}$$

$$\rho_{ij} = \rho_{ji}, \tag{2.13b}$$

$$\tilde{S}_{ijk} = S_{jki}. \tag{2.13c}$$

The restriction placed on the stiffness tensor by elastodynamic reciprocity is given by Eq. (2.13a) and is called the major symmetry of the stiffness (usually obtained by considering an assumed strain-energy function [67]). Likewise,

the symmetries required by reciprocity on the density and coupling tensors, Eqs. (2.13b) and (2.13c), respectively, are also called major symmetries.

2.2.2 Passivity

A passive mechanical medium is one that does not supply any mechanical energy. It can only respond to externally provided stimulus. This is expressed in terms of energy with the statement that net energy flux *into* a region of a passive material must be equal to or greater than zero. As with reciprocal media, any heterogeneous material constructed of passive materials must also be passive. This is true for standard elastic materials and generalized elastodynamic media like Willis materials. The restrictions imposed by passivity on Willis materials have also been derived by other authors (see Refs. [49, 64]), but they are provided in this section for completeness. The present derivation will follow the approach of Banerjee [69].

The net energy flux per period into a finite-sized region Ω with boundary Γ is the real part of the complex power [54], while the imaginary part is known as the reactive power, which does not contribute to the energy transmitted to Ω. The complex power in the regions Ω, denoted by P, is given by

$$P = \int_{\Gamma} \sigma_{ij} v_i^* n_j d\vec{x} + \int_{\Omega} f_i v_i^* d\vec{x} = \int_{\Omega} \left[\sigma_{ij} v_{i,j}^* + \dot{\mu}_i v_i^* \right] d\vec{x}, \tag{2.14}$$

where n_i is the unit outward normal, and the equation has been simplified using the divergence theorem and the dynamic equation given in Eq. (2.4).

Using the Willis relations, Eq. (2.14) may be expanded as

$$P = \int_{\Omega} \left[C_{ijkl} u_{k,l} v^*_{i,j} + S_{ijk} v_k v^*_{i,j} + \tilde{S}_{ijk} v_{j,k} v^*_i + \rho_{ij} \dot{v}_j v^*_i \right] d\vec{x}. \tag{2.15}$$

Through the careful choice of boundary conditions, the velocity and strain in the arbitrary region Ω may be imposed independently. Therefore, one may set the particle velocity v_i equal to zero to yield an inequality involving the stiffness, or one may set the strain equal to zero to yield an inequality involving the mass density, written respectively as

$$\Re\left\{C_{ijkl} v^*_{i,j} u_{k,l}\right\} = \frac{i\omega}{2}\left(C_{ijkl} - C^*_{klij}\right) \varepsilon^*_{ij} \varepsilon_{kl} \geq 0, \tag{2.16a}$$

$$\Re\left\{\rho_{ij} v^*_i \dot{v}_j\right\} = -\frac{i\omega}{2}\left(\rho_{ij} - \rho^*_{ji}\right) v^*_i v_j \geq 0. \tag{2.16b}$$

For non-zero strain and non-zero velocity, passivity requires

$$\Re\left\{\tilde{S}_{ijk} v^*_i v_{j,k} + S_{ijk} v_k v^*_{i,j}\right\} \geq -\Re\left\{C_{ijkl} v^*_{i,j} u_{k,l}\right\} - \Re\left\{\rho_{ij} v^*_i \dot{v}_j\right\}. \tag{2.17}$$

2.2.3 Reciprocal and Passive Media

If the medium is both reciprocal and passive, the major symmetries of the stiffness and density tensors can be exploited to simplify Eqs. (2.16) to yield

$$C''_{ijkl} \varepsilon^*_{ij} \varepsilon_{kl} \leq 0, \tag{2.18a}$$

$$\rho''_{ij} v^*_i v_j \geq 0, \tag{2.18b}$$

where $Y' \equiv \Re\{Y\}$ and $Y'' \equiv \Im\{Y\}$. In words, Eqs. (2.18) mean that for a passive material and using the $e^{-i\omega t}$ time convention, the imaginary part of the

stiffness tensor must be negative definite and the imaginary part of the density tensor must be positive definite. Equation (2.17) may also be simplified to give

$$\Re\left\{\varepsilon_{ij}\Re\{S_{ijk}\}v_k^*\right\} \leq -\varepsilon_{ij}^* C''_{ijkl}\varepsilon_{kl} + v_i^*\rho''_{ij}v_j. \tag{2.19}$$

In light of Eqs. (2.18), we find the right-hand side of Eq. (2.19) must be either zero (the lossless case) or positive. In the important limiting case of a lossless material, we find

$$\Im\{C_{ijkl}\} = \Im\{\rho_{ij}\} = \Re\{S_{ijk}\} = \Re\{\tilde{S}_{ijk}\} = 0. \tag{2.20}$$

These results were found using similar methods by Srivastava and Nemat-Nasser [49] and Srivastava [64].

The result that the coupling tensors must be purely imaginary in the lossless case is interesting, given the fact that complex coupling tensors have emerged from a derivation that only considers lossless media [48, 50]. This is counter to the stiffness and density tensors which are purely real unless losses are present. For those properties, the imaginary component is nonzero because the material response lags the excitation in lossy media. On the other hand, the imaginary part of the coupling tensors have been associated with asymmetry at the inclusion scale [48, 50], while the real part has been observed to be due to nonlocal coupling phenomena from "weak spatial dispersion effects associated with the finite phase velocity along the array" [52]. This explains the apparent discrepancy between the present derivation, which does not account for such nonlocal phenomena, and the complex-valued predictions of the above-mentioned derivation which assumes a periodic lattice.

The bounds imposed by reciprocity may be derived for coupling tensors accounting for nonlocal phenomena as well. As shown by Alù [52] and Sieck, *et al.* [51], local coupling phenomena are accounted for by coupling tensors which are *even* in wavenumber which requires, for example, that $S_{ijk}(\omega, \vec{k}) = S_{ijk}(\omega, -\vec{k})$. On the other hand, first-order nonlocal coupling phenomena are accounted for by coupling tensors which are *odd* in wavenumber; for example, $S_{ijk}(\omega, \vec{k}) = -S_{ijk}(\omega, -\vec{k})$. While this distinction does not affect the results of the passivity derivation, including the odd component of coupling in the reciprocity analysis leads to the statement

$$\tilde{S}^{\text{odd}}_{ijk} = -S^{\text{odd}}_{jki}. \tag{2.21}$$

Combining Eq. (2.21) with Eq. (2.17) and assuming lossless media results in purely real values for S^{odd}_{ijk} and $\tilde{S}^{\text{odd}}_{ijk}$. As mentioned in Section 2.1, all coupling tensors will be assumed to account only for local phenomena and will therefore be assumed to be even in wavenumber.

2.3 Causality

In general, the strain and velocity fields at a given time and location in a material depend upon the fields at other times (material memory) and locations (non-locality). By assuming that nothing in the future may affect the present state of the system (that is, the system is causal) one restricts the admissible functions that describe the material response [70, 71]. While causality is well known and often used in electromagnetism to provide restrictions

on the spectral shape of material properties for special cases, the principal of causality has primarily been used in the fields of acoustics and elastodynamics for measurement purposes [72, 73, 74]. Therefore, we will start our discussion of the effects of causality in a linear, local Willis material by deriving the Kramers-Krönig relations.

For the present analysis, it is assumed that only local effects are significant, and that all of the results will hold point-wise throughout the material. Despite the fact that lattice effects are known to be important in Willis materials [52], an analysis on the effects of non-local causality (i.e., accounting for finite propagation times) is beyond the scope of this work. For this case, a constitutive equation for a linear material relating a fields $\hat{y}_n(t)$ to the field $\hat{x}(t)$ may then be written in the time-domain as a sum of convolutions: [71]

$$\hat{x}(t) = \sum_n \int_0^\infty \left(\frac{\partial}{\partial s} \underline{A}_n(s) \right) \hat{y}_n(t-s) ds, \tag{2.22}$$

where $\underline{A}_n(s)$ are known as the history functions and are real valued. Note that $\underline{A}_n(s)$ and $\hat{y}_n(t)$ are not vectors, but a list of arbitrary tensors. As an example, $\hat{y}_1(t)$ could represent the strain field $\hat{\varepsilon}_{ij}(t)$ at a given material point as a function of time and $\underline{A}_1(s)$ would then represent the history function associated with the stiffness, $\underline{\mathcal{C}}_{ijkl}(s)$ (note that it is not the stiffness). In that case, $\hat{x}(t)$ would be the stress $\hat{\sigma}_{ij}(t)$ at the same material point as a function of time. The history functions are assumed to be smooth, except possibly at $s = 0$, and are purely real. Further, the history functions are assumed to go to zero as $s \to \infty$. For time-harmonic systems we may write

$\hat{x}(t) = \Re\{x(\omega)e^{-i\omega t}\}$ and $\hat{y}_n(t) = \Re\{y_n(\omega)e^{-i\omega t}\}$, and the operator $\Re\{\ \cdot\ \}$ and the time dependencies may be neglected by considering only time averaged quantities. Then, integrating Eqs. (2.22) by parts, multiplying the result by $e^{i\omega t}$ (the complex conjugate of our time convention $e^{-i\omega t}$), and time averaging yields

$$x(\omega) = \sum_n \left[\underline{A}_n(0) - i\omega \int_0^\infty \underline{A}_n(s) e^{-i\omega s} ds \right] y_n(\omega). \tag{2.23}$$

One can then define the complex, frequency-dependent material properties, A_n, as

$$A_n(\omega) \equiv \underline{A}_n(0) + \omega \int_0^\infty \underline{A}_n(s) \sin(\omega s) ds - i\omega \int_0^\infty \underline{A}_n(s) \cos(\omega s) ds, \tag{2.24}$$

or simply $A_n(\omega) = A'_n(\omega) + iA''_n(\omega)$, where $A'_n(\omega)$ and $A''_n(\omega)$ are the real and imaginary parts of $A_n(\omega)$, respectively, defined as

$$A'_n(\omega) = \underline{A}_n(0) + \omega \int_0^\infty \underline{A}_n(s) \sin(\omega s) ds \tag{2.25a}$$

$$A''_n(\omega) = -i\omega \int_0^\infty \underline{A}_n(s) \cos(\omega s) ds. \tag{2.25b}$$

Equation (2.23) therefore simplifies to $x(\omega) = \sum_n A_n(\omega) y_n(\omega)$, and Eq. (2.24) may then be re-written in the following useful form:

$$A_n(\omega) - \underline{A}_n(0) = (A'_n(\omega) - \underline{A}_n(0)) + iA''_n(\omega) = \int_0^\infty \underline{A}_n(t) i\omega e^{i\omega t} dt. \tag{2.26}$$

The left-hand side of Eq. (2.26), $A_n - \underline{A}_n(0)$, is found to be analytic for any finite value of ω and at ∞ on the upper half of the complex-ω plane. Thus, in the limit $\omega \to \infty$, $A'_n(\omega) \to \underline{A}_n(0)$ and $A''_n(\omega) = 0$. Then, since $A_n(\omega) - \underline{A}_n(0) = A_n(\omega) - A'_n(\infty)$ is analytic in the upper half complex-ω

plane, Cauchy's residue theorem allows one to express the material property, A_n, as

$$A_n'(\omega) - A_n'(\infty) = \frac{1}{\pi}\mathcal{P}\int_{-\infty}^{\infty} \frac{A_n''(\lambda)}{\lambda - \omega} d\lambda, \tag{2.27a}$$

$$A_n''(\omega) = -\frac{1}{\pi}\mathcal{P}\int_{-\infty}^{\infty} \frac{A_n'(\lambda) - \underline{A}(0)}{\lambda - \omega} d\lambda, \tag{2.27b}$$

where the $\mathcal{P}$ denotes the principal value of the integral. These relations are known as the Kramers-Krönig relations, and they explicitly relate $A_n''(\omega)$ to $A_n'(\omega) - A'(\infty)$ via the Hilbert transform [75]. Note that any constant in the integrands will integrate to zero because the denominator is an odd function of ω. Finally, since $A_n'(\omega)$ is even and $A_n''(\omega)$ is odd with respect to ω, the integrals in Eqs. (2.27) may be reduced to only positive values of λ to give

$$A_n'(\omega) - A_n'(\infty) = \frac{2}{\pi}\mathcal{P}\int_{0}^{\infty} \frac{\lambda A_n''(\lambda)}{\lambda^2 - \omega^2} d\lambda, \tag{2.28a}$$

$$A_n''(\omega) = -\frac{2}{\pi}\mathcal{P}\int_{0}^{\infty} \frac{\omega A_n'(\lambda)}{\lambda^2 - \omega^2} d\lambda. \tag{2.28b}$$

Equations (2.28) must hold for any physically realizable system, and may be used to check that a predicted dispersion relation for an arbitrary material property is causal. For a linear Willis material, the constitutive equations Eqs. (2.1) are therefore causal if the following relations between real and imag-

inary parts hold:

$$C'_{ijkl}(\omega) - C'_{ijkl}(\infty) = \frac{2}{\pi}\mathcal{P}\int_0^\infty \frac{\lambda C''_{ijkl}(\lambda)}{\lambda^2 - \omega^2} d\lambda,$$

$$C''_{ijkl}(\omega) = -\frac{2}{\pi}\mathcal{P}\int_0^\infty \frac{\omega C'_{ijkl}(\lambda)}{\lambda^2 - \omega^2} d\lambda, \quad (2.29a)$$

$$S'_{ijk}(\omega) - S'_{ijk}(\infty) = \frac{2}{\pi}\mathcal{P}\int_0^\infty \frac{\lambda S''_{ijk}(\lambda)}{\lambda^2 - \omega^2} d\lambda,$$

$$S''_{ijk}(\omega) = -\frac{2}{\pi}\mathcal{P}\int_0^\infty \frac{\omega S'_{ijk}(\lambda)}{\lambda^2 - \omega^2} d\lambda, \quad (2.29b)$$

$$\tilde{S}'_{ijk}(\omega) - \tilde{S}'_{ijk}(\infty) = \frac{2}{\pi}\mathcal{P}\int_0^\infty \frac{\lambda \tilde{S}''_{ijk}(\lambda)}{\lambda^2 - \omega^2} d\lambda,$$

$$\tilde{S}''_{ijk}(\omega) = -\frac{2}{\pi}\mathcal{P}\int_0^\infty \frac{\omega \tilde{S}'_{ijk}(\lambda)}{\lambda^2 - \omega^2} d\lambda, \quad (2.29c)$$

$$\rho'_{ij}(\omega) - \rho'_{ij}(\infty) = \frac{2}{\pi}\mathcal{P}\int_0^\infty \frac{\lambda \rho''_{ij}(\lambda)}{\lambda^2 - \omega^2} d\lambda,$$

$$\rho''_{ij}(\omega) = -\frac{2}{\pi}\mathcal{P}\int_0^\infty \frac{\omega \rho'_{ij}(\lambda)}{\lambda^2 - \omega^2} d\lambda. \quad (2.29d)$$

2.3.1 An Informative Limiting Case

Equations (2.29) provide explicit relationships between the real and imaginary parts of the dispersive properties of a causal Willis material. Unfortunately, the generality of these expressions does not lend itself to easy implementation in determining general theoretical restrictions imposed on Willis material properties by assuming causality. An important question, then, is: How can the Kramers-Krönig relations be used to learn more about Willis materials? Some answers to that question can be obtained by first acknowledging assumptions underlying the implementation of Eqs. (2.29) and then investigating limiting cases. In order to use these relationships, one must first

acknowledge the assumptions implicit in this formulation. The primary assumption relevant to the present study is that the history functions that are valid and associated material properties describe a material that is well represented as a continuum. That is to say, one must assume that all small scale physics underlying the dispersive nature of the medium are accurately represented by the history functions at every material point. For example, one does not need to explicitly consider molecular dynamics associated with relaxation in a viscoelastic medium to model the causal stress-strain response of the medium using a stiffness history function. Under the continuum hypothesis one must therefore assume that the upper limit of the integrals in Eqs. (2.29) is only infinite in the sense that it is sufficiently high to not restrict the accuracy of the relationships between real and imaginary parts of the material property.

Beyond these basic assumptions, it is also important to note that it is rarely, if ever, possible to know the real or imaginary parts of any material property at all frequencies. Numerous authors have addressed this difficulty by limiting their analysis to certain frequency ranges where simplifying assumptions may be made such that knowledge of the material response outside of that range is unnecessary to provide accurate relations between the real and imaginary parts of a material property. Common examples include investigation of regions of low loss near poles [70] and limiting analysis to regions of weak dispersion [72]. These specific cases and their implications on dispersive Willis material properties will be discussed in more detail in Sections 2.4.1 and 2.4.2, respectively.

One specific limiting case of interest is that of a passive, reciprocal, and lossless Willis material in the long wavelength limit. This case is of specific interest to the field of acoustic and elastic metamaterials which focuses on effective properties of a medium that result from deeply subwavelength microstructure. In the long wavelength limit, one can evaluate the Kramer-Krönig relations if the upper limit of Eqs. (2.29) is set to a frequency that is simultaneously much greater than the frequency of interest and well below the lowest microstructural resonance frequency. This interpretation of the the integral limits is permissible because of the continuum approximation [1]. In this case, the material properties are local in time and space, and all losses are negligible. While the upper frequency limit described here is difficult, if not impossible, to define from a mathematical standpoint, the value of this approximation to aid in physical reasoning based on a causality argument will become clear in the following paragraphs. For this case, Eq. (2.20) provides the passivity requirement that the imaginary parts of the stiffness and mass density tensors are zero and the real parts of the coupling tensors are also zero at all frequencies considered in the Kramer-Krönig relations. The requirements of causality summarized in Eqs. (2.29) then simplify to

$$C_{ijkl}(\omega) = C'_{ijkl}(\infty), \quad \rho_{ij}(\omega) = \rho'_{ij}(\infty), \quad \Im\{S_{ijk}(\omega)\} = \Im\{\tilde{S}_{ijk}(\omega)\} = 0. \tag{2.30}$$

Thus, Willis coupling appears to be prohibited by causality in this limiting case. However, multiple investigators have predicted the existence of non-zero Willis coupling tensors in passive, lossless, and reciprocal media in the

very long wavelength limit. For example, Nemat-Nasser and Srivastava [48] and Norris, *et al.* [50] used Bloch wave analyses to determine the effective coupling tensors for a one-dimensional elastic lattice, Sieck, *et al.* provided estimates for the analogous one-dimensional acoustic system [51], and Milton calculated coupling tensors for a two-dimensional periodic lattice [76]. In all of these works, complex valued coupling tensors have been predicted in the low-frequency limit when all constituent materials of the microstructure were assumed to be lossless. One thus concludes that while Eqs. (2.1) provide an accurate and insightful representation the behavior of materials with asymmetric microstructure (i.e., they properly describe the motion of the system), they are not a universally causal representation. While a causal representation may not be necessary for frequency domain analyses, effective medium theory that does not provide causal effective properties may pose problems for time-domain analyses and to interpretation of experimental data [72, 73, 74]. It is therefore important to investigate whether a causal representation can be found.

One common aspect of the studies mentioned above is that the lowest order dispersion of the imaginary parts of the coupling tensors is proportional to $-i\omega$. Since time-derivatives in the frequency domain may be substituted by multiplication by $-i\omega$, this form suggests a time derivative operation on the field variable may be hidden within the effective Willis coupling coefficient. This conclusion is supported by a simple model of a one-dimensional multi-degree of freedom "particle" with inherently asymmetric microstructure, such

as the one shown in Chapter 3.1.1. Analysis of that particle predicts that stress is related to the *acceleration* rather than the velocity, and the momentum density is related to the *strain rate* rather than the strain. Furthermore, Nassar, *et al.* also suggested that the low-order dispersion predicted by their model of Willis coupling was actually a time derivative on the field quantities being wrapped into the material property in the frequency domain [65]. Following these suggestions, the reciprocal Willis equations (Eqs. (2.1) with $\tilde{S}_{ijk} = S_{jki}$) can be re-written in the form

$$\sigma_{ij} = C_{ijkl}\varepsilon_{kl} - \frac{S_{ijk}}{i\omega}\dot{v}_k, \tag{2.31a}$$

$$\mu_i = -\frac{S_{jki}}{i\omega}\dot{\varepsilon}_{jk} + \rho_{ij}v_j. \tag{2.31b}$$

Then, defining $\Psi_{ijk} = -S_{ijk}/i\omega$, one obtains a new set of constitutive equations:

$$\sigma_{ij} = C_{ijkl}\varepsilon_{kl} + \Psi_{ijk}\dot{v}_k, \tag{2.32a}$$

$$\mu_i = \tilde{\Psi}_{ijk}\dot{\varepsilon}_{jk} + \rho_{ij}v_j, \tag{2.32b}$$

where $\tilde{\Psi}_{jki} = \Psi_{ijk}$ (equality from reciprocity) are purely real material properties in the low frequency limit that represents Willis coupling. This time domain formulation is particularly interesting because it clearly indicates that the generalized relationships of elastodynamics for stress and momentum degenerate to the common representations if strain and velocity are constant. In other words, the time domain formulation of Eqs. (2.32) implies that Willis coupling is the result of microstructure that does not influence the static stress-strain response of the heterogeneous medium or rigid body dynamics, but

that becomes observable under time-varying excitation. This is particularly interesting since it indicates that Willis coupling does not violate Galilean invariance of the stress field in a medium with uniform and constant velocity. As mentioned above, a similar set of constitutive equations were proposed by Nassar, *eta al.* after analyzing a one-dimensional periodic system of masses and springs [65]. Their proposal was based on the requirement that the imposed stress field be invariant under Galilean transformations and then writing the definition of the momentum in similar manner. Lastly, it is important to note that despite the fact that the time domain formulation was deduced from causality using a highly idealized dispersionless limiting case, Ψ_{ijk} is not restricted to be dispersionless in general. Indeed, previous work on the topic clearly indicates that this material property may be strongly dispersive when resonant subwavelength material inhomogeneities are present in a medium [49, 51].

Since Eqs. (2.32) are simply an alternative representation of the Willis equations, the restrictions on S_{ijk} due to passivity may be easily converted to restrictions on Ψ_{ijk} (the restrictions imposed by reciprocity are implicitly already included). In particular, for a reciprocal and passive system we require

$$\omega \left| \varepsilon_{ij} \Psi''_{ijk} v^*_k \right| \leq -\varepsilon^*_{ij} C''_{ijkl} \varepsilon_{kl} + v^*_i \rho''_{ij} v_j, \tag{2.33}$$

where we observe that the lossy component of Ψ_{ijk} is the imaginary part, analogous to the lossy parts of the stiffness and density tensors. Furthermore, using an analysis similar to that given above, the Kramer-Krönig relations for

Ψ_{ijk} may be written

$$\Psi'_{ijk}(\omega) - \Psi'_{ijk}(\infty) = \frac{2}{\pi}\mathcal{P}\int_0^\infty \frac{\lambda\Psi''_{ijk}(\lambda)}{\lambda^2 - \omega^2}d\lambda,$$

$$\Psi''_{ijk}(\omega) = -\frac{2}{\pi}\mathcal{P}\int_0^\infty \frac{\omega\Psi'_{ijk}(\lambda)}{\lambda^2 - \omega^2}d\lambda, \qquad (2.34)$$

which is identical in form to the relations in Eqs. (2.29).

2.4 Special Cases

In this section, additional requirements of material properties for three special cases of particular interest are considered. First, the case of media supporting wave propagation with very low loss is considered. Then, the case of media without any resonances is discussed. Finally, the requirements on the fully general elastodynamic material properties are reduced to the acoustic limit, where neither shear stress nor strain are supported.

2.4.1 Low Loss Regions

Propagation with low losses in wave energy is an important subject, and much has been written on the topic [70]. If the net power flux through a region is set equal to zero, then

$$C''_{ijkl} = \Psi''_{ijk} = \rho''_{ij} = 0. \qquad (2.35)$$

Since the imaginary parts of the material properties are identically zero, Eq. (2.28a) requires the real part to be constant in frequency. This result may seem surprising, since there are many examples of effective media constructed of

purely lossless components whose effective properties display nontrivial dispersion. Examples include media with resonant inhomogeneities [11, 12] and Bloch media [48]. However, these media are based on hidden degrees of freedom, such as shunt resonators which are inherently dispersive [11], or periodic media which account for long-range interactions [48].

While the presence of a band structure precludes the use of the lossless restrictions, Landau and Lifshitz [70] demonstrated that interesting requirements may be found in the lossless regions. If $A''(\lambda) = 0$ for λ in some passband, then the principal integral on the right-hand side of Eq. (2.28a) may be reduced to a normal integral for ω in the passband. Then, taking a derivative with respect to ω, one may write

$$\frac{\partial A'}{\partial \omega} = \frac{2}{\pi} \int_0^\infty \frac{2\lambda\omega}{(\lambda^2 - \omega^2)^2} A''(\lambda) d\lambda. \tag{2.36}$$

Notice that over the entire range of integration, the integrand in Eq. (2.36) takes the sign of $A''(\lambda)$. But for the stiffness and density, passivity requires the imaginary part of the material properties to keep the same sign for all frequencies. Therefore, the sign of $\partial A'/\partial\omega$ is the same as the sign of $A''(\omega)$ in the passbands. It should be noted that since passivity only places a restriction on the *magnitude* of the coupling tensors, a similar statement for the coupling tensors cannot be made.

2.4.2 Low Dispersion Regions

In the regions of loss the Kramers-Krönig relations may still yield information about the slope of $A'(\omega)$. Assuming non-negligible $A''(\omega)$, O'Donnell,

et al. [72] were able expand the principal value integral in Eq. (2.28b) about the pole in an infinite power series equivalent to

$$A''(\omega) = -\frac{\pi}{2}\omega\frac{\partial A'}{\partial \omega} - \frac{\pi^3}{24}\omega^3\frac{\partial^3 A'}{\partial \omega^3} + \cdots . \tag{2.37}$$

For either small ω or for $A''(\omega)$ approximately proportional to ω (a property of regions of low dispersion), the higher-order terms become negligible, and we find the sign of $\partial A'/\partial\omega$ has the opposite sign of $A''(\omega)$. This holds for all of the material properties, including the coupling terms.

The cases of Landau and Lifshitz [70] and of O'Donnell, *et al.* [72] lead to opposite conclusions, so the situations in which they are applicable should be clearly delineated. First, the two approaches start from different underlying assumptions, and thus are described using different relationships. Since Landau and Lifshitz assume very small $A''(\omega)$, they start with the Kramers-Krönig relation for $A'(\omega)$. On the other hand, O'Donnell, *et al.* make no assumption on $A''(\omega)$, and use the Kramers-Krönig relation for $A''(\omega)$. Furthermore, O'Donnell, *et al.* tacitly assume the dominant contribution to the principal value integral comes from the pole, which implies there are no resonances of $A'(\lambda)$ for λ close to ω. An example where this assumption breaks down is a low-loss material displaying band structure due to sub-wavelength resonances. In a passband far from any band gap, the dominant contribution to the integral in Eq. (2.28b) is the pole, and the limit of O'Donnell, *et al.* holds. However, close to the edge of the passband, the relatively large values of $A''(\omega)$ in the band gap dominate, and the limit of Landau and Lifshitz becomes

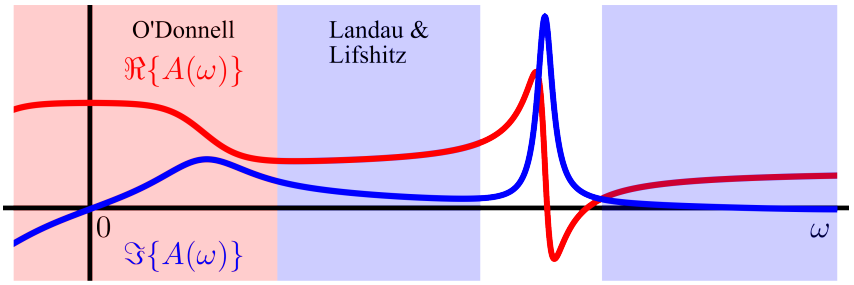

Figure 2.1: Demonstration of the O'Donnell [72] and the Landau and Lifshitz [70] approximations. The O'Donnell approximation is applicable for slowly varying real part far from sharp imaginary peaks (red region). The Landau and Lifshitz approximation is applicable for low imaginary part near a resonance or near relatively sharp imaginary peaks (blue region).

appropriate. Figure 2.1 provides an illustration of these two approximations and their approximate domains of applicability.

2.4.3 Acoustic Limit

Because of the recently increased interest in acoustic metamaterials, the causal form of the Willis equations, Eqs. (2.32), is specialized here to the fluid case where shear is not supported. Instead of using the Cauchy stress and strain tensors, the acoustic pressure P and the volumetric strain ε_V, which are both scalars, will be used.

The volumetric strain is defined as the trace of the strain tensor, and the pressure is defined as negative one-third of the trace of the Cauchy stress:

$$\varepsilon_V = \operatorname{tr} \varepsilon_{ij} = \varepsilon_{ii}, \tag{2.38a}$$

$$P = -\frac{1}{3}\operatorname{tr} \sigma_{ij} = -\frac{\sigma_{ii}}{3}. \tag{2.38b}$$

In the limit of acoustic disturbances the stress and strain are written as $\sigma_{ij} = -P\delta_{ij}$ and $\varepsilon_{ij} = \varepsilon_V \delta_{ij}/3$, respectively. Then Eqs. (2.32) become

$$-3P = \frac{1}{3} C_{iikk} \varepsilon_V + \Psi_{iik} \dot{v}_k, \tag{2.39a}$$

$$\mu_i = \frac{1}{3} \tilde{\Psi}_{ijj} \dot{\varepsilon}_V + \rho_{ij} v_j, \tag{2.39b}$$

where we have taken the trace of the first equation. We now define $\kappa \equiv C_{iijj}/9$, $\psi_i \equiv \Psi_{jji}/3$, and $\tilde{\psi}_i \equiv \tilde{\Psi}_{ijj}/3$ such that

$$-P = \kappa \varepsilon_V + \psi_i \dot{v}_i, \tag{2.40a}$$

$$\mu_i = \tilde{\psi}_i \dot{\varepsilon}_V + \rho_{ij} v_j. \tag{2.40b}$$

For a passive and reciprocal medium we require $\kappa'' \leq 0$, the requirements on ρ_{ij} do not change, $\tilde{\psi}_i = \psi_i$, and the passivity restrictions on the Willis coupling coefficient are given by

$$\omega \Re\{\varepsilon_V \psi_i'' v_i^*\} \leq -|\varepsilon_V|^2 \kappa'' + v_i^* \rho_{ij}'' v_j. \tag{2.41}$$

Additionally, the limits discussed in Section 2.4.1 still apply.

2.5 Summary

Restrictions on the range of physically meaningful Willis material properties have been derived based on the principles of reciprocity, passivity, and causality. These restrictions are summarized in Table 2.1. Reciprocity leads to minor symmetries of the stiffness and coupling tensors. Passivity leads to restrictions on the imaginary parts of the stiffness and mass density tensors

Table 2.1: Summary of the physical restrictions imposed on Willis material properties. The form of the Willis equations corresponding to the causal coupling coefficient Ψ_{ijk} given here is presented in Eqs. (2.32).

Property	Symbol	Reciprocity	Passive and Reciprocal
Stiffness	C_{ijkl}	$C_{ijkl} = C_{klij}$	$\Im\{C_{ijkl}\} \leq 0$
Mass Density	ρ_{ij}	$\rho_{ij} = \rho_{ji}$	$\Im\{\rho_{ij}\} \geq 0$
Coupling	S_{ijk}, $\tilde{S}_{ijk}$	$\tilde{S}_{ijk} = S_{jki}$	$\Re\{S_{ijk}\}$ bounded
Causal Coupling	$\Psi_{ijk} = \dfrac{S_{ijk}}{-i\omega}$	$\tilde{\Psi}_{ijk} = \Psi_{jki}$	$\Im\{\Psi_{ijk}\}$ bounded

and the real parts of the coupling tensors. Causality results in the Kramers-Krönig equations and relate the dispersion relations of the real and imaginary parts of the material properties. The standard representation of the linear Willis constitutive equations is shown to be acausal, and a potential alternative representation has been presented.

The restrictions derived in this chapter are an excellent check for the homogenization methods presented in Chapter 3. The micromechanical models presented in Chapter 3 and experimentally confirmed in Chapter 4 assume purely passive and reciprocal constituent materials, and so all of the requirements summarized in Table 2.1 should (and do) hold. The homogenization model developed in Chapter 5, on the other hand, is approximate and so reciprocity may not hold in all cases. These results will be discussed in their respective chapters.

Chapter 3

Physical Interpretation of Willis Coupling

Analyses of periodic materials have shown that Willis coupling has at least two physical origins: inherently asymmetric microstructure which is often referred to as local coupling [48, 50] and nonlocal effects associated with multiple scattering [52, 51]. This chapter provides simple models which may be used to obtain some physical understanding of local Willis coupling. The first section presents models which describe Willis coupling arising from inherently asymmetric media, while the second section uses expansions by volume averages of microstructural constitutive equations to obtain the Willis equations. All of these models are presented for one-dimensional systems, and demonstrate that Willis coupling arises from the misalignment of a material's center of mass and its centroid. In addition to providing physical insight, these models may also be used in future unit cell homogenization methods.

3.1 Inherently Asymmetric Media

The first models described here are coupled effective material elements consisting of masses and springs. Then, as a generalization of the mass-spring models, a model is derived where an arbitrary reciprocal two-port network is

used to determine the material properties of a one-dimensional system.

3.1.1 Mass-Spring Models

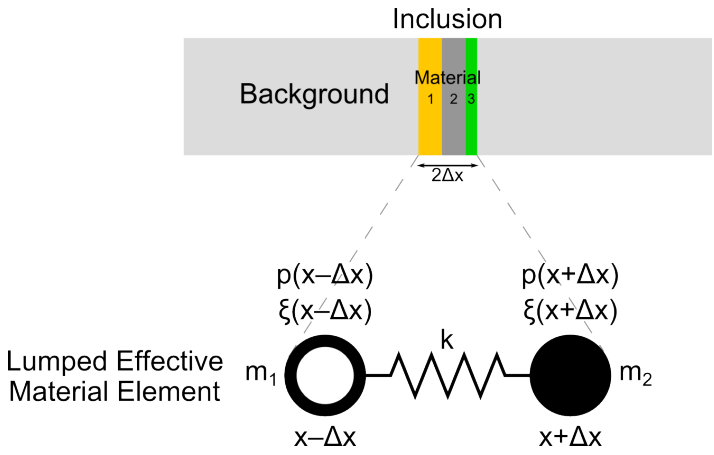

Figure 3.1: Simple asymmetric model of an effective material element, consisting of three material layers (1, 2, and 3) embedded in a background matrix. For long-wavelength excitations, the three-layer inclusion may be modeled as an effective material element with two masses (m_1 at position $x - \Delta x$ and m_2 at position $x + \Delta x$) and a spring with constant k. The pressure p and displacement ξ are evaluated on the boundaries of the element, $x - \Delta x$ and $x + \Delta x$.

Consider an effective material element, such as the layered inclusion in Fig. 3.1, which may be represented in the long-wavelength limit by two unequal lumped masses and a spring between them. Let the first mass be $m_1 = \rho_1 S \Delta x$ at $x - \Delta x$ and the second mass be $m_2 = \rho_2 S \Delta x$ at $x + \Delta x$, and let the spring have a spring constant $k = \kappa / 2\Delta x$. In these expressions, S is the cross-sectional area and Δx is the width of the fluid element.

There are two equations of motion for each of the masses within the

unit cell are given by

$$\rho_1 \Delta x \ddot{\xi}(x - \Delta x) = p(x - \Delta x) - \frac{\kappa}{2\Delta x}(\xi(x - \Delta x) - \xi(x + \Delta x)), \tag{3.1}$$

$$\rho_2 \Delta x \ddot{\xi}(x + \Delta x) = -p(x + \Delta x) + \frac{\kappa}{2\Delta x}(\xi(x - \Delta x) - \xi(x + \Delta x)), \tag{3.2}$$

where $\xi(x)$ is the displacement at the field point x, $p(x)$ is the pressure field, and the over-dots denote a time derivative. These equations may be rearranged to yield the equivalent equations

$$\frac{p(x - \Delta x) - p(x + \Delta x)}{2\Delta x} = \frac{\rho_1}{2}\ddot{\xi}(x - \Delta x) + \frac{\rho_2}{2}\ddot{\xi}(x + \Delta x), \tag{3.3}$$

$$\begin{aligned} -\frac{p(x - \Delta x) + p(x + \Delta x)}{2} = &- \frac{\kappa}{2\Delta x}(\xi(x - \Delta x) - \xi(x + \Delta x)) \\ &- \rho_1 \frac{\Delta x}{2}\ddot{\xi}(x - \Delta x) + \rho_2 \frac{\Delta x}{2}\ddot{\xi}(x + \Delta x). \end{aligned} \tag{3.4}$$

Now, expand each function about the point x and neglect terms $O[\Delta x^2]$:

$$-\frac{\partial}{\partial x}p(x) = \frac{\rho_1 + \rho_2}{2}\ddot{\xi}(x) + \frac{\rho_2 - \rho_1}{2}\Delta x \frac{\partial}{\partial x}\ddot{\xi}(x), \tag{3.5}$$

$$-p(x) = \frac{\rho_2 - \rho_1}{2}\Delta x \ddot{\xi}(x) + \kappa \frac{\partial}{\partial x}\xi(x). \tag{3.6}$$

Since $\partial\xi(x)/\partial x$ is the volume strain $\varepsilon(x)$ and $\dot{\xi}(x)$ is the particle velocity $v(x)$, and noting that $-\partial p(x)/\partial x$ is the time-derivative of the momentum density $\dot{\mu}(x)$ in accordance with the conservation of linear momentum (one-dimensional form of Eq. (1.7)), these equations may be written in the following form (where the explicit x dependence is omitted)

$$\mu = \frac{\rho_1 + \rho_2}{2}v + \frac{\rho_2 - \rho_1}{2}\Delta x \dot{\varepsilon}, \tag{3.7}$$

$$-p = \frac{\rho_2 - \rho_1}{2}\Delta x \dot{v} + \kappa\varepsilon. \tag{3.8}$$

From this form we readily identify the approximate effective density as $\rho = (\rho_1 \Delta x + \rho_2 \Delta x)/2\Delta x$, the effective bulk modulus as κ, and the (reciprocal, passive, and causal) Willis coupling coefficients as $\psi = \tilde{\psi} = \Delta x(\rho_2 - \rho_1)/2$. Thus, the effective constitutive equations for this effective material element are coupled:

$$\mu = \rho v + \tilde{\psi}\dot{\varepsilon}, \tag{3.9}$$

$$-p = \psi \dot{v} + \kappa \varepsilon. \tag{3.10}$$

Note that $k = O[\Delta x^{-1}]$, so the Willis coupling terms are higher-order expansions of the effective constitutive equations Equations (3.9) and (3.10) are the one-dimensional acoustic equivalent of Eqs. (1.8) and (1.9), respectively. Notice that $\tilde{\psi} = \psi$, and so the system satisfies reciprocity.

The physical explanation for the presence of Willis coupling in this simple system is that the centroid of the system is not aligned with the center of mass. For example, if pressure is applied to the effective material element with no pressure gradient, the smaller mass will move farther than the larger mass, while the center of mass remains stationary. The center of mass *has* to remain stationary because the net force applied to the element is zero, but the centroid moves significantly, as one of the boundaries has a significant displacement while the other boundary does not. Similarly, if a net force were applied to the effective material element, again the smaller mass would move farther than the larger mass, and the motion of the center of mass would be as though it contained all of the mass and no spring were present, as required

by basic physics.

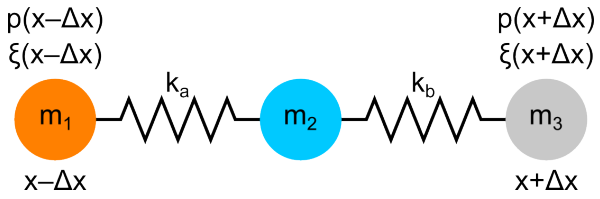

Figure 3.2: Simple asymmetric model of a effective material element, consisting of three potentially unequal masses, m_1 (with equilibrium position $x - \Delta x$), m_2, and m_3 (with equilibrium position $x + \Delta x$), connected by springs, k_a and k_b. three material layers (1, 2, and 3) embedded in a background matrix. The pressure p and displacement ξ are evaluated on the boundaries of the element, $x - \Delta x$ and $x + \Delta x$.

Since Willis coupling may arise from asymmetric mass distribution, as shown above, the natural question is whether it may also arise from asymmetry in the stiffness. To answer this question, consider an effective material element which, in the long-wavelength limit, may be described by three masses and two springs, as shown in Fig. 3.2. As above, the effective material properties are determined by relating the pressure on the boundaries to the motion of the boundaries. For conciseness, define $P_L = p(x - \Delta x)$, $P_R = p(x + \Delta x)$, $x_1 = \xi(x - \Delta x)$, $x_2 = \xi(x + \Delta x)$, and x_2 as the displacement of m_2. Then, Newton's second law for the three masses with time-harmonic motion may be written

$$-\omega^2 m_1 x_1 = P_L - k_a(x_1 - x_2), \tag{3.11}$$

$$-\omega^2 m_2 x_2 = \quad k_a(x_1 - x_2) - k_b(x_2 - x_3), \tag{3.12}$$

$$-\omega^2 m_3 x_3 = \quad k_b(x_2 - x_3) - P_R. \tag{3.13}$$

To simplify the analysis, solve Eq. (3.12) for x_2 and substitute into the other equations. Writing the resultant system of equations matrix form yields

$$\boldsymbol{A}\begin{bmatrix} x_1 \\ x_3 \end{bmatrix} = \begin{bmatrix} -P_L \\ P_R \end{bmatrix}, \tag{3.14}$$

where

$$\boldsymbol{A} = \begin{bmatrix} \omega^2 m_1 - k_a + \frac{k_a^2}{k_a+k_b-\omega^2 m_2} & \frac{k_a k_b}{k_a+k_b-\omega^2 m_2} \\ \frac{k_a k_b}{k_a+k_b-\omega^2 m_2} & \omega^2 m_3 - k_b + \frac{k_b^2}{k_a+k_b-\omega^2 m_2} \end{bmatrix}. \tag{3.15}$$

Now, notice that to $O[\Delta x^2]$ we may write

$$\begin{bmatrix} p(x) \\ \frac{\partial}{\partial x}p(x) \end{bmatrix} = \begin{bmatrix} -\frac{1}{2} & \frac{1}{2} \\ \frac{1}{2\Delta x} & \frac{1}{2\Delta x} \end{bmatrix} \begin{bmatrix} -P_L \\ P_R \end{bmatrix} \equiv \boldsymbol{M}_1 \begin{bmatrix} -P_L \\ P_R \end{bmatrix}, \tag{3.16}$$

$$\begin{bmatrix} \xi(x) \\ \frac{\partial}{\partial x}\xi(x) \end{bmatrix} = \begin{bmatrix} \frac{1}{2} & \frac{1}{2} \\ -\frac{1}{2\Delta x} & \frac{1}{2\Delta x} \end{bmatrix} \begin{bmatrix} x_1 \\ x_3 \end{bmatrix} \equiv \boldsymbol{M}_2 \begin{bmatrix} x_1 \\ x_3 \end{bmatrix}. \tag{3.17}$$

Then we may relate the pressure and its derivative at the centroid of the effective material element to the displacement and its derivative at the centroid through

$$\begin{bmatrix} p(x) \\ \frac{\partial}{\partial x}p(x) \end{bmatrix} = \boldsymbol{M}_1 \boldsymbol{A} \boldsymbol{M}_2^{-1} \begin{bmatrix} \xi(x) \\ \frac{\partial}{\partial x}\xi(x) \end{bmatrix}, \tag{3.18}$$

where we may identify the effective material properties with

$$\boldsymbol{M}_1 \boldsymbol{A} \boldsymbol{M}_2^{-1} \equiv \begin{bmatrix} \omega^2\psi & \kappa \\ \omega^2\rho & \omega^2\tilde{\psi} \end{bmatrix}. \tag{3.19}$$

Explicitly carrying out the matrix multiplications leads to the conclusions

$$\rho = \frac{1}{2\Delta x}\frac{(k_a+k_b)(m_1+m_2+m_3) - m_2\omega^2(m_1+m_3)}{k_a+k_b-m_2\omega^2}, \tag{3.20}$$

$$\kappa = \frac{\Delta x}{2}\frac{4k_a k_b - (k_a+k_b)(m_1+m_2+m_3)\omega^2 + m_4\omega^2(m_1+m_3)}{k_a+k_b-m_2\omega^2}, \tag{3.21}$$

$$\psi = \tilde{\psi} = \frac{m_3-m_1}{2} + \frac{m_2}{2}\frac{k_b-k_a}{k_a+k_b-m_2\omega^2}. \tag{3.22}$$

In the quasi-static limit, where $\omega \to 0$, the material properties are written as the simple and non-trivial expressions

$$\rho|_{\omega\to 0} = \frac{m_1 + m_2 + m_3}{2\Delta x}, \tag{3.23}$$

$$\kappa|_{\omega\to 0} = 2\Delta x \frac{k_a k_b}{k_a + k_b}, \tag{3.24}$$

$$\psi|_{\omega\to 0} = \frac{m_3 - m_1}{2} + \frac{m_2}{2}\frac{k_b - k_a}{k_a + k_b}. \tag{3.25}$$

These expressions reduce to the material properties derived with only two masses if $m_2 \to 0$ and $k = k_a k_b/(k_a + k_b)$. As expected, the density in the quasi-static limit is the total mass divided by the total length and the bulk modulus is the bulk modulus of the two springs in series. The Willis coupling coefficients (again equal as required by reciprocity) may be non-trivial if there is an asymmetric distribution of mass or if there is an asymmetric distribution of stiffness.

The interpretation of Willis coupling as the misalignment of the centroid and center of mass still holds for the three-mass scenario depicted in Fig. 3.2, even for $m_1 = m_3$ where the equilibrium centroid equals the center of mass. For intuition, consider letting $m_1 = m_3 = 0$, $k_a \to 0$, and $k_b \to \infty$. Then, applying an equal force on both sides will result in the motion at $x - \Delta x$ being much greater than at $x + \Delta x$, while the mass m_2 would not move (there are equal forces acting on it). Thus, the asymmetry of the stiffness leads the centroid to move away from the center of mass with equal magnitude forces on the boundaries.

These analyses demonstrate that Willis coupling may arise from even very simple systems. Furthermore, it demonstrates that Willis coupling arises from interpreting the geometric center of a system as the material center.

3.1.2 Transmission Line Model

The mass-spring systems described above are special cases of a more general concept known as a two-port network. Specifically, Fig. 3.1 illustrates a two-port network where access to the system is only available at two points: the masses. Any two-port network may be used to relate the kinematic and dynamic variables at the ports, and if the associated wavelengths are sufficiently long relative to the size of the network, it may also be considered an effective material element. A common way to describe a linear two-port network is to use electrical circuit diagrams describing transmission lines. These circuit diagrams may be used to represent acoustical networks by interpreting the voltage as the pressure, the current as the volume velocity, and the network elements as acoustical impedances. While this approach is most useful for describing more complicated one-dimensional systems, the basic principles used to describe the simple mass-spring-mass system are still the fundamental principles for the transmission line models.

Any linear, reciprocal, time-invariant two-port network may be reduced to a simple T-network of acoustic impedances, as shown in Fig. 3.3. Loading such a T-network by either pressure or volume velocity sources on both sides can be used to estimate the effective material properties, as shown below.

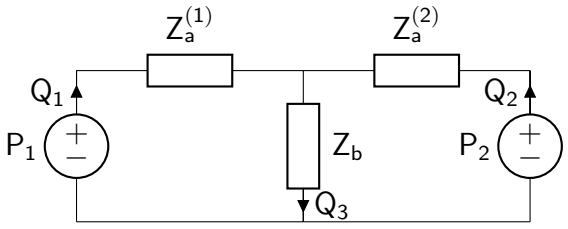

Figure 3.3: The general propagation T-network being driven by two pressure sources.

Defining pressure sources P_1 and P_2 and volume velocities Q_1, Q_2, and Q_3 as shown in Fig. 3.3, the circuit equations may be written in matrix form as

$$\begin{bmatrix} P_1 \\ P_2 \\ 0 \end{bmatrix} = \begin{bmatrix} Z_a^{(1)} & 0 & Z_b \\ 0 & Z_a^{(2)} & Z_b \\ 1 & 1 & -1 \end{bmatrix} \begin{bmatrix} Q_1 \\ Q_2 \\ Q_3 \end{bmatrix} \tag{3.26}$$

or, by incorporating the third equation into the first two,

$$\begin{bmatrix} P_1 \\ P_2 \end{bmatrix} = \begin{bmatrix} Z_a^{(1)} + Z_b & Z_b \\ Z_b & Z_a^{(2)} + Z_b \end{bmatrix} \begin{bmatrix} Q_1 \\ Q_2 \end{bmatrix} \tag{3.27}$$

The goal is to transform these equations into constitutive equations. If the total phase change across the T-network is much less than one, we may approximate the pressure and pressure gradient fields at the geometric center as

$$p(x) \approx \frac{1}{2}\left(p(x-\Delta x) + p(x+\Delta x)\right) = \frac{1}{2}\left(P_1 + P_2\right), \tag{3.28a}$$

$$\frac{\partial}{\partial x}p(x) \approx \frac{1}{2\Delta x}\left(p(x+\Delta x) - p(x-\Delta x)\right) = \frac{1}{2\Delta x}\left(-P_1 + P_2\right). \tag{3.28b}$$

Similarly, the velocity and velocity gradient fields at the geometric center may

be approximated as

$$v(x) \approx \frac{1}{2}\left(v(x-\Delta x)+v(x+\Delta x)\right) = \frac{1}{2S}\left(Q_1 - Q_2\right), \tag{3.29a}$$

$$\frac{\partial}{\partial x}v(x) \approx \frac{1}{2\Delta x}\left(v(x+\Delta x)-v(x-\Delta x)\right) = \frac{1}{V}\left(-Q_1 - Q_2\right), \tag{3.29b}$$

where S is the cross-sectional area and $V = 2S\Delta x$ is the volume of the system. The expressions defined in Eqs. 3.28 and 3.29 represent the average value and average slope of the functions $p(x)$ and $v(x)$ in the material element. Because each domain is assumed to behave as an uncoupled fluid element, the pressure and velocity may then be related through the one-dimensional form of the dynamic equation in Eq. (1.7), $-\partial p/\partial x = \dot{\mu}$, and through the definition of the volume strain rate, $\partial v/\partial x = \dot{\varepsilon}_V$. Then the circuit equations may be transformed to

$$\begin{bmatrix} p \\ -\dot{\mu} \end{bmatrix} = \frac{1}{2}\begin{bmatrix} 1 & 1 \\ -\Delta x^{-1} & \Delta x^{-1} \end{bmatrix}\begin{bmatrix} Z_a^{(1)}+Z_b & Z_b \\ Z_b & Z_a^{(2)}+Z_b \end{bmatrix}\begin{bmatrix} S & -V/2 \\ -S & -V/2 \end{bmatrix}\begin{bmatrix} v \\ \dot{\varepsilon}_V \end{bmatrix}, \tag{3.30}$$

or

$$\begin{bmatrix} -p \\ \dot{\mu} \end{bmatrix} = S\begin{bmatrix} \frac{1}{2}(Z_a^{(2)}-Z_a^{(1)}) & \frac{\Delta x}{2}(Z_a^{(1)}+Z_a^{(2)}+4Z_b) \\ \frac{1}{2\Delta x}(Z_a^{(1)}+Z_a^{(2)}) & \frac{1}{2}(Z_a^{(2)}-Z_a^{(1)}) \end{bmatrix}\begin{bmatrix} v \\ \dot{\varepsilon}_V \end{bmatrix}. \tag{3.31}$$

Since this analysis assumes time-harmonic motion ($e^{-i\omega t}$ convention), we may therefore identify the material properties as

$$\kappa = -i\omega\frac{V}{4}\left(Z_a^{(1)}+Z_a^{(2)}+4Z_b\right), \tag{3.32a}$$

$$\rho = \frac{1}{-i\omega}\frac{S}{2\Delta x}\left(Z_a^{(1)}+Z_a^{(2)}\right), \tag{3.32b}$$

$$\psi = \tilde{\psi} = \frac{1}{-i\omega}\frac{S}{2}\left(Z_a^{(2)}-Z_a^{(1)}\right). \tag{3.32c}$$

As with the mass-spring-mass system, the Willis coupling coefficient determined in this manner is only non-zero for an asymmetric network (i.e., $Z_a^{(1)} \neq Z_a^{(2)}$). Furthermore, since any linear, time-invariant, reciprocal two-port network may be written as a T-network, in one-dimensional systems with no nonlocal interactions the *only* way that a system will demonstrate Willis coupling is because it consists of an asymmetric microstructure.

Since the material elements are assumed to be passive, reciprocal, and causal, the material properties as defined in Eqs. (3.32) should satisfy the requirements of Table 2.1. Passivity in circuit elements is enforced by requiring the real parts of $Z_a^{(1)}$, $Z_a^{(2)}$, and Z_b to be positive. Thus, the modulus consists of positive real quantities V and ω multiplying impedances with positive real parts, all multiplied by $-i$, and so $\Im\{\kappa\} \leq 0$. The mass density is similar except for being divided by $-i$ rather than multiplied, and so $\Im\{\rho\} \geq 0$. Finally, since

$$\frac{2\omega}{S}\left|\Im\{\psi\}\right| = \Re\{Z_a^{(2)} - Z_a^{(1)}\} \leq \Re\{Z_a^{(1)} + Z_a^{(2)}\} = \frac{2\omega\Delta x}{S}\left|\Im\{\rho\}\right|, \qquad (3.33)$$

the Willis coupling coefficient must therefore satisfy the inequality $|\Im\{\psi\}| \leq (L/2)|\Im\{\rho\}|$ and is therefore bounded, as expected from the more general analysis provided in Chapter 2.

An important assumption made during the derivation of the material properties listed in Eqs. (3.32) was that the total phase change across the element is much less than one. In order to understand this assumption, combine the constitutive equations with the dynamic equation to yield the wave

equation for one-dimensional Willis materials:

$$\nabla^2 v - \frac{\kappa}{\rho}\ddot{v} = 0. \tag{3.34}$$

Willis coupling does not explicitly modify the wave equation, so we may conclude that the total phase change across the system may be written as

$$|\theta| = 2\omega\Delta x \left|\sqrt{\frac{\rho}{\kappa}}\right| = i2 \left|1 + \frac{4Z_b}{Z_a^{(1)} + Z_a^{(2)}}\right|^{-1/2} \ll 1, \tag{3.35}$$

which therefore implies

$$4|Z_b| \gg |Z_a^{(1)} + Z_a^{(2)}|. \tag{3.36}$$

For systems of layered standard materials, this condition is satisfied for very low frequencies where $Z_a^{(1)}, Z_a^{(2)} \sim i\omega$ (mass terms) and $Z_b \sim 1/i\omega$ (spring term). In this particular limit, the system may be represented by two equivalent masses connected by a spring, as demonstrated in Section 3.1.1.

Example: Layered Media

One of the benefits of extracting material properties from a transmission line approach is the ease with which it may be extended to layered media. The transmission line for a standard material of length l_i with mass density ρ_i, bulk modulus κ_i and cross-sectional area S_i may be represented in an $ABCD$ matrix form as [77]

$$\begin{bmatrix} P_1 \\ u_1 \end{bmatrix} = \begin{bmatrix} A_i & B_i \\ C_i & D_i \end{bmatrix} \begin{bmatrix} P_2 \\ u_2 \end{bmatrix} = \begin{bmatrix} \cos(k_i l_i) & -iZ_i \sin(k_i l_i) \\ -\frac{i}{Z_i}\sin(k_i l_i) & \cos(k_i l_i) \end{bmatrix} \begin{bmatrix} P_2 \\ u_2 \end{bmatrix}, \tag{3.37}$$

where $k_i = \omega\sqrt{\rho_i/\kappa_i}$ and $Z_i = \sqrt{\kappa_i\rho_i}/S_i$. Then the total $ABCD$ matrix for n layers is simply

$$\begin{bmatrix} A & B \\ C & D \end{bmatrix} = \begin{bmatrix} A_1 & B_1 \\ C_1 & D_1 \end{bmatrix} \begin{bmatrix} A_2 & B_2 \\ C_2 & D_2 \end{bmatrix} \cdots \begin{bmatrix} A_n & B_n \\ C_n & D_n \end{bmatrix}. \tag{3.38}$$

Then this $ABCD$ matrix may be converted to an impedance matrix using the fact that the determinant of each $ABCD$ matrix for the layer is one. The impedance matrix is written as

$$\begin{bmatrix} Z_{11} & Z_{12} \\ Z_{21} & Z_{22} \end{bmatrix} = \frac{1}{C} \begin{bmatrix} A & -1 \\ -1 & D \end{bmatrix}. \tag{3.39}$$

Finally, we may determine the acoustic impedances:

$$Z_a^{(1)} = Z_{11} + Z_{21} = \frac{A-1}{C}, \tag{3.40a}$$

$$Z_a^{(2)} = Z_{21} + Z_{22} = \frac{D-1}{C}, \tag{3.40b}$$

$$Z_b = -Z_{21} = \frac{1}{C}. \tag{3.40c}$$

Thus we may write the material properties as

$$\kappa = -i\omega\frac{V}{4}\frac{A+D+2}{C}, \tag{3.41a}$$

$$\rho = \frac{1}{-i\omega}\frac{S}{L}\frac{A+D-2}{C}, \tag{3.41b}$$

$$\psi = \frac{1}{-i\omega}\frac{S}{2}\frac{D-A}{C}, \tag{3.41c}$$

where $L = \sum_i l_i$ for the heterogeneous multi-layered effective material element.

For a nontrivial example, consider the asymmetric unit cell described by Nemat-Nasser and Srivastava [48]. This unit cell consists of three materials in five slabs. The first and last slabs (material 1) have $\rho_1 = 1000$ kg/m^3 and

$\kappa_1 = 8\times10^{11}$ Pa, the second and fourth slabs (material 2) have $\rho_2 = 300$ kg/m^3 and $\kappa = 3 \times 10^8$ Pa, and the third slab (material 3) has $\rho_3 = 8000$ kg/m^3 and $\kappa_3 = 300 \times 10^{11}$ Pa. The thicknesses of these slabs are, in order, 1.2 mm, 0.3 mm, 0.8 mm, 0.1 mm, and 1.2 mm. The compressibility $\overline{D}$, mass density $\overline{\rho}$, and coupling parameter $\overline{S}_2$ used by Nemat-Nasser and Srivastava are equivalent (at low frequencies) to $1/\kappa$ (the compressibility β), ρ, and $-i\omega\psi/\kappa$, respectively. (In general $\overline{\rho} = \rho - i\omega\psi^2/\kappa$; see Appendix A.) The effective material properties predicted by the present transmission-line model are shown in Fig. 3.4. The present predictions are very similar to the exact material properties derived by Nemat-Nasser and Srivastava for low frequencies (first bandpass) for all three material properties, but above the first bandpass the two predictions differ significantly. Thus, as expected, the transmission line model derived above is best suited for low frequency predictions. This is primarily due to the fact that the transmission line model assumes the element is much smaller than an effective wavelength within the element, which assumption is violated above the first band. Since the present model does not account for nonlocal behavior it does not predict any real component of the Willis coupling terms (the part associated with lattice interactions) while the exact model does.

3.2 Expansion by Averages

Another method by which the effective material properties may be determined is by using expansions by averages, which is described in detail in Appendix B. This method demonstrates that Willis coupling is a natural con-

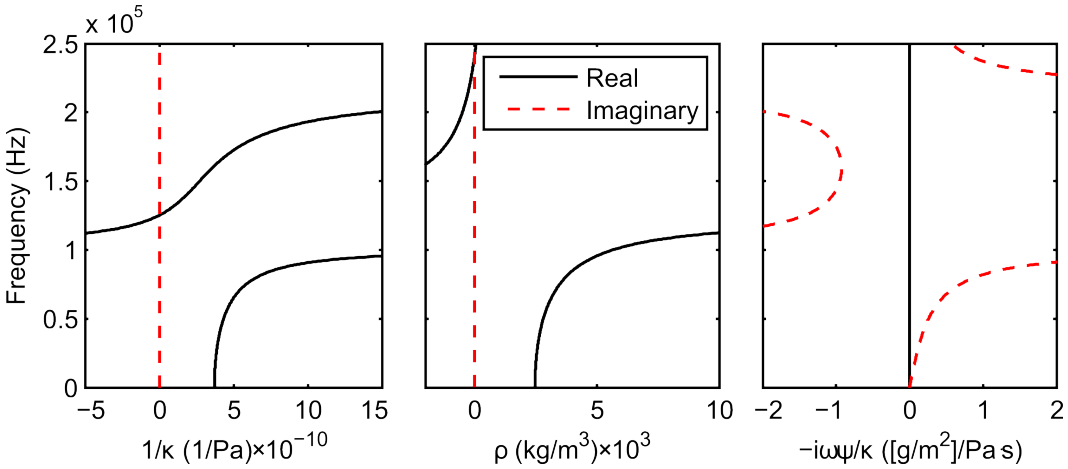

Figure 3.4: Predicted material properties (compressibility $1/\kappa$, mass density ρ, and a coupling coefficient $-i\omega\psi/\kappa$) for the asymmetric unit cell described by Nemat-Nasser and Srivastava [48].

sequence of interpreting the geometric center of a volume element as the center of mass of the element and is thus an artifact of homogenization of asymmetric elements.

Consider the average momentum density in a representative domain Ω:

$$\langle \vec{\mu} \rangle = \langle \rho \vec{v} \rangle = \frac{1}{\Omega} \int_{\Omega} \rho(\vec{x}') \vec{v}(\vec{x}') \, d\vec{x}'. \tag{3.42}$$

If the constituent materials within Ω are fully elastic Willis materials, then the average momentum density is expanded in the more complicated form

$$\langle \vec{\mu} \rangle = \left\langle \boldsymbol{\rho} \cdot \vec{v} + \tilde{\boldsymbol{\Psi}} : \dot{\boldsymbol{\varepsilon}} \right\rangle. \tag{3.43}$$

For simplicity, the analysis presented in this section assumes a one-dimensional system composed of standard materials (i.e., no Willis coupling). These assumptions may not be necessary for finite-element based approaches.

Assume the length of a representative volume element of an inhomogeneous system is $2\Delta x$ such that if the area of the surface normal to the direction of inhomogeneity is S the volume of Ω is $2S\Delta x$. Further assume that largest field wavenumber of interest k is small enough that $k\Delta x \ll 1$. Under these assumptions, the results of Appendix B may be applied to the average momentum density to write

$$\langle \mu \rangle = \frac{1}{2\Delta x}\int_{x-\Delta x}^{x+\Delta x} \mu(x')dx' = \frac{1}{2\Delta x}\int_{x-\Delta x}^{x+\Delta x} \rho(x')v(x')dx' \tag{3.44}$$

$$= \frac{1}{2\Delta x}\int_{x-\Delta x}^{x+\Delta x} \rho(x')\times \left[\langle v\rangle + \left\langle \frac{\partial v}{\partial x}\right\rangle (x'-x) + \frac{1}{2}\left\langle \frac{\partial^2 v}{\partial x^2}\right\rangle \left((x'-x)^2 - \frac{\Delta x^2}{3}\right) + O[(k\Delta x)^3]\right] dx' \tag{3.45}$$

$$= \langle\rho\rangle\langle v\rangle + \langle (x'-x)\rho(x')\rangle \left\langle \frac{\partial v}{\partial x}\right\rangle + \frac{1}{2}\left\langle (x'-x)^2\rho(x')\right\rangle \left\langle \frac{\partial^2 v}{\partial x^2}\right\rangle - \frac{\Delta x^2}{6}\langle\rho\rangle \left\langle \frac{\partial^2 v}{\partial x^2}\right\rangle + O[(k\Delta x)^3], \tag{3.46}$$

where x is the geometric center of the domain and

$$\langle (x'-x)\rho(x')\rangle = \frac{1}{2\Delta x}\int_{x-\Delta x}^{x+\Delta x} (x'-x)\rho(x')dx', \tag{3.47}$$

$$\left\langle (x'-x)^2\rho(x')\right\rangle = \frac{1}{2\Delta x}\int_{x-\Delta x}^{x+\Delta x} (x'-x)^2\rho(x')dx'. \tag{3.48}$$

Again, from Appendix B, the average momentum and the average velocity in Eq. (3.46) may be expanded in terms of the velocity at x such that the

momentum density may be written

$$\begin{aligned}\mu(x)+&\frac{\Delta x^2}{3}\frac{\partial^2}{\partial x^2}\mu(x)+O[(k\Delta x)^3]\\ &=\langle\rho\rangle v(x)+\langle(x'-x)\rho(x')\rangle\frac{\partial}{\partial x}v(x)\\ &\quad+\frac{1}{2}\left\langle(x'-x)^2\rho(x')\right\rangle\frac{\partial^2}{\partial x^2}v(x)+\frac{\Delta x^2}{6}\langle\rho\rangle\frac{\partial^2}{\partial x^2}v(x)+O[(k\Delta x)^3].\end{aligned} \tag{3.49}$$

Note that $\mu(x)=\langle\rho\rangle v(x)+O[k\Delta x]$. Then, substituting this expression into the second term on the left of Eq. (3.49) and simplifying yields

$$\begin{aligned}\mu(x)=&\langle\rho\rangle v(x)+\langle(x'-x)\rho(x')\rangle\frac{\partial}{\partial x}v(x)\\ &+\frac{1}{2}\left[\left\langle(x'-x)^2\rho(x')\right\rangle-\frac{\Delta x^2}{3}\langle\rho\rangle\right]\frac{\partial^2}{\partial x^2}v(x)+O[(k\Delta x)^3].\end{aligned} \tag{3.50}$$

Thus, to $O[(k\Delta x)^2]$ and assuming all relevant fields may be treated as continuous, the average fields are related in the same way as the fields at the geometric center. Recognizing $\partial v(x)/\partial x$ as $\dot{\varepsilon}(x)$ in one dimensional systems, the momentum density may then be written as

$$\mu(x)=\langle\rho\rangle v(x)+\langle(x'-x)\rho(x')\rangle\,\dot{\varepsilon}(x)+O[(k\Delta x)^2]. \tag{3.51}$$

From Eq. (3.51), the effective density and Willis coupling coefficient may be identified as $\langle\rho\rangle$ and $\langle(x'-x)\rho(x')\rangle$, respectively, to $O[(k\Delta x)^3]$. It is interesting to note that if the material properties also varied smoothly, the momentum density may have been further simplified to

$$\mu(x)=\langle\rho\rangle v(x)+\frac{\Delta x^2}{3}\left\langle\frac{\partial\rho}{\partial x}\right\rangle\dot{\varepsilon}(x)+O\left[(k\Delta x)^3\right]. \tag{3.52}$$

In this form, the dependence of the Willis coupling on the asymmetry of the system becomes apparent through the presence of the average density gradient.

The average strain may be treated in a similar way. The average strain may be written as

$$\langle \varepsilon \rangle = \langle -\beta p \rangle = -\frac{1}{2\Delta x} \int_{x-\Delta x}^{x+\Delta x} \beta(x') p(x') dx', \tag{3.53}$$

where $\beta(x)$ is the microscopic compressibility. This is the exact same form as Eq. (3.44), and so the same conclusions may be made:

$$\varepsilon(x) = -\langle \beta \rangle p(x) + \langle (x' - x)\beta(x') \rangle \frac{\partial}{\partial x} p(x) + O[(k\Delta x)^2]. \tag{3.54}$$

Newton's second law for the finite volume element may be written $-\langle \partial p/\partial x \rangle = \langle \dot{\mu} \rangle$, or, expanding the pressure and momentum density fields, $-\partial p/\partial x = \dot{\mu} + O[(k\Delta x)^2]$, and so the second term on the right-hand side of Eq. (3.54) may be substituted to yield

$$\varepsilon(x) = -\langle \beta \rangle p(x) + \langle (x' - x)\beta(x') \rangle \langle \rho \rangle \dot{v}(x) + O[(k\Delta x)^2], \tag{3.55}$$

where the additional terms in the momentum density are all higher order. This equation may then be rearranged to give an expression for the pressure in terms of kinematic quantities:

$$-p(x) = \frac{1}{\langle \beta \rangle} \varepsilon(x) - \frac{\langle (x' - x)\beta(x') \rangle}{\langle \beta \rangle} \langle \rho \rangle \dot{v}(x) + O[(k\Delta x)^2]. \tag{3.56}$$

Thus, the constitutive equations derived by assuming the momentum density is the total momentum over the volume element divided by its volume and the

average strain is the total strain of the element may then be written as

$$\mu = \rho^{\text{eff}} v + \tilde{\psi}^{\text{eff}} \dot{\varepsilon} + O[(k\Delta x)^2], \tag{3.57a}$$

$$-p = \kappa^{\text{eff}} \varepsilon + \psi^{\text{eff}} \dot{v} + O[(k\Delta x)^2], \tag{3.57b}$$

where the x dependence has been suppressed and the effective material properties are given by

$$\rho^{\text{eff}} = \langle \rho \rangle, \tag{3.58a}$$

$$\kappa^{\text{eff}} = \frac{1}{\langle \beta \rangle}, \tag{3.58b}$$

$$\psi^{\text{eff}} = \langle (x' - x)\rho(x') \rangle, \tag{3.58c}$$

$$\tilde{\psi}^{\text{eff}} = -\frac{\langle (x' - x)\beta(x') \rangle}{\langle \beta \rangle} \langle \rho \rangle . \tag{3.58d}$$

Notice that Willis coupling is only manifest, i.e., the Willis coupling coefficients are nonzero, if the mass density or compressibility is not even about the centroid of the element, as predicted by multiple authors [48, 50]. It should be further noted, however, that these other authors did not provide long-wavelength approximations, nor did they provide any physical explanation for the presence of Willis coupling in asymmetric effective material elements. Thus, the derivation and explanations given here provide a much more intuitive guide to design a strongly coupled effective material element in the long-wavelength limit.

For linear, reciprocal systems the expressions for $\tilde{\psi}$ and ψ in Eq. (3.58) must be equivalent. While not a full proof, this may be shown to be the case for ideal adiabatic gases at uniform ambient temperature with low density

contrast. The compressibility of a one-dimensional material may be defined as

$$\beta \equiv \left[\rho \frac{\partial P}{\partial \rho}\right], \tag{3.59}$$

where P is the total pressure. By assuming the material is adiabatic, the pressure may be related the density by

$$P\rho^{-\gamma} = \text{constant}, \tag{3.60}$$

where γ is the adiabatic gas constant. Thus, the compressibility may be written as

$$\beta = \left[\rho\left(\gamma \frac{P}{\rho}\right)\right]^{-1} = \frac{1}{\gamma P} = \frac{1}{\rho}\frac{1}{\gamma RT}, \tag{3.61}$$

where the last equality comes from the ideal gas law in the form $P = \rho RT$ with the gas constant R and absolute temperature T. If all constituent parts of the material are at the same temperature, then we may write

$$\tilde{\psi}^{\text{eff}} = -\left\langle \frac{x' - x}{\rho(x')} \right\rangle \frac{\langle \rho \rangle}{\langle 1/\rho \rangle}. \tag{3.62}$$

Now, since the system is required to have low density contrast, we may write $\rho(x') = \langle \rho \rangle (1 + \epsilon \tilde{\rho}(x')/\langle \rho \rangle)$, where $\epsilon \ll 1$ and $\langle \rho' \rangle = 0$. The function $\rho'(x')$ represents the variation of the mass density about the mean of the system. Then we may write

$$\left\langle \frac{1}{\rho} \right\rangle = \left\langle \frac{1}{\langle \rho \rangle}\left[1 + \epsilon \frac{\tilde{\rho}(x')}{\langle \rho \rangle}\right]^{-1} \right\rangle \tag{3.63}$$

$$= \left\langle \frac{1}{\langle \rho \rangle}\left(1 - \epsilon \frac{\tilde{\rho}(x')}{\langle \rho \rangle} + \epsilon^2 \frac{\tilde{\rho}^2(x')}{\langle \rho \rangle^2} + O[\epsilon^3]\right) \right\rangle \tag{3.64}$$

$$= \frac{1}{\langle \rho \rangle} + \epsilon^2 \frac{\langle \tilde{\rho}^2 \rangle}{\langle \rho \rangle^3} + O[\epsilon^3], \tag{3.65}$$

and

$$\left\langle \frac{x'-x}{\rho(x')} \right\rangle = \left\langle \frac{x'-x}{\langle\rho\rangle} \left[1+\epsilon\frac{\tilde{\rho}(x')}{\langle\rho\rangle}\right]^{-1} \right\rangle \tag{3.66}$$

$$= \left\langle \frac{x'-x}{\langle\rho\rangle} \left(1-\epsilon\frac{\tilde{\rho}(x')}{\langle\rho\rangle}+\epsilon^2\frac{\tilde{\rho}^2(x')}{\langle\rho\rangle^2}+O[\epsilon^3]\right) \right\rangle \tag{3.67}$$

$$= -\epsilon\frac{\langle(x'-x)\tilde{\rho}(x')\rangle}{\langle\rho\rangle^2}+\epsilon^2\frac{\langle(x'-x)\tilde{\rho}^2(x')\rangle}{\langle\rho\rangle^3}+O[\epsilon^3], \tag{3.68}$$

or, substituting back in for $\tilde{\rho}$ in the first term on the right,

$$\left\langle \frac{x'-x}{\rho} \right\rangle = \frac{1}{\langle\rho\rangle}\left\langle (x'-x)\left[1-\frac{\rho}{\langle\rho\rangle}\right]\right\rangle+\epsilon^2\frac{\langle(x'-x)\tilde{\rho}^2(x')\rangle}{\langle\rho\rangle^3}+O[\epsilon^3] \tag{3.69}$$

$$= -\frac{\langle(x'-x)\rho(x')\rangle}{\langle\rho\rangle^2}+\epsilon^2\frac{\langle(x'-x)\tilde{\rho}^2(x')\rangle}{\langle\rho\rangle^3}+O[\epsilon^3]. \tag{3.70}$$

Thus, to leading order in ϵ, we may write

$$\tilde{\psi}^{\text{eff}} = \frac{\langle(x'-x)\rho(x')\rangle}{\langle\rho\rangle^2}\frac{\langle\rho\rangle}{1/\langle\rho\rangle} = \langle(x'-x)\rho(x')\rangle = \psi^{\text{eff}}. \tag{3.71}$$

Thus, the Willis coupling coefficients given in Eqs. (3.58) are reciprocal for systems of ideal adiabatic gases with low mass-density contrast at uniform ambient temperature. In addition, we find that for systems with low mass-density contrast Willis coupling is $O[\epsilon]$.

Equations 3.58 provide a useful physical interpretation of the Willis coupling coefficients. They suggest that if a strongly coupled material element is desired, it should be designed to have strong asymmetry of the mass density. This approach is implemented for the physical sample considered in Chapter 4. However, Eqs. (3.58) do not provide a practical method for experimental demonstration of Willis coupling because the microstructure and

microstructural fields of a sample are rarely accessible. An alternative approach for purely mechanical systems known or known to possess structural asymmetry is to assume that the Willis equations of the form of Eqs. (3.57) and volume average:

$$\langle \mu \rangle = \rho^{\text{eff}} \langle v \rangle + \tilde{\psi}^{\text{eff}} \langle \dot{\varepsilon} \rangle, \tag{3.72a}$$

$$-\langle p \rangle = \kappa^{\text{eff}} \langle \varepsilon \rangle + \psi^{\text{eff}} \langle \dot{v} \rangle. \tag{3.72b}$$

As was the case in Section 3.1, the volume averaged field quantities are directly related to their values on the boundaries, and so knowledge of the motion and dynamics on the boundaries is sufficient to determine the effective material properties. Actually, in the long-wavelength limit, where this analysis method is applicable, the average field quantities in Eqs. (3.72) are equivalent to the definitions provided in Eqs. (3.28) and (3.29), and so Eqs. (3.72) are equivalent to Eq. (3.31). This method also underlies the reflection-transmission measurement method described in Chapter 4, and is likely to lead to a useful homogenization method for future finite-element analyses.

3.3 Conclusions

Simple mechanical models have been used to verify that Willis coupling arises from inherent asymmetry in the microstructure of a material. The two-mass one-spring system and the three-mass two-spring system demonstrated that Willis coupling arising from asymmetry of the constituent materials may be considered the result of an element's center of mass being misaligned with

the centroid. Additionally, the mass-spring systems and their generalization, the transmission-line model, provide a way to determine the effective material properties of a one-dimensional layered element. Interestingly, the generality of the transmission-line model demonstrated that local Willis coupling may *only* arise from microstructural asymmetry in one-dimensional purely mechanical media. Note that there may be additional mechanisms which generate Willis coupling in higher dimensions. The idea that Willis coupling comes from a misalignment of the center of mass and centroid was then reinforced by expanding the definitions of the average momentum density and the average strain. This interpretation is the basis for the design of the material sample considered in Chapter 4 All of these results are also consistent with the requirements of a reciprocal system.

Chapter 4

Experimental Evidence of One-Dimensional Willis Coupling

Experimental confirmation usually provides the most compelling evidence for a theory, and such is the case for the theory developed in Chapter 3. Furthermore, experimental methods allow one to characterize some complicated systems which are difficult to describe analytically. One method by which the material properties may be determined in terms of measured scattering parameters is presented and validated in this chapter.

The first section in this chapter describes a method by which material properties may be extracted from experimentally obtained data. This method is a generalization of the extraction technique described by Fokin, *et al.* [78], and extends the approach to account for Willis coupling. The second section describes a plane wave tube-based experiment used to infer the material properties of an effective material element using the above-mentioned method, and also describes the effective material element developed for this purpose. The final section compares the theoretical predictions of the material properties based on the analyses presented in Chapter 3 with the inferred values.

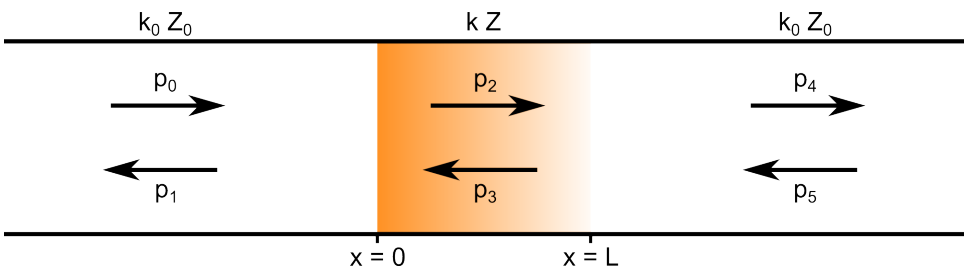

Figure 4.1: Schematic of a three-medium reflection-transmission problem.

4.1 Experimental Determination of Willis Properties

Consider a plane wave tube experiment consisting of a background material (usually air) with density and bulk modulus ρ_0 and κ_0, respectively, and an effective material element with density, bulk modulus, and Willis coupling coefficients ρ, κ, and $\tilde{\psi} = \psi$, respectively (see Fig. 4.1 for a schematic representation). The motion in the effective material element is determined by combining the Willis constitutive relations in Eqs. (3.9) and (3.10) with the dynamic equation $-\partial p/\partial x = \dot{\mu}$ to give the equation

$$\kappa \frac{\partial \varepsilon}{\partial x} + \psi \frac{\partial \dot{v}}{\partial x} = \psi \ddot{\varepsilon} + \rho \dot{v}. \tag{4.1}$$

Since in one dimension $\partial \dot{v}/\partial x = \ddot{\varepsilon}$, Eq. (4.1) reduces to the wave equation for particle velocity of a standard material. Therefore, the wavenumber of the effective material element is given by the standard dispersion relation $k^2 = \omega^2 \rho/\kappa$. The impedance, however, is not the same as a standard material. The specific acoustic impedance of the effective material element may be written as

$$Z \equiv \frac{p}{v} = -\frac{\kappa \varepsilon + \psi \dot{v}}{v}. \tag{4.2}$$

For a time-harmonic system with a propagating wave in the $\pm x$ direction, such that $v = v_0 e^{\pm ikx}$, the strain may be written as $\varepsilon = \nabla v/(-i\omega) = \mp kv/\omega = \mp v\sqrt{\rho/\kappa}$. For such a wave, the specific acoustic impedance may be written

$$Z^{\pm} = -i\omega\psi \pm \sqrt{\kappa\rho} = \sqrt{\kappa\rho}\left[i\frac{\omega\psi}{\sqrt{\kappa\rho}} \pm 1\right] \equiv Z[iW \pm 1], \tag{4.3}$$

where $Z = \sqrt{\kappa\rho}$ is the "uncoupled specific acoustic impedance" and $W = \omega\psi/Z$ is a non-dimensional number which indicates the importance of Willis coupling in the specific acoustic impedance. Notice that the sign of the iW term does not change with propagation direction, and is therefore a manifestation of the asymmetric nature of a Willis material. This geometric asymmetry can lead to directionally-dependent reflection coefficients, as demonstrated below.

Using the impedance relation given in Eq. (4.3), the pressure field from a propagating velocity field may be written

$$p = Z^{\pm} v = Z[iW \pm 1] v_0 e^{\pm ikx}, \tag{4.4}$$

where v_0 is the particle velocity amplitude. Therefore, a strictly forward (backward) propagating velocity wave in a one-dimensional Willis material is accompanied by a strictly forward (backward) propagating pressure wave, just as is the case for a standard material. The relative phase of the pressure and velocity waves in a Willis material are not the same for different propagation directions, however, which is not the same as for a standard material. For example, the phase of a forward propagating wave at $x = 0$ with $v_0 \in \mathbb{R}$ is

$\theta^+ = \tan^{-1} W$, while for a backward propagating wave is $\theta^- = \pi - \tan^{-1} W$ instead of $\pi + \tan^{-1} W$, as would be the case for a standard material.

Since any time-harmonic one-dimensional linear acoustic field may be decomposed into the sum of a forward and backward propagating wave, the pressure and particle velocity in the entire system may be written as

$$p = \begin{cases} p_0 e^{ik_0 x} + p_1 e^{-ik_0 x} & x < 0 \\ p_2 e^{ikx} + p_3 e^{-ikx} & 0 < x < L \\ p_4 e^{ik_0(x-L)} + p_0 e^{-ik_0(x-L)} & x > L \end{cases}, \tag{4.5}$$

and

$$v = \begin{cases} \frac{p_0}{Z_0^+} e^{ik_0 x} + \frac{p_1}{Z_0^-} e^{-ik_0 x} & x < 0 \\ \frac{p_2}{Z^+} e^{ikx} + \frac{p_3}{Z^-} e^{-ik_0 x} & 0 < x < L \\ \frac{p_4}{Z_0^+} e^{ik_0(x-L)} + \frac{p_0}{Z_0^-} e^{-ik_0(x-L)} & x > L \end{cases}, \tag{4.6}$$

where p_0, p_1, etc. are the forward and backward propagating waves depicted in Fig. (4.1). If the there is no backscatter from a termination such that $p_5 = 0$, then the reflection coefficient $R \equiv p_1/p_0$ is the scattering coefficient S_{11} and the transmission coefficient $T \equiv p_4/p_0$ is the scattering coefficient S_{21}. (If there is backscatter the scattering coefficients may be determined using the methods described in Appendix C; once the scattering coefficients are known, proceed as presented here.) In this case, continuity of pressure and particle velocity at $x = 0$ and $x = L$ lead to the four equations

$$\begin{bmatrix} 1 & -1 & -1 & 0 \\ \frac{1}{Z_0^+} & -\frac{1}{Z^+} & -\frac{1}{Z^-} & 0 \\ 0 & e^{ikL} & e^{-ikL} & -1 \\ 0 & \frac{e^{ikL}}{Z^+} & \frac{e^{-ikL}}{Z^-} & -\frac{1}{Z_0^+} \end{bmatrix} \begin{bmatrix} S_{11} \\ p_2/p_0 \\ p_3/p_0 \\ S_{21} \end{bmatrix} = \begin{bmatrix} -1 \\ -\frac{1}{Z_0^+} \\ 0 \\ 0 \end{bmatrix}. \tag{4.7}$$

Solving these equations for the reflection and transmission coefficients S_{11} and S_{21} yields

$$S_{11} = \frac{(Z/Z_0)^2(1+W^2) - 1 + 2iW(Z/Z_0)}{(Z/Z_0)^2(1+W^2) + 1 + 2i(Z/Z_0)\cot kL}, \tag{4.8}$$

$$S_{21} = \frac{2iZZ_0 \csc kL}{Z^2(1+W^2) + Z_0^2 + 2iZZ_0 \cot kL}. \tag{4.9}$$

Since S_{11} and S_{21} may be measured (see Appendix C), Eqs. (4.8) and (4.9) constitute two equations with three unknowns: Z, k and W, and so one more independent equation is necessary. Consider a second experiment where the material orientation is inverted (or, equivalently, where the source is moved to the opposite side). This "backward" experiment will yield information for the scattering coefficients S_{12} and S_{22} rather than S_{11} and S_{21}. The setup of the problem is the same except $W \to -W$ because ψ changes sign with orientation inversion. Thus, the transmission coefficient remains the same so $S_{12} = S_{21}$ (as required by reciprocity), but the reflection coefficient is written

$$S_{22} = \frac{Z^2(1+W^2) - Z_0^2 - 2iWZZ_0}{Z^2(1+W^2) + Z_0^2 + 2iZZ_0 \cot kL}. \tag{4.10}$$

With this third equation, we may invert for each of the three unknowns:

$$k = \pm\frac{1}{L}\cos^{-1}\left(\frac{1 - S_{11}S_{22} + S_{12}^2}{2S_{12}}\right) \mp \frac{2\pi m}{L}, \tag{4.11}$$

$$W = \pm\frac{S_{22} - S_{11}}{\sqrt{4S_{12}^2 - (1 - S_{11}S_{22} + S_{12}^2)^2}}, \tag{4.12}$$

$$Z = \pm\frac{Z_0}{\sqrt{1+W^2}}\sqrt{\frac{(1+S_{11})(1+S_{22}) - S_{12}^2}{(1-S_{11})(1-S_{22}) - S_{12}^2}}, \tag{4.13}$$

where m is the number of full wavelengths within the material. As discussed by Fokin, *et al.* [78], the signs of Z and k are not independent of each other.

The choice of sign for Z and k are dictated by the fact that for a passive system the real part of Z must be positive. Following the method used by Fokin, *et al.*, the effective impedance and wavenumber may be written as

$$Z = \frac{Z_0 r}{(1 - S_{11})(1 - S_{22}) - S_{12}^2}, \tag{4.14}$$

$$k = \frac{i \log(x)}{L} + \frac{2\pi m}{L} \tag{4.15}$$

where

$$r = \pm\sqrt{(1 - S_{11}S_{22} + S_{12}^2)^2 - 4S_{12}^2}, \tag{4.16}$$

$$x = \frac{1 - S_{11}S_{22} + S_{12}^2 + r}{2S_{12}}. \tag{4.17}$$

The sign of r is chosen such that the real part of Z is positive. Finally, W is written as

$$W = \pm\frac{S_{22} - S_{11}}{ir}. \tag{4.18}$$

The sign of the Willis number is positive in the quasi-static limit, and is determined at higher frequencies by requiring W be a continuous function of frequency. The material properties are then found using

$$\kappa = \frac{Z\omega}{k}, \qquad \rho = \frac{Zk}{\omega}, \qquad \psi = \frac{WZ}{\omega}. \tag{4.19}$$

Thus, the properties of a one-dimensional effective material element may be determined from knowledge of the scattering coefficients using Eqs. (4.14)-(4.19). The following section discusses an experimental apparatus used to determine scattering coefficients.

4.2 Experimental Apparatus

A plane wave impedance tube-based experiment was designed and used to demonstrate the method to experimentally determine material properties described in the previous section (see Fig. 4.2 for a schematic description). The plane wave impedance tube, shown in Fig. 4.3, was a BSWA SW477 impedance tube with the tube extension. This 30-mm-diameter tube has a source built into one side, four microphone ports, and a sample staging area. A custom built anechoic termination was used, and consisted of a foam plug followed by a layered foam wedge. The plug came with the purchase of the impedance tube, and the wedge was constructed of adhesive-backed foam sheets, stacked and manually cut into the shape of a cone. The absorption coefficient of the termination was measured to be above 0.95 throughout the frequency range of interest, which is 1–2 kHz (see Fig 4.4).

Measurements were made using a DataPhysics Quatro system and the associated software SignalCalc. A source signal, $V_0(t)$, consisting of a swept sine wave from 500–2000 Hz over 5.2 s (0.195 Hz spectral resolution, decimated to 48.8 Hz in post-processing) was generated using SignalCalc and sent to the DataPhysics Quatro output port. The source signal was then split with a BNC T-splitter and sent to the built-in source of the impedance tube and to an input port of the DataPhysics Quatro, thus allowing measurement of the signal received by the source to be used as a reference signal. Another input port of the DataPhysics Quatro was used to power and acquire the signal from the microphone. The microphone (see Fig. 4.3 for a picture) was a

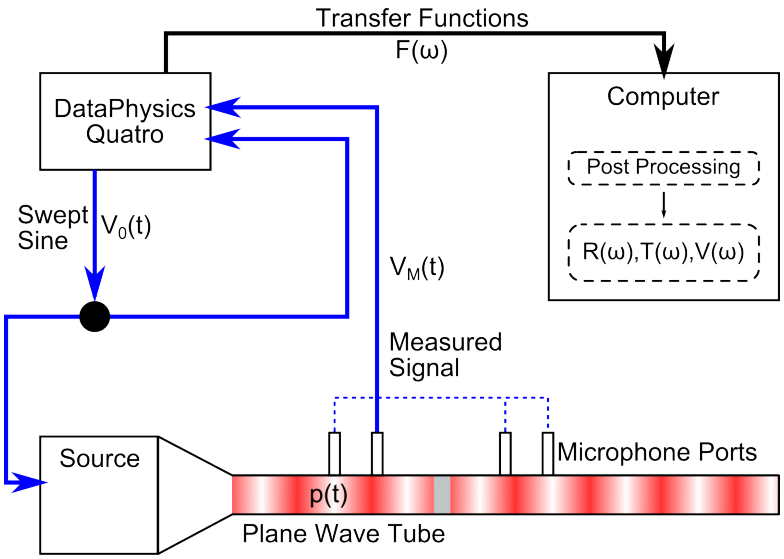

Figure 4.2: Schematic of the experimental apparatus. A voltage signal, $V_0(t)$, is generated by the DataPhysics Quatro system, and split using a BNC T-splitter into a source signal, and a reference signal. The source signal is transformed into an acoustic pressure signal $p(t)$ by the transducer built into the plane wave tube. A microphone is used to measure the propagated pressure signal and convert it to another voltage signal, $V_M(t)$, which is then recorded by the DataPhysics Quatro. The DataPhysics Quatro exports the transfer function $F(\omega)$ between the reference and measured voltage signals to a computer for storage. This process is repeated with the microphone in each of the four microphone ports. The resultant four transfer functions are then post-processed to calculate the reflection, transmission, and backscatter coefficients, $R(\omega)$, $T(\omega)$, and $V(\omega)$, respectively.

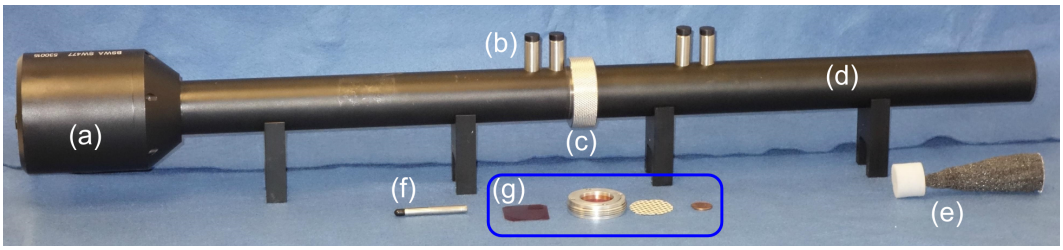

Figure 4.3: Picture of the plane wave impedance tube used for measurements of the effective material element. The tube consists of (a) a built-in source, (b) microphone ports, (c) a sample stage, and (d) a tube extension with additional microphone ports. The tube extension was terminated anechoically using (e) a foam plug and a foam wedge. A single microphone (f) was used to measure the acoustic pressure within the plane wave tube. The effective material element used in the experiment (g) is shown in greater detail in Fig. 4.5.

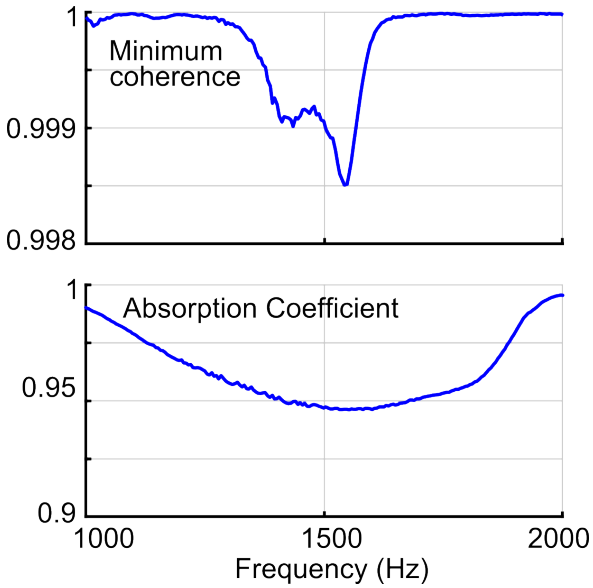

Figure 4.4: Minimum coherence of experiments used in the analyses presented here and anechoic termination absorption coefficient as a function of frequency.

PCB 6.3 mm (1/4 inch) pressure microphone. Due to the measurement technique implemented [79], no calibration was needed, although the microphone was implicitly assumed to have a time-invariant sensitivity on the time-scale of the experiment. For each measurement the microphone was placed in a microphone port and plastic plugs that came with the purchase of the plane wave tube were used in the other three ports. Twenty averages were used, measuring the signal from 0 to 10 kHz. The coherence in the frequency range of interest was consistently greater than 0.9985 for all measurements discussed here (see Fig 4.4).

A custom-built sample holder was built for these experiments (see Fig. 4.5). The holder consists of three aluminum rings with an inner diameter of 30 mm to match the impedance tube. The central and largest component is threaded to be perfectly centered in the sample stage of the impedance tube. The two side components are used to uniformly clamp thin layers of material samples to the outside edge of the central component using steel screws. There is a slight circular depression on the sides of the central ring, as well as a slight circular embossing on the side rings, used to position the sample layers. The width of the central ring is approximately 5.9 mm, and the width of the fully assembled holder (with the sample layers described below in place) is 12.7 mm ($\pm$0.2 mm). The central ring of the sample holder acts as an air-cavity, thus allowing for measurement of a three-medium effective material element consisting of two thin, but arbitrary, layers bordering a 5.9-mm-thick layer of air. The side rings of the sample holder are treated as extensions of the plane

wave tube and do not contribute to the overall length of the effective material element. Therefore, using the sample layers described below, the length of the effective material element is approximately 6.0 mm.

The material layers used for the experiments described here are (see Fig. 4.5(a) for pictures) a 0.125-mm-thick membrane (DuPont^{TM} Kapton$^{®}$ FPC, Young's modulus $E = 2.758$ GPa, Poisson ratio $\nu = 0.34$, and mass density $\rho = 1420$ kg/m^3; property values provided by manufacturer) and a 0.45-mm-thick perforated sheet of electrical insulating paper (Copaco), where the perforations were 3.1 mm diameter circles creating a surface void fraction of about 0.24. The membrane was cut a little large for the central ring depression and squeezed into place with the side ring in order to impose a small amount of tension on the membrane. The tension was used to ensure the membrane did not buckle and to reduce the effects of nonlinearity in the measurements. As mentioned above, the two sample layers were separated by a 5.9-mm-thick layer of air with a total volume of 4.2×10^{-6} m^3. The air is assumed to have a wave-speed of 343 m/s and a mass density of 1.201 kg/m^3.

Since the effective material element is asymmetric, its orientation within the plane wave tube is important. The "forward" orientation is defined as having the membrane closest to the source, and the "backward" orientation is defined as having the perforated paper closest to the source. These orientations are shown schematically in Fig. 4.6. A single-microphone-based technique was used to determine the reflection and transmission coefficients for both orientations [79]. The reflection and transmission coefficients determined were the

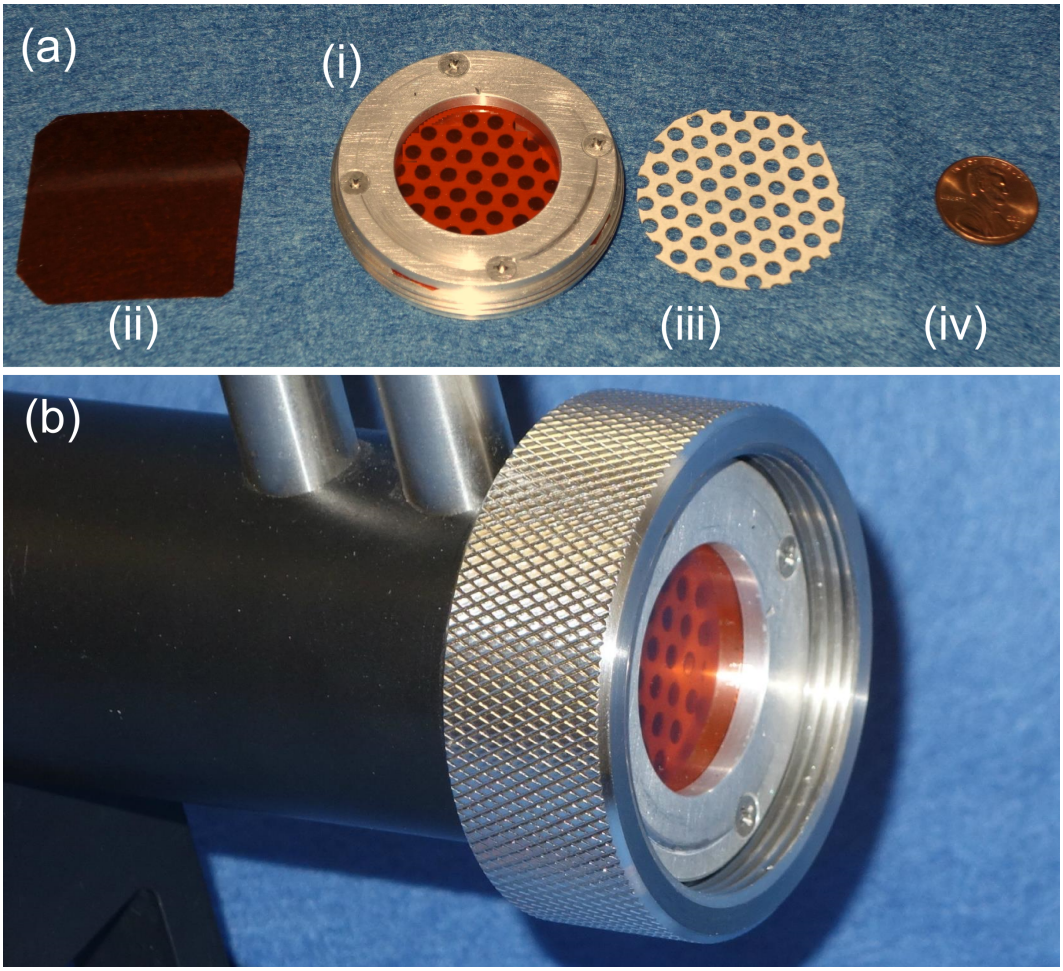

Figure 4.5: (a) Picture of (i) the threaded aluminum component holder with material layers used in the experiments inserted, (ii) sample of 0.125-mm-thick Kapton® membrane, (iii) sample of 0.45-mm-thick perforated electrical insulating paper (Copaco), and (iv) penny for scale. (b) Picture of component holder inserted into the impedance tube.

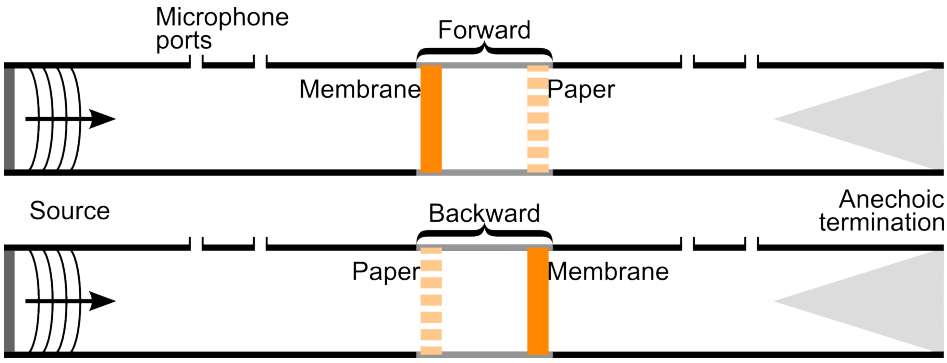

Figure 4.6: Schematic of the experimental apparatus with the effective material element described in the text and shown in Fig. 4.7 in the forward and reverse orientations.

reflection at the source-side edge of the effective material element, $R(\omega)$, the transmission coefficient at the termination-side edge of the effective material element, $T(\omega)$, and the reflection coefficient at the termination-side edge of the effective material element (which is non-zero due to the imperfect nature of the anechoic termination), $V(\omega)$. These reflection and transmission coefficients were then used to determine the four coefficients of the scattering matrix of the effective material element, S_{11}, S_{12}, S_{21}, and S_{22}. The details of determining the scattering coefficients from the measured signals are presented in Appendix C. Once the scattering coefficients are determined, Eqs. (4.14)-(4.19) may be used to determine the properties of the effective material element.

4.3 Theoretical Prediction of Effective Material Properties

As described above, the effective material element consists of a membrane element, and air cavity, and a perforated sheet of paper. In order to use the theoretical development from Chapter 3 to predict the effective material properties, a model of the microstructure must be developed and the average kinematics and dynamics determined. Since smallest wavelength of interest (17 cm in air) is much larger than the width of the effective material element, a lumped-element description of the system is appropriate. The membrane may be modeled as a mass, M_m, with springs, k_m, that represent both the bending stiffness and the in-plane tension. The cavity is well represented by a spring k_a. Finally, the holes dominate the acoustic response of the perforated paper, and may be modeled as a mass M_p which is the air mass being pushed through the holes. These elements are shown schematically in Fig. 4.7.

Acoustic energy may also be lost in the motion of this system. For example, viscous drag of the air through the holes in the paper lead to a loss of acoustic energy, and there may be losses associated with the bending of the membrane. The losses associated with the bending of the membrane may be easily accommodated by allowing k_m be complex. The losses associated with the perforated paper are accommodated by including a frequency-dependent imaginary-valued spring constant $\tilde{k}_h$.

Due to the relative simplicity of the effective material element, one may determine the values of the spring constants and masses used to model

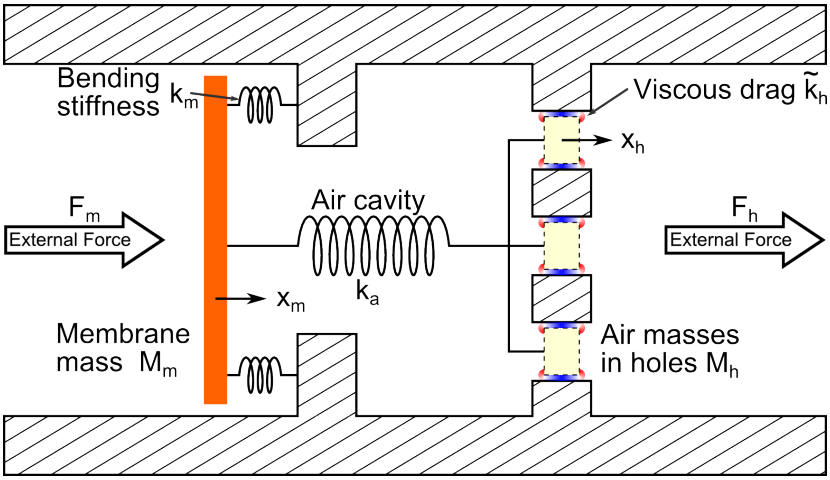

Figure 4.7: Mechanical schematic of the dominating properties of the components of the effective material element.

the element using the material properties and dimensions of the membrane, air cavity, and air-filled holes in the perforated sheet. The work of Bongard, *et al.* provides a detailed model for the membrane mass, $M_m = 1.8830\rho_m hS$, and stiffness, $k_m = a^4/(192SD)$, where ρ_m is the membrane density, h is the membrane thickness, a is the membrane radius, $S = \pi a^2$ is the surface area, and $D = Eh^3/12(1-\nu^2)$ [80]. For the effective material element considered here, these become $M_m = 0.23$ g and $k_m = 27.1$ kN/m. While the Bongard model of a membrane provides reasonable results (see, for example, Fig. 4.8), it does not account for tension or pre-stress in the membrane or for any losses. The quality of model-predicted behavior of the element is only as good as the material property inputs to the model. Since the effects of the membrane tension and losses on the values of M_m and k_m are not known, an alternative approach to determining these parameters is to infer them from the measured

data. The real and imaginary parts of M_m and k_m may be inferred from measurements of the effective mass density and then used for comparison with the other effective material properties, as discussed more fully below. The movement of air in the holes in the perforated paper dominate the response of that component of the asymmetric element at low frequencies. The perforated paper may therefore be modeled as the mass of the air in the holes plus the mass of the entrained fluid near them. The expression for the effective mass of this component of the effective material element is $M_h = \rho_{\text{air}} S(h + \Delta h) = 5.5 \times 10^{-3}$ g, where ρ_{air} is the mass density of air and $\Delta h = 16a/3\pi$ is excess length to account for the entrained air [5]. The viscous losses associate with the air motion in the pores was derived by Morse and Ingard to be $\tilde{k}_h \approx -i \ln(a/h) S \sqrt{2\rho\omega^3\mu_v}/4$, where μ_v is the coefficient of viscosity [81], or for the present case, $\tilde{k}_h \approx -i1.56(f/1000)^{3/2}$ N/m, where f is assumed to be in Hz. Finally, in the long wavelength limit the air cavity is dominated by its compressibility, and may be modeled as a spring with stiffness $k_a = S\rho_{\text{air}} c_{\text{air}}^2 = 16.8$ kN/m, where c_{air} is the sound speed in air [5]. Table 4.1 summarizes the values of the spring constants and masses discussed above, as well as the values inferred from the measured data (described below).

Given the mechanical model of the effective material element element given above, the positions of the boundary masses satisfy the equations

$$M_m \frac{\partial^2 x_m}{\partial t^2} = F_m - k_a(x_m - x_h) - k_m x_m, \tag{4.20a}$$

$$M_h \frac{\partial^2 x_h}{\partial t^2} = F_h + k_a(x_m - x_h) - \tilde{k}_h x_h, \tag{4.20b}$$

Table 4.1: Summary of the values of the spring constants and masses used in the mechanical model shown in Fig. 4.7. Two sets of values are presented for the membrane properties, one based on the material properties published by the manufacturer and a clamped-plate model, and one inferred from the measured effective mass density values. The inferred values are presented in square brackets. The properties of the cavity and the perforated paper are derived assuming standard conditions for air, with a wave speed of 343 m/s and a mass density of 1.201 kg/m^3. Frequencies are assumed to be in Hz.

Property	**Symbol**	**Membrane**
Mass	M_m	0.23 g [0.16 g]
Stiffness	k_m	27.1 kN/m $\left[19.3 - i1.5\left(\frac{f}{1000}\right)^{-3/2}\ \text{kN/m}\right]$
		Cavity
Mass	–	–
Stiffness	k_a	16.8 kN/m
		Perforated Paper
Mass	M_h	5.5×10^{-3} g
Stiffness	k_h	$-i1.56\left(\frac{f}{1000}\right)^{3/2}$ N/m

where x_m and x_h are the displacements of the membrane and the air masses in the holes of the paper, respectively, and F_m and F_h are the external forces acting on the membrane and air masses, respectively (see the schematic in Fig. 4.7). Assuming time harmonic motion with angular frequency ω, these equations may be written as the matrix equation

$$\begin{bmatrix} F_m \\ F_h \end{bmatrix} = \begin{bmatrix} k_m + k_a - \omega^2 M_m & -k_a \\ -k_a & \tilde{k}_h + k_a - \omega^2 M_h \end{bmatrix} \begin{bmatrix} x_m \\ x_h \end{bmatrix}. \tag{4.21}$$

This equation may be transformed into a matrix equation for the average force per volume $\langle f \rangle$ and average pressure $\langle p \rangle$ in terms of the average particle velocity $\langle v \rangle$ and and average strain $\langle \varepsilon \rangle$. These average quantities may be defined in matrix form as

$$\begin{bmatrix} \langle f \rangle \\ -\langle p \rangle \end{bmatrix} = \begin{bmatrix} 1/V & 1/V \\ -1/2S & 1/2S \end{bmatrix} \begin{bmatrix} F_m \\ F_h \end{bmatrix}, \tag{4.22a}$$

$$\begin{bmatrix} \langle v \rangle \\ \langle \varepsilon \rangle \end{bmatrix} = \begin{bmatrix} -1/2i\omega & -1/2i\omega \\ -1/L & 1/L \end{bmatrix} \begin{bmatrix} x_m \\ x_h \end{bmatrix}. \tag{4.22b}$$

Using these relations and the results from Section 3.2, Eq. (4.21) may be written as

$$\begin{aligned} \begin{bmatrix} \langle f \rangle \\ -\langle p \rangle \end{bmatrix} = \begin{bmatrix} 1/V & 1/V \\ -1/2S & 1/2S \end{bmatrix} \begin{bmatrix} k_m + k_a - \omega^2 M_m & -k_a \\ -k_a & \tilde{k}_h + k_a - \omega^2 M_h \end{bmatrix} \\ \times \begin{bmatrix} -1/2i\omega & -1/2i\omega \\ -1/L & 1/L \end{bmatrix}^{-1} \begin{bmatrix} \langle v \rangle \\ \langle \varepsilon \rangle \end{bmatrix}, \end{aligned} \tag{4.23}$$

or

$$\langle f \rangle = \rho^{\text{eff}} \langle v \rangle + \tilde{\psi}^{\text{eff}} \langle \dot{\varepsilon} \rangle, \tag{4.24a}$$

$$-\langle p \rangle = \kappa^{\text{eff}} \langle \varepsilon \rangle + \psi^{\text{eff}} \langle \dot{v} \rangle, \tag{4.24b}$$

where the effective material properties are

$$\rho^{\text{eff}} = -\frac{k_m + k_h}{\omega^2 V} + \frac{M_m + M_h}{V}, \tag{4.25a}$$

$$\kappa^{\text{eff}} = \frac{L}{4S}(k_m + \tilde{k}_h + 4k_a) - \frac{\omega^2 L}{4S}(M_m + M_h), \tag{4.25b}$$

$$\psi^{\text{eff}} = \tilde{\psi}^{\text{eff}} = \frac{k_m - \tilde{k}_h}{\omega^2 2S} - \frac{M_m - M_h}{2S}. \tag{4.25c}$$

As expected from reciprocity, the two Willis coupling coefficients are equal. The experimentally inferred material properties may be compared with these independently obtained theoretical predictions.

4.4 Comparison of Experimentally and Theoretically Predicted Properties

The three experimentally inferred material properties and the non-dimensional number W are presented in Fig. 4.8, along with the prediction associated with the simple model described above using the Bongard model to describe the membrane (labeled "Analytical Membrane" in the figure) and using the measured effective density to infer the membrane properties (labeled "Inferred Membrane" in the figure). The values of M_m and the real part of k_m for the "Inferred Membrane" approach are determined by fitting the model in Eqs. (4.24) and (4.25) to the real part of the effective density calculated from the experimental data at $f = 1$ kHz and at the density zero-crossing, which occurs at approximately 1713 Hz. The imaginary part of k_M is determined by fitting the model to the imaginary part of the effective density calculated from the experimental data at 1 kHz and assuming the imaginary part of the

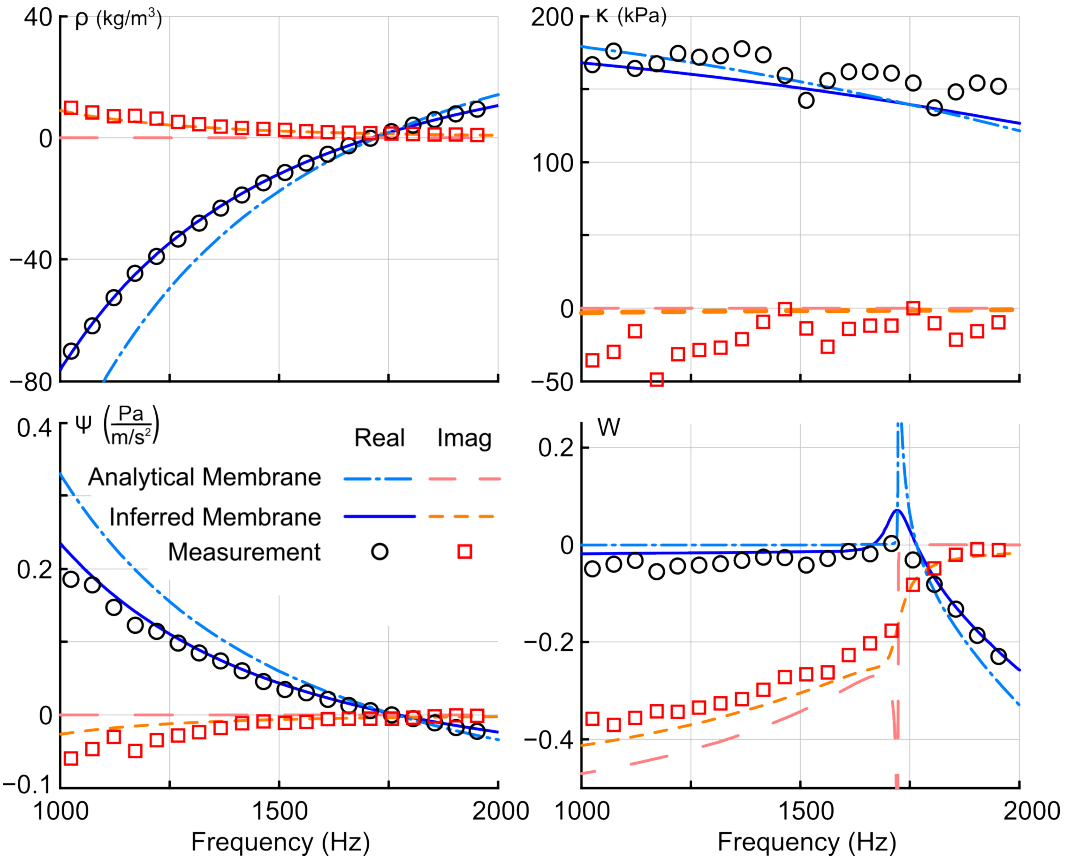

Figure 4.8: Effective bulk modulus κ, mass density ρ, Willis coupling coefficient ψ, and non-dimensional number W extracted from the asymmetric element and measurements described in the text (real part: circles; imaginary part: squares). Two different predictions of the behavior of the effective material element are shown based on the mechanical model developed in this work. One uses the analytical approach of Bongard for the membrane properties with vendor-supplied material properties for the membrane materials and the dimensions used in the experimental setup (real part: dot-dashed lines; imaginary part: long dashed lines). The second is obtained by inferring the membrane parameters from the measured effective density values (real part: solid lines; imaginary part: dashed lines) at 1 kHz and the frequency of zero effective density to get improved estimates of the effective behavior using the same mechanical model.

density follows an $\omega^{-7/2}$ dependence (as observed in the data). For these fits, the model parameters become $M_m = 0.16$ g and $k_m = (19.3 - i1.5[f/1000]^{-3/2})$ kN/m, where the frequency f is assumed to be in Hz. The losses associated with the bending of the membrane dominate the losses of the heterogeneous element and may be treated as the only lossy component, since the other primary contributor to loss is the viscous losses associated with air flow through the perforated plate, which is estimated to contribute less than 1% of the losses of the membrane. The fact that the values of the fit parameters which were estimated from the experimentally obtained data are of the same order of magnitude as the values given by the membrane model advanced by Bongard, *et al.* gives high confidence that the model that uses experimentally obtained data to estimate the values of the lumped-parameter membrane element is a good estimate of the as-built asymmetric effective material element.

For all four quantities shown in Fig. 4.8, the "Inferred Membrane" predicted and measurement-extracted material properties exhibit very similar behavior. The predicted and extracted effective density values are very similar at all frequencies shown despite the model only being fit at two frequencies. The real part of the density is nearly -80 kg/m^3 near 1000 Hz, increases smoothly to zero around 1713 Hz, and continues on to positive values. The imaginary part of the effective density is about 9 kg/m^3 at 1000 Hz and decreases with frequency nearly as $\omega^{-7/2}$. The imaginary parts of the stiffness are negative and relatively close to zero (greater than -50 kPa) for the entire frequency range inspected, while the real parts are positive and around 150

kPa. The measurement data show relatively minor variations that do not appear in the model predictions. The oscillations occur roughly every 330 Hz, which corresponds to a wavelength in air of about 1.0 m or 1.3 impedance tube lengths and may be the result of a resonance of the entire experimental apparatus. Another possible source of these oscillations is that the stiffness may be especially sensitive to errors associated with measurements near pressure nodes, which are present due to the standing-wave nature of the system. These variations also appear to a lesser extent in the extracted values of ψ and W. The real parts of the Willis coupling coefficient are about 0.2 Pa/(m/s^2) at 1000 Hz and decay smoothly as a function of frequency and displaying a zero-crossing at approximately 1773 Hz. The imaginary parts are about -0.5 Pa/(m/s^2) at 1000 Hz and rise asymptotically toward zero. The real part of the non-dimensional quantity W is nearly zero for frequencies less than about 1720 Hz and then decreases nearly linearly to -0.25 by 2000 Hz, while the imaginary part is about -0.4 at 1000 Hz, increases slowly to about -0.2 by 1720 Hz, and then shows a rapid increase approaching 0 with increasing frequency. It is notable that the quantity W appears to demonstrate a behavior analogous to that of a damped resonator, with the real part peaking at the "resonance frequency" of approximately 1720 Hz. Indeed, if the lossy behavior of k_m is neglected, the predicted values of W go through a pole at 1724 Hz.

The values of W presented in Fig. 4.8 clearly demonstrate that Willis coupling must be accounted for when calculating the effective specific acoustic impedance of this material element. For example, at 2 kHz the spe-

cific acoustic impedance in the forward direction is predicted to be $Z = (1.2 - i0.26)$ kPa/(m/s), and in the backward direction is predicted to be $Z_B = (-1.1 - i0.33)$ kPa/(m/s), which has a phase approximately 29° greater than $-Z$. Figure 4.9 presents a plot of the specific acoustic impedance in the forward and backward directions as a function of frequency. Throughout the frequency range presented, the magnitude or the phase of the specific acoustic impedance depends noticeably on the direction of propagation. This effect was seen by Bradley in the study of periodic media with asymmetric unit cells, though he did not interpret his findings in terms of effective material properties [82]. In particular, the splitting of the real part of the impedance found in Fig. 4.9 is also seen in the first band of Fig. 8 in Ref. [82]. The agreement of the two theoretical predictions with the experimentally obtained effective properties then strongly suggests that this system exhibits non-trivial Willis coupling. Thus, despite the fact that Willis coupling may be termed a "higher-order effect", it is clearly important in this case.

Two brief comments should be made on the interpretation of the effective properties of this simple element as material properties. The first is in regards to element size and the validity of the effective medium approximation. One of the primary requirements of using homogenization methods to approximate a heterogeneous structure as an effective material is that the wavelength in the medium be much larger than a representative volume element, or $k_{\text{eff}}L \ll 1$. The predicted and measured effective wavenumber times the effective material element length are shown in Fig. 4.9, as well as for the

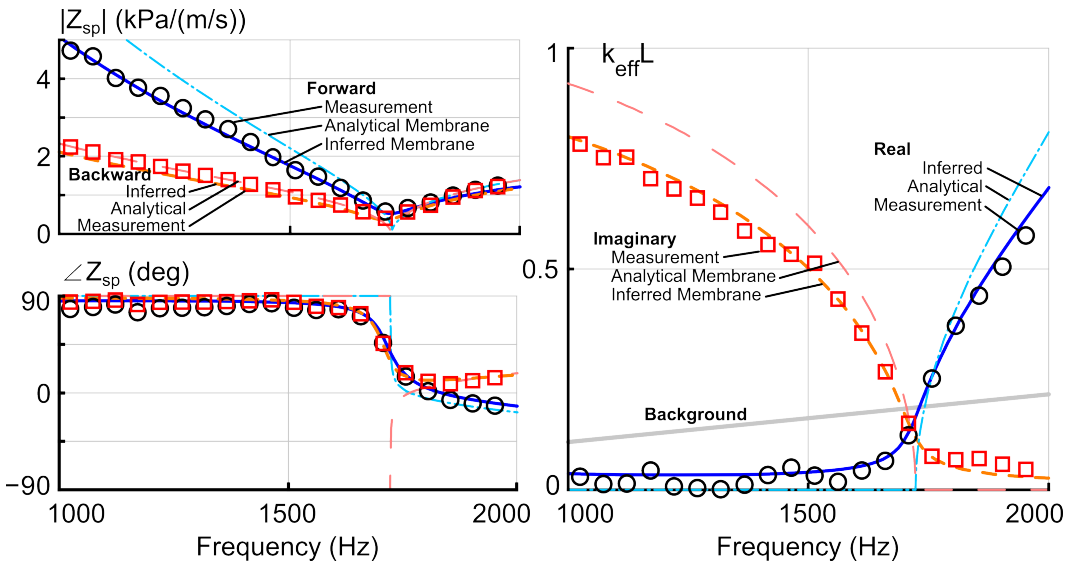

Figure 4.9: Measured and predicted (using the analytical membrane properties and the measurement-inferred membrane properties) values of the effective wavenumber times the length of the effective material element described in the main text (5.9 mm) and the specific acoustic impedance of the effective material element in the forward (membrane-cavity-pores) and backward (pores-cavity-membrane) directions.

background medium (air). All of the values of $k_{\text{eff}}L$ and k_0L are less than one throughout the frequency range of interest, and are much less than one near the density zero-crossing around 1730 Hz. Therefore, the effective wavelength is long enough when compared to the effective material element length to be considered a representative material element. It is interesting to note that below 1730 Hz the wavenumber is almost completely imaginary, and so no wave propagation occurs within the element at low frequencies. The second important comment about this measurement and model is in regards to the inability to measure the response of an effective material composed of an infinite number of these elements from the single element that has been measured. First, because the measurement was made on a single volume element, any nonlocal interactions that would take place in a material composed of large numbers of these elements are clearly omitted by both the model and measurement presented here. Thus, it is likely that placing two or more of these effective material elements in series would lead to a different set of effective properties, which is contrary to the concept of a material. Indeed, it has been shown that many unit cells are necessary for a system to be a material [83]. On the other hand, if several of these elements were dispersed randomly within some matrix as inclusions, the macroscopic material properties of this metamaterial would be determined by a (weighted) average of the matrix properties and the effective inclusion material properties, which is the approach taken in Chapter 5. Then, in the sense of an isolated inclusion, the properties derived above may be treated as the effective material properties.

4.5 Effects of Neglecting Willis Coupling

It is instructive to analyze the material properties extracted using conventional methods which do not account for the inherent asymmetry of the effective material element. This analysis may be performed following the approach developed by Fokin, *et al.* [78], which the extraction technique described above reduces to in the limit of symmetric effective material elements, or $S_{22} = S_{11}$. Since this extraction technique only allows for a single reflection and transmission coefficient, each orientation of a effective material element with asymmetric microstructure will yield different reflection coefficients and thus differing estimates for the extracted material properties. The extracted bulk modulus and mass density for the forward orientation (membrane-cavity-pores; see Fig. 4.6) and the inverted orientation (pores-cavity-membrane) of the effective material element described above using the approach by Fokin, *et al.* are presented in Fig. 4.10. Since this approach tacitly assumes symmetry, there are no extracted values for the Willis coupling coefficient or the associated non-dimensional parameter W.

As may be seen in Fig. 4.10, the two orientations of the effective material element yield noticeably different material properties. The bulk modulus, in particular, shows remarkably different overall trends for both the real and imaginary parts for the different orientations. The bulk modulus in the backward orientation has a similar trend to the properties extracted when the effects of Willis coupling are taken into account, though the values of the real part are lower than the values presented in Fig. 4.8. The bulk modulus in the

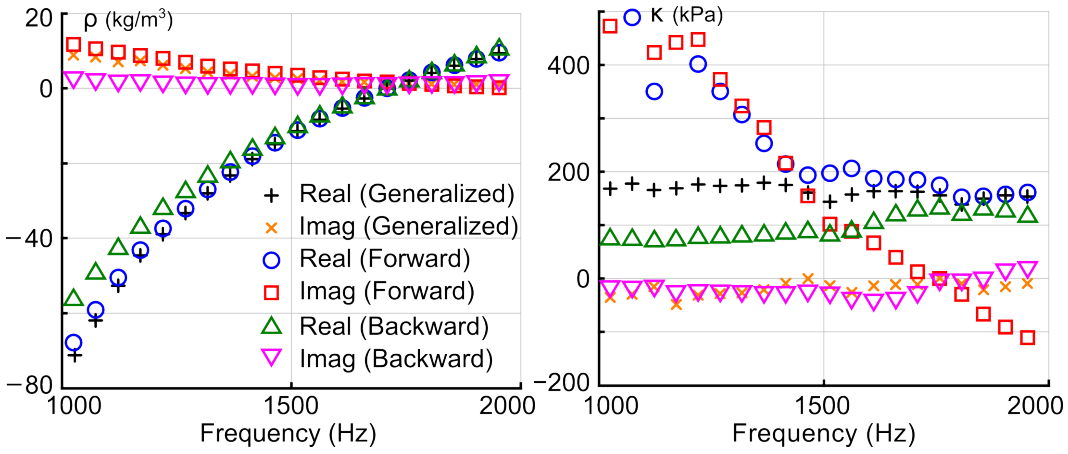

Figure 4.10: Effective density and bulk modulus inferred from the effective material element described in the main text using the approach of Fokin, *et al* [78]. using (1) the forward measurement and (2) the backward measurement (see Fig. 4.6 for a schematic). The effective properties inferred using the generalized Fokin method described in the text and presented in Fig. 4.8 is also provided for comparison.

forward orientation, however, exhibits a completely different frequency dependence, with nearly linearly decreasing real and imaginary parts as a function of increasing frequency from 1000 Hz to approximately 1400 Hz. For that case, the real part levels out around 150 kPa for higher frequencies and the imaginary part continues to decrease. Notice, in particular, that the imaginary part of the bulk modulus changes sign at approximately 1758 Hz, which is inconsistent with the fact that all constituent materials are reciprocal and passive, as discussed in Section 2.2.3. The imaginary part of the bulk modulus in the backward orientation also changes sign at this frequency, though the magnitudes are close enough to zero that this may be experimental error. This demonstration of unphysical material properties through the breaking of

passivity is typical of published effective material properties where microstructural asymmetry is present but not accounted for [78, 84, 85].

The inconsistency of the extracted material properties using the two effective material element orientations and the fact that the imaginary part of the bulk modulus changes sign in a passive, reciprocal system suggest that the extraction method of Fokin, *et al.* is not appropriate for effective material elements with asymmetric microstructures. The extraction process described in this paper, which is an extension of the method of Fokin, *et al.* to account for Willis coupling, requires measurements in both orientations and results in material properties which are consistent with requirements of a passive, reciprocal system. The method developed here is therefore a more appropriate extraction method for effective material elements with subwavelength asymmetric structure as illustrated by the simple example provided in this work. It should be noted that this generalized extraction technique is also valid for symmetric microstructures; homogenization of symmetric effective material elements will simply result in $W = 0$ within experimental error.

4.6 Conclusions and Perspectives

Theoretical and experimental means for determining the effective material properties of a effective material element exhibiting Willis coupling have been derived and implemented. The model predictions agree very well with the experimentally extracted material property values. Furthermore, the effective material properties extracted using a conventional method that does

not account for microstructural asymmetry leads to inconsistent and unphysical results, strengthening the conclusion that Willis coupling is important to account for in the measured effective material element.

While the homogenization methods presented in Chapter 3 and here do indeed yield effective material properties, the systems they describe cannot be accurately described as "materials". As discussed in Chapter 1, a material is a system where the largest length scale associated with the microstructure is much smaller than the smallest length scale of interest. Since the homogenization methods discussed are concerned only with a single material element, the smallest length scale of interest *is* the largest length scale of the microstructure. If a "material" is desired, details of how the material element interacts with the surrounding elements (or how it does not interact with them) must be included. This is the topic taken up in Chapter 5.

Chapter 5

Prediction of Macroscopic Willis Properties

The homogenization theory of Chapters 3 and 4 is focused on extracting the material properties of a single unit rather than extracting bulk material properties. As mentioned in Chapter 1, published bulk homogenization methods have been restricted to periodic media [48, 50, 51]. These homogenization methods are not appropriate to describe the important class of composite materials consisting of randomly distributed inhomogeneities within a matrix material. An alternative homogenization approach that is appropriate for describing three-dimensional composites consisting of materials with known properties is presented in this chapter.

The structure of this chapter is as follows. Section 5.1 presents a derivation of the homogenization technique, and the associated approximations are explicitly stated. In particular, the important approximation of long-wavelength in an elastic host material relative to the size of inhomogeneities embedded within is presented and discussed. Under this approximation homogenization for arbitrarily anisotropic and dynamic ellipsoidal inhomogeneities may be performed analytically up to a double integral, which may be easily calculated numerically. The resultant effective properties take

the form of a coupled constitutive equation, as described by Milton and Willis [59]. Finally, the dilute homogenization technique is extended to higher inhomogeneity volume fractions by employing differential effective medium methods. In Section 5.2 the utility and limits of the homogenization method is demonstrated with several examples, and compared with published methods where applicable. Section 5.3 summarizes the findings and draws conclusions about the utility of the model.

5.1 Theoretical Development

This section covers the mathematical foundations and approximations of the homogenization technique employed in this work. A brief qualitative overview of the technique is first presented, followed by a rigorous derivation. Whenever an approximation is made in the derivation, a discussion of the physical interpretation and the limits for which the approximation is valid is given.

5.1.1 Qualitative Description

The goal of this homogenization method is to estimate the effective properties of very general elastic metamaterials consisting of inhomogeneities embedded randomly within an elastic matrix material. The resulting model predicts the effective properties of materials with arbitrarily ellipsoidal inhomogeneities that may demonstrate sub-wavelength dynamic behavior which may yield effective frequency dependent stiffness, density, and Willis coupling

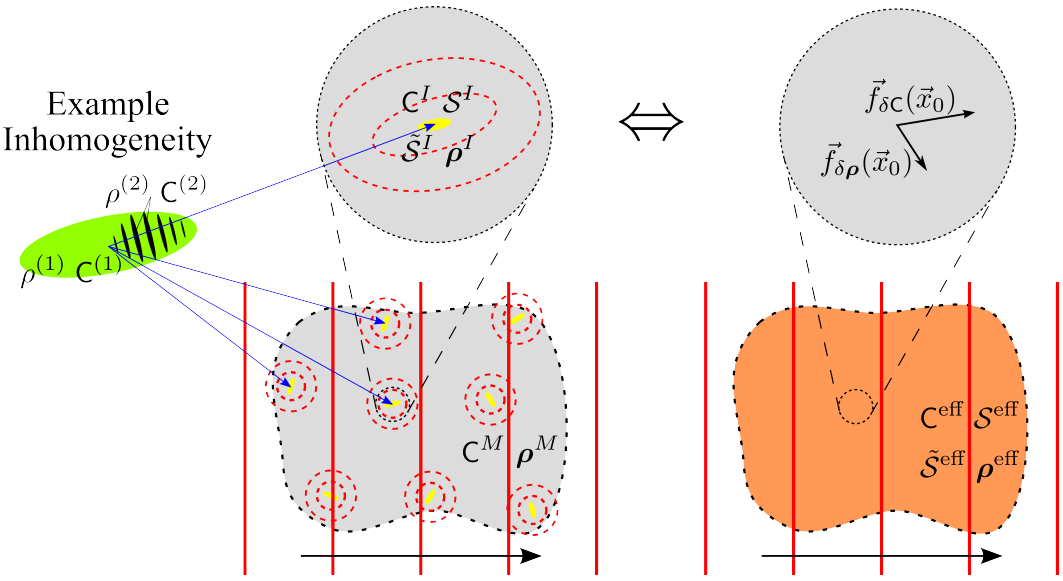

Figure 5.1: A schematic of the homogenization method. The scattered field (red dashed lines) from the inhomogeneities (yellow ellipses) due to an incident field (red solid lines) may be considered point sources in a matrix (gray background). Effective material properties are obtained by matching the resulting strain and velocity fields with the global wave propagation at each frequency. The inhomogeneities and matrix may display frequency dependent stiffness, density, and Willis coupling parameters. These frequency dependent properties are assumed to be the result of homogenized dynamic structure on the scale of the inclusion which is schematized by the figure on the left, though this homogenization is not provided in this work.

on the microscale (which is the metamaterial approximation). In the present approach, the inhomogeneities may be treated as body force sources within the homogeneous matrix material when subjected to external stimulus. The magnitude of those body force sources is shown to be proportional to the material property contrast between the inhomogeneity and the host material. If the inhomogeneities are very small and well separated relative to a wavelength,

the volume averaged fields within the inhomogeneities and the volume fraction of the heterogeneities are sufficient to describe their effect on the macroscopic field quantities. Using well-established micromechanical methods [35], the variation of the strain and velocity fields due to the presence of inhomogeneities may be fully described using a Green's function based on the matrix material properties and the geometry of the inhomogeneities. Comparing the resulting strain and velocity fields with a coupled constitutive equation allows effective material properties to be identified. A schematic of the homogenization approach is shown in Fig. 5.1. It should be noted that the inhomogeneities may themselves be heterogeneous media in order to generate frequency-dependent effective microscale properties, but these effective properties will not be derived in this document. While the initial development given here assumes there is only one kind of inhomogeneity with a single geometric orientation, these results are extended to more higher volume fractions using a differential effective medium theory [33].

While the homogenization technique derived below is only approximate it is very general, and provides the first homogenization method to allow for the estimation of the effective properties of random heterogeneous media displaying macroscopic Willis coupling. Previous homogenization models which account for Willis coupling rely on periodic lattices and have only been demonstrated for one-dimensional systems [48, 49, 86, 50], and to the authors' knowledge no numerical homogenization schemes to address random media displaying this type of coupling have been developed. The present method

permits the homogenization of fully three-dimensional elastic systems of randomly distributed arbitrarily ellipsoidal inhomogeneities which is valuable for the future design of acoustic and elastic metamaterials.

5.1.2 Dynamic Response of Heterogeneous Materials

As presented in Chapter 1 (Eq. (1.7), repeated for convenience), the fully three-dimensional dynamic equation of linear elasticity (neglecting body forces) may be written as

$$\nabla \cdot \boldsymbol{\sigma} = \dot{\vec{\mu}}. \tag{5.1}$$

where $\boldsymbol{\sigma}$ is the Cauchy stress and $\vec{\mu}$ is the momentum density. These equations describe the material response to an imposed deformation or traction and must be supplemented with constitutive equations. In order to account for Willis coupling in either the inhomogeneities or in the matrix, the Willis equations from Eq. (1.8) and (1.9),

$$\boldsymbol{\sigma} = \mathsf{C} : \boldsymbol{\varepsilon} + \mathcal{S} \cdot \dot{\vec{u}} \qquad \text{and} \qquad \vec{\mu} = \tilde{\mathcal{S}} : \boldsymbol{\varepsilon} + \boldsymbol{\rho} \cdot \dot{\vec{u}}, \tag{5.2}$$

are the constitutive equations of choice. Note that these equations are not the causal form of the Willis constitutive equations. In the case of this derivation it is more convenient to use this form, and since time-harmonic signals are assumed at the outset there is no loss of accuracy in the model description. Also note that non-local Willis coupling is ignored in the derivation below.

Combining the Willis constitutive response with the dynamical equa-

tion yields

$$\nabla \cdot [\mathsf{C} : \boldsymbol{\varepsilon}] - i\omega \nabla \cdot [\mathcal{S} \cdot \vec{u}] + i\omega \left[\tilde{\mathcal{S}} : \boldsymbol{\varepsilon}\right] + \omega^2 \boldsymbol{\rho} \cdot \vec{u} = 0. \tag{5.3}$$

An elegant way to deal with the spatial dependence of the material properties in piece-wise heterogeneous media, is to introduce contrast tensors defined as

$$\delta \boldsymbol{X}(\vec{x}) \equiv \boldsymbol{X}(\vec{x}) - \boldsymbol{X}^{\mathrm{M}}, \tag{5.4}$$

for $X \in \{\mathsf{C}, \mathcal{S}, \tilde{\mathcal{S}}, \boldsymbol{\rho}\}$, where the superscript M denotes the matrix material. Clearly, the contrast tensors are zero in the matrix. The spatially varying material properties can then be inserted into Eq. (5.3) to yield

$$\begin{aligned} \nabla \cdot \left(\mathsf{C}^{\mathrm{M}} : \boldsymbol{\varepsilon}\right) + \nabla \cdot \left(\mathcal{S}^{\mathrm{M}} \cdot \vec{u}\right) + i\omega \left(\tilde{\mathcal{S}}^{\mathrm{M}} : \boldsymbol{\varepsilon}\right) + \omega^2 \boldsymbol{\rho}^{\mathrm{M}} \cdot \vec{u} \\ = -\vec{f}^{\Delta \mathsf{C}} - \vec{f}^{\Delta \mathcal{S}} - \vec{f}^{\Delta \tilde{\mathcal{S}}} - \vec{f}^{\Delta \boldsymbol{\rho}}, \end{aligned} \tag{5.5}$$

where

$$\vec{f}^{\Delta \mathsf{C}} = \nabla \cdot [\delta \mathsf{C}(\vec{x}) : \boldsymbol{\varepsilon}], \tag{5.6a}$$

$$\vec{f}^{\Delta \mathcal{S}} = \nabla \cdot [\delta \mathcal{S}(\vec{x}) \cdot \dot{\vec{u}}], \tag{5.6b}$$

$$\vec{f}^{\Delta \tilde{\mathcal{S}}} = -\delta \tilde{\mathcal{S}}(\vec{x}) : \dot{\boldsymbol{\varepsilon}}, \tag{5.6c}$$

$$\vec{f}^{\Delta \boldsymbol{\rho}} = -\delta \boldsymbol{\rho}(\vec{x}) \cdot \ddot{\vec{u}}. \tag{5.6d}$$

As the notation implies, the material contrast terms may be treated as force source distributions in a homogeneous matrix material. The effect of these sources on the overall response of the material may therefore be described using the Green's function approach described below. Since the displacement field is a vector quantity and the source terms are vector quantities, the Green's

function, $\boldsymbol{G}$, is a second rank tensor that satisfies Eq. (5.7), which is provided in index notation for clarity,

$$C^{\mathrm{M}}_{ikjl}G_{jm,lk} - i\omega S^{\mathrm{M}}_{ijk}G_{km,j} + i\omega \tilde{S}^{\mathrm{M}}_{ijk}G_{jm,k} + \omega^2 \rho^{\mathrm{M}}_{ij}G_{jm} = -\delta_{im}\delta(\vec{x}). \tag{5.7}$$

Equation (5.7) is the equation for a point-source driven wave motion in a general Willis material, where $\boldsymbol{G}(\vec{x})$ is the frequency domain Green's function and $\delta(\vec{x})$ is the three-dimensional Dirac delta function. The Green's function gives the displacement field at the position $\vec{x}$ due to a point force source at the origin (or at a source location $\vec{x}'$ if the arguments of $\boldsymbol{G}(\vec{x})$ and $\delta(\vec{x})$ are replaced by $\vec{x} - \vec{x}'$). Furthermore, $\boldsymbol{G}(\vec{x})$ is material, geometry, and frequency dependent, in general.

The displacement field may then be implicitly written as

$$\vec{u}(\vec{x}) = \vec{u}^0(\vec{x}) + \boldsymbol{G} \overset{\Omega}{\star} \left\{ \vec{f}^{\delta \mathsf{C}} + \vec{f}^{\Delta \mathcal{S}} + \vec{f}^{\Delta \tilde{\mathcal{S}}} + \vec{f}^{\delta \rho} \right\}, \tag{5.8}$$

where $\vec{u}^0(\vec{x})$ is the solution to the homogeneous boundary value problem. The binary operator $\overset{\Omega}{\star}$ is a tensorial spatial convolution over the domain Ω which is defined for two arbitrary tensors $\boldsymbol{A}$ and $\boldsymbol{B}$ as

$$\boldsymbol{A} \overset{\Omega}{\star} \boldsymbol{B} \equiv \int_{\Omega} \boldsymbol{A}(\vec{x} - \vec{x}') : \boldsymbol{B}(\vec{x}') d\vec{x}'.$$

Note that for time harmonic systems

$$\frac{\partial}{\partial t} \int_{\Omega} \boldsymbol{G}(\vec{x} - \vec{x}') \cdot \vec{f}(\vec{x}') d\vec{x}' = \int_{\Omega} \dot{\boldsymbol{G}}(\vec{x} - \vec{x}') \cdot \vec{f}(\vec{x}') d\vec{x}',$$

and so

$$\frac{\partial}{\partial t} \left[\boldsymbol{G} \overset{\Omega}{\star} \vec{f} \right] = \dot{\boldsymbol{G}} \overset{\Omega}{\star} \vec{f}. \tag{5.9}$$

Thus the integral equation for the velocity may be written as

$$\dot{\vec{u}}(\vec{x}) = \dot{\vec{u}}^0(\vec{x}) + \dot{\boldsymbol{G}} \overset{\Omega}{\star} \left\{ \vec{f}^{\delta \mathsf{C}} + \vec{f}^{\Delta \mathcal{S}} + \vec{f}^{\Delta \tilde{\mathcal{S}}} + \vec{f}^{\delta \rho} \right\}. \tag{5.10}$$

Another property of convolutions, $\nabla(\boldsymbol{A} \overset{\Omega}{\star} \boldsymbol{B}) = (\nabla \boldsymbol{A}) \overset{\Omega}{\star} \boldsymbol{B} = \boldsymbol{A} \overset{\Omega}{\star} (\nabla \boldsymbol{B})$, then allows us to write

$$\nabla \vec{u}(\vec{x}) = \nabla \vec{u}^0(\vec{x}) + (\nabla \boldsymbol{G})^{\mathsf{T}} \overset{\Omega}{\star} \left\{ \vec{f}^{\delta \mathsf{C}} + \vec{f}^{\Delta \mathcal{S}} + \vec{f}^{\Delta \tilde{\mathcal{S}}} + \vec{f}^{\delta \rho} \right\}. \tag{5.11}$$

As stated in Chapter 1, the raised sanserif T in Eq. (5.11) denotes another tensorial transpose which places the first two dimensions at the end of the list of dimensions (e.g., $G^{\mathsf{T}}_{ij,k} = G_{ki,j}$).

Now consider a heterogeneous material consisting of two material phases; matrix and inhomogeneity. To mathematically distinguish between the matrix and the inhomogenities, define a Heaviside step function $\theta(\vec{x})$ which is equal to zero if $\vec{x}$ is in the matrix and equal to one if $\vec{x}$ is in the inhomogeneity. Now define $\Delta \boldsymbol{X}$ such that $\delta \boldsymbol{X}(\vec{x}) = \theta(\vec{x}) \Delta \boldsymbol{X} = \theta(\vec{x})(\boldsymbol{X}^{\mathrm{I}} - \boldsymbol{X}^{\mathrm{M}})$ for $\boldsymbol{X} \in \{\mathsf{C}, \mathcal{S}, \tilde{\mathcal{S}}, \boldsymbol{\rho}\}$, where the superscript I denotes a property of the inhomogeneity. Since the contrast tensors are only non-zero in the inhomogeneities, the convolution volume integrals reduce to integrals over the domain of the inhomogeneities Ω_{I}. The velocity and displacement gradient fields are then written as

$$\dot{\vec{u}}(\vec{x}) = \dot{\vec{u}}^0(\vec{x}) + \dot{\boldsymbol{G}} \overset{\Omega_{\mathrm{I}}}{\star} \left\{ \nabla' \cdot \left(\Delta \mathsf{C} : \boldsymbol{\varepsilon} + \Delta \mathcal{S} \cdot \dot{\vec{u}} \right) + i\omega \Delta \tilde{\mathcal{S}} : \boldsymbol{\varepsilon} + i\omega \Delta \boldsymbol{\rho} \cdot \dot{\vec{u}} \right\} \tag{5.12a}$$

$$\begin{aligned} \nabla \vec{u}(\vec{x}) &= \nabla \vec{u}^0(\vec{x}) + \\ (\nabla \boldsymbol{G})^{\mathsf{T}} &\overset{\Omega_{\mathrm{I}}}{\star} \left\{ \nabla' \cdot \left(\Delta \mathsf{C} : \boldsymbol{\varepsilon} + \Delta \mathcal{S} \cdot \dot{\vec{u}} \right) + i\omega \Delta \tilde{\mathcal{S}} : \boldsymbol{\varepsilon} + i\omega \Delta \boldsymbol{\rho} \cdot \dot{\vec{u}} \right\}, \end{aligned} \tag{5.12b}$$

where $\nabla' \cdot \boldsymbol{X}(\vec{x}')$ is the divergence of $\boldsymbol{X}(\vec{x}')$ with respect to $\vec{x}'$. Note that the solution to the homogeneous boundary value problem $\vec{u}^0(\vec{x})$ is still accounted for when $\vec{x} \in \Omega_\mathrm{I}$. By an extension of the properties of derivatives of convolutions to tensorial spatial convolutions, the velocity and displacement gradient fields become

$$\dot{\vec{u}}(\vec{x}) = \dot{\vec{u}}^0(\vec{x}) + \nabla \dot{\boldsymbol{G}} \overset{\Omega_\mathrm{I}}{*} \left(\Delta \mathsf{C} : \boldsymbol{\varepsilon} + \Delta \mathcal{S} \cdot \dot{\vec{u}} \right) + i\omega \dot{\boldsymbol{G}} \overset{\Omega_\mathrm{I}}{\star} \left(\Delta \tilde{\mathcal{S}} : \boldsymbol{\varepsilon} + \Delta \boldsymbol{\rho} \cdot \dot{\vec{u}} \right), \tag{5.13a}$$

$$\begin{aligned} \nabla \vec{u}(\vec{x}) &= \nabla \vec{u}^0(\vec{x}) + \\ \nabla \left(\nabla \boldsymbol{G} \right)^\mathsf{T} &\overset{\Omega_\mathrm{I}}{*} \left(\Delta \mathsf{C} : \boldsymbol{\varepsilon} + \Delta \mathcal{S} \cdot \dot{\vec{u}} \right) + i\omega (\nabla \boldsymbol{G})^\mathsf{T} \overset{\Omega_\mathrm{I}}{\star} \left(\Delta \tilde{\mathcal{S}} : \boldsymbol{\varepsilon} + \Delta \boldsymbol{\rho} \cdot \dot{\vec{u}} \right), \end{aligned} \tag{5.13b}$$

where the binary operator $\overset{\Omega}{*}$ is another tensorial spatial convolution over the domain Ω which is defined for arbitrary $\boldsymbol{A}$ and $\boldsymbol{B}$ as

$$\boldsymbol{A} \overset{\Omega}{*} \boldsymbol{B} \equiv \int_\Omega \boldsymbol{A}(\vec{x} - \vec{x}') \cdot \boldsymbol{B}(\vec{x}') d\vec{x}'.$$

Using Eq. (5.13b), the strain field can then be written as

$$\begin{aligned} \boldsymbol{\varepsilon}(\vec{x}) = \boldsymbol{\varepsilon}^0(\vec{x}) + \frac{1}{2} \left[\nabla (\nabla \boldsymbol{G})^\mathsf{T} + \nabla (\nabla \boldsymbol{G}^T)^\mathsf{T} \right] &\overset{\Omega_\mathrm{I}}{*} \left(\Delta \mathsf{C} : \boldsymbol{\varepsilon} + \Delta \mathcal{S} \cdot \dot{\vec{u}} \right) \\ + i \frac{\omega}{2} \left[(\nabla \boldsymbol{G})^\mathsf{T} + (\nabla \boldsymbol{G}^T)^\mathsf{T} \right] &\overset{\Omega_\mathrm{I}}{\star} \left(\Delta \tilde{\mathcal{S}} : \boldsymbol{\varepsilon} + \Delta \boldsymbol{\rho} \cdot \dot{\vec{u}} \right). \end{aligned} \tag{5.14}$$

This formulation of the velocity and strain is analogous to the formulation given by Sabina and Willis [87].

5.1.3 Micromechanics

The (exact) velocity and strain fields given in Eq. (5.13a) and Eq. (5.14) are expressed as integral equations whose kernel is an as yet undetermined Green's tensor. In the following, note that common micromechanical methods

allow these integral equations to be expressed as relatively simple algebraic equations. The micromechanical approximation is that inhomogeneities only interact with other inhomogeneities and affect macroscopic behavior through volume-averaged quantities. This approximation is valid if the phase of the wave in the matrix varies insignificantly over an inclusion dimension; that is, $k^{\mathrm{M}}a \ll 1$ where k^{M} is the largest wavenumber in the matrix and a is the largest dimension of an inhomogeneity. This condition is also called the long-wavelength limit, and is of particular interest in the field of metamaterials [88]. Also note that $k^{\mathrm{eff}}a$ must also be small, where k^{eff} is the largest wavenumber in the effective material (post-homogenization).

Another consequence of using the long-wavelength limit is that the dynamic equation must be approximated for consistency. In performing an order analysis of Willis materials it is useful to introduce the nondimensional quantities $\mathcal{W} = \mathcal{S}/Z_0$ and $\tilde{\mathcal{W}} = \tilde{\mathcal{S}}/Z_0$, where $Z_0 = \sqrt{|\mathsf{C}||\boldsymbol{\rho}|}$ is the characteristic specific acoustic impedance of the material and $|\cdot|$ denotes the characteristic amplitude of the argument. The quantities $\mathcal{W}$ and $\tilde{\mathcal{W}}$ are the tensorial form of the non-dimensional quantity W in Chapter 4. Assuming the constituent materials are reciprocal and passive, the requirements of Chapter 2 result in $|\tilde{\mathcal{W}}| = |\mathcal{W}|$. For $\vec{y} = \vec{x}/d$ and $\boldsymbol{H} = \boldsymbol{G}|\mathsf{C}|d$, Eq. (5.7) may be in the dimensionless form

$$\frac{C^{\mathrm{M}}_{ikjl}}{|\mathsf{C}^{\mathrm{M}}|}H_{jm,lk} + ik^{\mathrm{M}}a\left(\tilde{W}^{\mathrm{M}}_{ijk} - W^{\mathrm{M}}_{ijk}\right)H_{jm,k} + (k^{\mathrm{M}})^2a^2\frac{\rho^{\mathrm{M}}_{ij}}{|\boldsymbol{\rho}^{\mathrm{M}}|}H_{jm} = 0, \qquad (5.15)$$

where partial differentiation is now with respect to $\vec{y}$ and $k \sim \omega\sqrt{|\mathsf{C}|/|\boldsymbol{\rho}|}$ is assumed, which is equivalent to assuming $|\mathcal{W}|^2 \ll 1$. Note that in the

case of strong coupling, or $|\mathcal{W}|^2 \gg 1$, the wavenumber is approximately $k = i|W|\omega\sqrt{|\mathsf{C}|/|\boldsymbol{\rho}|}$. The characteristic amplitudes of the three coefficients in Eq. (5.15) are, in order from left to right, 1, $2k^{\mathrm{M}}a|\mathcal{W}|$, and $(k^{\mathrm{M}})^2a^2$. Thus, to be consistent with the long-wavelength approximation we must neglect the second and third terms, and Eq. (5.7) reduces to

$$C^{\mathrm{M}}_{ijkl}G_{jm,lk} = -\delta_{im}\delta(\vec{x})\delta(t), \tag{5.16}$$

where $\boldsymbol{G}$ is now the elasto-static Green's tensor. This approximation is equivalent to applying the elastic-viscoelastic correspondence principle and extending it to consider the dispersive effects of subwavelength inclusion dynamics [89]. The long-wavelength approximation is of significant importance as it allows one to estimate the effective material properties of interest to acoustic and elastic metamaterials if the frequency dependent properties of the constituents are known. This is valuable for metamaterial design efforts which may consider heterogeneities with non-spherical geometry and elastic anisotropy of all constituent materials.

Using the results of Appendix B, it may be shown that to linear spatial order

$$\langle \boldsymbol{Y} \circ \boldsymbol{Z} \rangle = \frac{1}{\Omega_{\mathrm{I}}}\int_{\Omega_{\mathrm{I}}} \boldsymbol{Y} \circ \boldsymbol{Z} d\vec{x} \approx \frac{1}{\Omega_{\mathrm{I}}}\int_{\Omega_{\mathrm{I}}} \langle \boldsymbol{Y} \rangle \circ \langle \boldsymbol{Z} \rangle d\vec{x} = \langle \boldsymbol{Y} \rangle \circ \langle \boldsymbol{Z} \rangle, \tag{5.17}$$

for arbitrary tensors $\boldsymbol{Y}$ and $\boldsymbol{Z}$ with the appropriate contraction symbol for $\circ$. Equations (5.17) are also known as the mean or average field approximation, and is treated in numerous textbooks; e.g., Refs. [35, 90]. Given this approximation, the volume averaged strain and velocity fields in a heterogeneous

medium where Willis coupling is non-negligible may be written as

$$\langle \boldsymbol{\varepsilon} \rangle = \langle \boldsymbol{\varepsilon}^0 \rangle + \mathsf{T}_1 : (\Delta \mathsf{C} : \langle \boldsymbol{\varepsilon} \rangle + \Delta \mathcal{S} \cdot \langle \dot{\vec{u}} \rangle) + \mathcal{T}_2 \cdot (\Delta \tilde{\mathcal{S}} : \langle \boldsymbol{\varepsilon} \rangle + \Delta \boldsymbol{\rho} \cdot \langle \dot{\vec{u}} \rangle), \quad (5.18a)$$

$$\langle \dot{\vec{u}} \rangle = \langle \dot{\vec{u}}^0 \rangle + \mathcal{T}_3 : (\Delta \mathsf{C} : \langle \boldsymbol{\varepsilon} \rangle + \Delta \mathcal{S} \cdot \langle \dot{\vec{u}} \rangle) + \boldsymbol{T}_4 \cdot (\Delta \tilde{\mathcal{S}} : \langle \boldsymbol{\varepsilon} \rangle + \Delta \boldsymbol{\rho} \cdot \langle \dot{\vec{u}} \rangle), \quad (5.18b)$$

where $\langle \boldsymbol{X}^0 \rangle$ is the homogeneous field $\boldsymbol{X}^0$ averaged over the domain of the inclusion and

$$\mathsf{T}_1 = \frac{1}{\Omega_\mathrm{I}} \int_{\Omega_\mathrm{I}} \int_{\Omega_\mathrm{I}} \mathsf{N}(\vec{x} - \vec{x}') d\vec{x} d\vec{x}', \quad (5.19a)$$

$$\mathcal{T}_2 = \frac{i\omega}{2\Omega_\mathrm{I}} \int_{\Omega_\mathrm{I}} \int_{\Omega_\mathrm{I}} \mathcal{M}(\vec{x} - \vec{x}') d\vec{x} d\vec{x}', \quad (5.19b)$$

$$\mathcal{T}_3 = -\frac{i\omega}{\Omega_\mathrm{I}} \int_{\Omega_\mathrm{I}} \int_{\Omega_\mathrm{I}} \nabla \boldsymbol{G}(\vec{x} - \vec{x}') d\vec{x} d\vec{x}', \quad (5.19c)$$

$$\boldsymbol{T}_4 = \frac{\omega^2}{\Omega_\mathrm{I}} \int_{\Omega_\mathrm{I}} \int_{\Omega_\mathrm{I}} \boldsymbol{G}(\vec{x} - \vec{x}') d\vec{x} d\vec{x}', \quad (5.19d)$$

with

$$\begin{aligned} \mathsf{N}(\vec{x}) =& \frac{1}{2} \left[\nabla \left(\nabla \boldsymbol{G} \right)^\mathsf{T} (\vec{x}) + \nabla \left(\nabla \boldsymbol{G}^T \right)^\mathsf{T} (\vec{x}) \right] \\ \Leftrightarrow \quad & N_{ijkl}(\vec{x}) = \frac{1}{2} \left[G_{ik,jl}(\vec{x}) + G_{jk,il}(\vec{x}) \right], \end{aligned} \quad (5.20a)$$

$$\begin{aligned} \mathcal{M}(\vec{x}) =& \frac{1}{2} \left[(\nabla \boldsymbol{G})^\mathsf{T} (\vec{x}) + (\nabla \boldsymbol{G}^T)^\mathsf{T} (\vec{x}) \right] \\ \Leftrightarrow \quad & M_{ijk}(\vec{x}) = \frac{1}{2} \left[G_{ik,j}(\vec{x}) + G_{jk,i}(\vec{x}) \right]. \end{aligned} \quad (5.20b)$$

The expressions for $\mathsf{N}(\vec{x})$ and $\mathcal{M}(\vec{x})$ have been provided in index notation in Eqs. (5.20) for clarity.

In order to maintain consistency with the long-wavelength approximation an order analysis must be performed on Eqs. (5.18). First, if we define

$\vec{h} = \vec{u}/a$, then we may write $\nabla_{\vec{x}}\vec{u} = \nabla_{\vec{y}}\vec{h}$ and $\dot{\vec{u}} = -i\omega a\vec{h}$. Also, note that $|\mathsf{T}_1| \sim 1/|\mathsf{C}^{\mathrm{M}}|$, $|\mathcal{T}_2| \sim |\mathcal{T}_3| \sim a\omega/|\mathsf{C}^{\mathrm{M}}|$, and $|\boldsymbol{T}_4| \sim a^2\omega^2/|\mathsf{C}^{\mathrm{M}}|$. Then, Eqs. (5.18) may be written in terms of orders of magnitude as

$$|\vec{h}| = |\vec{h}^0| + |\vec{h}|\left(1 + k^{\mathrm{M}}aW^{\mathrm{M}}\right) + |\vec{h}|\left(k^{\mathrm{M}}aW^{\mathrm{M}} + (k^{\mathrm{M}}a)^2\right), \tag{5.21a}$$

$$a\omega|\vec{h}| = a\omega|\vec{h}^0| + a\omega|\vec{h}|\left(1 + k^{\mathrm{M}}aW^{\mathrm{M}}\right) + a\omega|\vec{h}|\left(k^{\mathrm{M}}aW^{\mathrm{M}} + (k^{\mathrm{M}}a)^2\right), \tag{5.21b}$$

where we have assumed $|\Delta\boldsymbol{X}| \sim |\boldsymbol{X}^{\mathrm{M}}|$. Since $k^{\mathrm{M}}aW^{\mathrm{M}} \ll 1$ and $(k^{\mathrm{M}}a)^2 \ll 1$ in the long-wavelength limit we find that most of the terms should be neglected at this order of approximation, leaving

$$\langle\boldsymbol{\varepsilon}\rangle = \langle\boldsymbol{\varepsilon}^0\rangle + \mathsf{T}_1 : \Delta\mathsf{C} : \langle\boldsymbol{\varepsilon}\rangle, \tag{5.22a}$$

$$\langle\dot{\vec{u}}\rangle = \langle\dot{\vec{u}}^0\rangle + \mathcal{T}_3 : \Delta\mathsf{C} : \langle\boldsymbol{\varepsilon}\rangle. \tag{5.22b}$$

Expressions for T_1 and $\mathcal{T}_3$ may be written down analytically for isotropic spherical heterogeneities and with some numerical integration for ellipsoids in a long-wavelength system (see Appendix D). Equations (5.22) can then be inverted to obtain an expression for the volume averaged strain and velocity fields in the heterogeneity as a function of the macroscopic field values,

$$\langle\boldsymbol{\varepsilon}\rangle = \mathsf{A}^{\varepsilon} : \langle\boldsymbol{\varepsilon}^0\rangle + \mathcal{A}^{\varepsilon v} \cdot \langle\dot{\vec{u}}^0\rangle, \tag{5.23a}$$

$$\langle\dot{\vec{u}}\rangle = \mathcal{A}^{v\varepsilon} : \langle\boldsymbol{\varepsilon}^0\rangle + \boldsymbol{A}^{v} \cdot \langle\dot{\vec{u}}^0\rangle, \tag{5.23b}$$

where

$$\mathsf{A}^{\varepsilon} = \left[\mathsf{I} - \mathsf{T}^{1} : \Delta\mathsf{C}\right]^{-1}, \tag{5.24a}$$

$$\mathcal{A}^{\varepsilon v} = 0, \tag{5.24b}$$

$$\mathcal{A}^{v\varepsilon} = -\mathcal{T}_{3} : \Delta\mathsf{C} : \left[\mathsf{I} - \mathsf{T}^{1} : \Delta\mathsf{C}\right]^{-1}, \tag{5.24c}$$

$$\boldsymbol{A}^{v} = \boldsymbol{\delta}, \tag{5.24d}$$

where $\mathsf{I} \Leftrightarrow I_{ijkl} = (\delta_{ik}\delta_{jl} + \delta_{il}\delta_{jk})/2$ is the fourth order symmetric identity tensor.

Because the tensors A^{ε}, $\mathcal{A}^{\varepsilon v}$, $\mathcal{A}^{v\varepsilon}$, and $\boldsymbol{A}^{v}$ map the macroscopic velocity and strain to the volume averaged microscopic velocity and strain, these four tensors are called "localization tensors" and are a generalized form of the strain localization tensors used in micromechanics. In particular, A^{ε} calculates the microscopic strain due to the macroscopic strain, $\mathcal{A}^{\varepsilon v}$ calculates the microscopic strain due to the macroscopic velocity, $\mathcal{A}^{v\varepsilon}$ calculates the microscopic velocity due to the macroscopic strain, and $\boldsymbol{A}^{v}$ calculates the microscopic velocity due to the macroscopic velocity. Note that in the long-wavelength approximation the macroscopic velocity does not generate a microscopic strain regardless of the coupling tensors. This is due to the fact that the coupling of the velocity to the strain requires a non-negligible phase gradient of the displacement or velocity field on the scale of the inhomogeneity.

In summary, by assuming long wavelengths in the matrix material (the micromechanical approximation) the exact integral equations for the microscopic displacement and velocity fields may be approximated as algebraic equa-

tions which may be solved explicitly in terms of the imposed fields and the localization tensors. While the solution is approximate, it applies to a wide variety of interesting systems, including randomly distributed, fully dynamic inhomogeneities with anisotropic material properties and Willis coupling on the microscale.

5.1.4 Effective Material Properties for Dilute Concentrations

The localization tensors derived in the previous section may be used to predict the effective material properties by extending standard micromechanical homogenization techniques to include the Willis material parameters. This is done by first assuming that both the matrix and the inhomogeneities obey the Willis equations

$$\boldsymbol{\sigma}^{\mathrm{X}} = \mathsf{C}^{\mathrm{X}} : \boldsymbol{\varepsilon}^{\mathrm{X}} + \mathcal{S}^{\mathrm{X}} \cdot \dot{\vec{u}}^{\mathrm{X}}, \tag{5.25a}$$

$$\vec{\mu}^{\mathrm{X}} = \tilde{\mathcal{S}}^{\mathrm{X}} : \boldsymbol{\varepsilon}^{\mathrm{X}} + \rho^{\mathrm{X}} \dot{\vec{u}}^{\mathrm{X}}, \tag{5.25b}$$

where X = M, I, or eff. Then, using a simple approximation of the overall properties of a two-phase heterogeneous material consisting of inhomogeneities perfectly bonded to the matrix, we may write

$$\boldsymbol{Y}^{\mathrm{eff}} = (1-\phi)\langle \boldsymbol{Y} \rangle^{\mathrm{M}} + \phi \langle \boldsymbol{Y} \rangle^{\mathrm{I}} \quad \text{or} \quad \langle \boldsymbol{Y} \rangle^{\mathrm{M}} = \frac{1}{1-\phi} \left[\boldsymbol{Y}^{\mathrm{eff}} - \phi \langle \boldsymbol{Y} \rangle^{\mathrm{I}} \right], \tag{5.26}$$

for $\boldsymbol{Y} \in \{\boldsymbol{\sigma}, \vec{\mu}, \boldsymbol{\varepsilon}, \vec{v}\}$, where the superscript eff denotes the effective, or macroscopic, property and $\phi \equiv \Omega_{\mathrm{I}}/[\Omega_{\mathrm{I}} + \Omega_{\mathrm{M}}]$ is the inhomogeneity volume fraction. The averaged fields $\langle \boldsymbol{Y} \rangle^{\mathrm{M}}$ and $\langle \boldsymbol{Y} \rangle^{\mathrm{I}}$ are averaged field $\boldsymbol{Y}$ in the matrix and inhomogeneity, respectively, of a representative volume element (RVE). If the

inhomogeneities have sufficient spatial separation, interactions between inhomogeneities are negligible, and the RVE may consist of a single inhomogeneity in a matrix. In that case, $\langle \boldsymbol{\varepsilon} \rangle$ and $\langle \dot{\vec{u}} \rangle$ in Eq. (5.23) may be used to represent $\langle Y \rangle^{\mathrm{I}}$. This is the dilute approximation, which is expressed mathematically as $k^{\mathrm{M}} d \ll k^{\mathrm{M}} L$, where d is the characteristic inhomogeneity size and L is a characteristic distance between inhomogeneities. Since $\phi \sim d^3/L^3$, the limit where the dilute approximation is strictly valid is $\phi^{1/3} \ll 1$.

Combining Eqs. (5.26) and (5.25) with Eq. (5.23), an effective constitutive equation for the heterogeneous material may be found. Under a dilute concentration of heterogeneities in the matrix ($\phi \ll 1$), the effective macroscopic field quantities (here denoted with a superscript g for 'global') may be approximated by the field quantities of a homogeneous matrix; that is, $\vec{u}^{\mathrm{g}} \approx \vec{u}^{0}$. This is equivalent to the classical Eshelby method, and is valid up to $O(\phi)$ [35]. Thus,

$$\langle \boldsymbol{\sigma} \rangle^{\mathrm{M}} = \frac{\boldsymbol{\sigma}^{\mathrm{g}} - \phi \langle \boldsymbol{\sigma} \rangle^{\mathrm{I}}}{1-\phi} = \frac{\boldsymbol{\sigma}^{\mathrm{g}} - \phi \mathsf{C}^{\mathrm{I}} : \langle \boldsymbol{\varepsilon} \rangle^{\mathrm{I}} - \phi \mathcal{S}^{\mathrm{I}} \cdot \langle \dot{\vec{u}} \rangle}{1-\phi}, \tag{5.27}$$

and also

$$\begin{aligned} \langle \boldsymbol{\sigma} \rangle^{\mathrm{M}} &= \mathsf{C}^{\mathrm{M}} : \langle \boldsymbol{\varepsilon} \rangle^{\mathrm{M}} + \mathcal{S}^{\mathrm{M}} \cdot \langle \dot{\vec{u}} \rangle^{\mathrm{M}} \\ &= \frac{\mathsf{C}^{\mathrm{M}} : \boldsymbol{\varepsilon}^{\mathrm{g}} + \mathcal{S}^{\mathrm{M}} \cdot \dot{\vec{u}}^{\mathrm{g}} - \phi \left(\mathsf{C}^{\mathrm{M}} : \langle \boldsymbol{\varepsilon} \rangle^{\mathrm{I}} + \mathcal{S}^{\mathrm{M}} \cdot \langle \dot{\vec{u}} \rangle^{\mathrm{I}} \right)}{1-\phi}, \end{aligned} \tag{5.28}$$

where we have substituted the matrix strain and velocity similar to the substitution of the matrix stress in Eq. (5.27), which combine to give

$$\boldsymbol{\sigma}^{\mathrm{g}} = \mathsf{C}^{\mathrm{M}} : \boldsymbol{\varepsilon}^{\mathrm{g}} + \mathcal{S}^{\mathrm{M}} \cdot \dot{\vec{u}}^{\mathrm{g}} + \phi \left[\Delta \mathsf{C} : \langle \boldsymbol{\varepsilon} \rangle^{\mathrm{I}} + \Delta \mathcal{S} \cdot \langle \dot{\vec{u}} \rangle^{\mathrm{I}} \right]. \tag{5.29}$$

Substituting the field quantities within the inhomogeneities for the general quantities using the localization tensors in Eqs. (5.23), one can write

$$\begin{aligned}\boldsymbol{\sigma}^{\mathrm{g}} = &\left[\mathsf{C}^{\mathrm{M}} + \phi\left(\Delta\mathsf{C} : \bar{\mathsf{A}}^{\varepsilon} + \Delta\mathcal{S}\cdot\bar{\mathcal{A}}^{v\varepsilon}\right)\right] : \boldsymbol{\varepsilon}^{\mathrm{g}} \\ &+ \left[\mathcal{S}^{\mathrm{M}} + \phi\left(\Delta\mathsf{C} : \bar{\mathcal{A}}^{\varepsilon v} + \Delta\mathcal{S}\cdot\bar{\boldsymbol{A}}^{v}\right)\right]\cdot\dot{\vec{u}}^{\mathrm{g}}.\end{aligned} \tag{5.30}$$

Similarly, the macroscopic momentum may be written as

$$\begin{aligned}\vec{\mu}^{\mathrm{g}} = &\left[\tilde{\mathcal{S}}^{\mathrm{M}} + \phi\left(\Delta\tilde{\mathcal{S}} : \bar{\mathsf{A}}^{\varepsilon} + \Delta\boldsymbol{\rho}\cdot\bar{\mathcal{A}}^{v\varepsilon}\right)\right] : \boldsymbol{\varepsilon}^{\mathrm{g}} \\ &+ \left[\boldsymbol{\rho}^{\mathrm{M}} + \phi\left(\Delta\tilde{\mathcal{S}} : \bar{\mathcal{A}}^{\varepsilon v} + \Delta\boldsymbol{\rho}\cdot\bar{\boldsymbol{A}}^{v}\right)\right]\cdot\dot{\vec{u}}^{\mathrm{g}}.\end{aligned} \tag{5.31}$$

Notice that the macroscopic stress and momentum fields are related to both the macroscopic strain and velocity fields via the localization tensors, which are linear operators. Thus, by matching Eqs. (5.30) and (5.31) with the assumed form of the effective medium provided in Eq. (5.25), the effective material satisfies a set of effective Willis equations where

$$\mathsf{C}^{\mathrm{eff}} = \mathsf{C}^{\mathrm{M}} + \phi\left(\Delta\mathsf{C} : \bar{\mathsf{A}}^{\varepsilon} + \Delta\mathcal{S}\cdot\bar{\mathcal{A}}^{v\varepsilon}\right), \tag{5.32a}$$

$$\mathcal{S}^{\mathrm{eff}} = \mathcal{S}^{\mathrm{M}} + \phi\left(\Delta\mathsf{C} : \bar{\mathcal{A}}^{\varepsilon v} + \Delta\mathcal{S}\cdot\bar{\boldsymbol{A}}^{v}\right), \tag{5.32b}$$

$$\tilde{\mathcal{S}}^{\mathrm{eff}} = \tilde{\mathcal{S}}^{\mathrm{M}} + \phi\left(\Delta\tilde{\mathcal{S}} : \bar{\mathsf{A}}^{\varepsilon} + \Delta\boldsymbol{\rho}\cdot\bar{\mathcal{A}}^{v\varepsilon}\right), \tag{5.32c}$$

$$\boldsymbol{\rho}^{\mathrm{eff}} = \boldsymbol{\rho}^{\mathrm{M}} + \phi\left(\Delta\tilde{\mathcal{S}} : \bar{\mathcal{A}}^{\varepsilon v} + \Delta\boldsymbol{\rho}\cdot\bar{\boldsymbol{A}}^{v}\right). \tag{5.32d}$$

As should be expected, the effective material properties are tacitly frequency dependent based on the dispersion relations of the constitutive materials but independent of the imposed fields.

It is interesting that in Eqs. (5.32) even if $\mathcal{S}^{\mathrm{I}} = \tilde{\mathcal{S}}^{\mathrm{I}} = \mathcal{S}^{\mathrm{M}} = \tilde{\mathcal{S}}^{\mathrm{M}} = 0$ and $\boldsymbol{\rho}^{\mathrm{I}} = \rho^{\mathrm{I}}\boldsymbol{\delta}$, $\boldsymbol{\rho}^{\mathrm{M}} = \rho^{\mathrm{M}}\boldsymbol{\delta}$ (i.e., the constituent materials satisfy standard constitutive equations), the effective coupling tensors may be non-zero depending on

the localization tensors and associated Green's tensors. Further, Eqs. (5.32) clearly show that coupling may exist even when $\mathcal{S}^{\mathrm{M}} = \mathcal{S}^{\mathrm{I}} = \tilde{\mathcal{S}}^{\mathrm{M}} = \tilde{\mathcal{S}}^{\mathrm{I}} = 0$ and $\Delta\boldsymbol{\rho} = 0$, which is a slight modification from the original observation made by Willis [47], but consistent with later works on the topic [48, 50]. It is noteworthy that one observes this result in the long-wavelength and dilute limit considered here which implies that Willis coupling may arise from purely local interactions in addition to the existence of nonlocal interactions associated with an infinite periodic lattice of scatterers, as noted elsewhere [50, 86].

5.1.5 Effective Material Properties at Elevated Volume Fractions

As stated above, all of these results rely on the assumption of dilute concentrations which is of limited interest. However, well established methods have been developed to extend this type of development to higher concentrations [35, 90]. For example, self-consistent models are based on the idea that if a portion of an effective medium were replaced by the representative volume element of the material the homogenization would cause no change in the effective properties. Another example is differential effective medium (DEM) theory, which approximates the overall response of non-dilute concentrations of inhomogeneities by iteratively taking a dilute concentration, homogenising, then treating the resulting effective material as the matrix for another dilute concentration to homogenize. Using these types of methods, the results from this section may be extended to greater concentrations of inhomogeneities.

Following the derivation shown in Ref. [35], the DEM equations which

extend the present long-wavelength dilute effective material approximation may be written as

$$(1-\phi)\frac{d\mathsf{C}^{\text{eff}}}{d\phi} = \left[\mathsf{C}^{\text{I}} - \mathsf{C}^{\text{eff}}\right] : \mathsf{A}^{\varepsilon}_{\text{DEM}} + \left[\mathcal{S}^{\text{I}} - \mathsf{S}^{\text{eff}}\right] \cdot \mathcal{A}^{v\varepsilon}_{\text{DEM}}, \tag{5.33a}$$

$$(1-\phi)\frac{d\mathcal{S}^{\text{eff}}}{d\phi} = \left[\mathsf{C}^{\text{I}} - \mathsf{C}^{\text{eff}}\right] : \mathcal{A}^{\varepsilon v}_{\text{DEM}} + \left[\mathcal{S}^{\text{I}} - \mathsf{S}^{\text{eff}}\right] \cdot \boldsymbol{A}^{v}_{\text{DEM}}, \tag{5.33b}$$

$$(1-\phi)\frac{d\tilde{\mathcal{S}}^{\text{eff}}}{d\phi} = \left[\tilde{\mathcal{S}}^{\text{I}} - \tilde{\mathcal{S}}^{\text{eff}}\right] : \mathsf{A}^{\varepsilon}_{\text{DEM}} + \left[\boldsymbol{\rho}^{\text{I}} - \boldsymbol{\rho}^{\text{eff}}\right] \cdot \mathcal{A}^{v\varepsilon}_{\text{DEM}}, \tag{5.33c}$$

$$(1-\phi)\frac{d\boldsymbol{\rho}^{\text{eff}}}{d\phi} = \left[\tilde{\mathcal{S}}^{\text{I}} - \tilde{\mathcal{S}}^{\text{eff}}\right] : \mathcal{A}^{\varepsilon v}_{\text{DEM}} + \left[\boldsymbol{\rho}^{\text{I}} - \boldsymbol{\rho}^{\text{eff}}\right] \cdot \boldsymbol{A}^{v}_{\text{DEM}}, \tag{5.33d}$$

with the initial conditions $\mathsf{C}^{\text{eff}}(\phi = 0) = \mathsf{C}^{\text{M}}$, $\mathcal{S}^{\text{eff}}(\phi = 0) = \mathcal{S}^{\text{M}}$, $\tilde{\mathcal{S}}^{\text{eff}}(\phi = 0) = \tilde{\mathcal{S}}^{\text{M}}$, and $\boldsymbol{\rho}^{\text{eff}}(\phi = 0) = \boldsymbol{\rho}^{\text{M}}$, and the localization tensors for the long-wavelength case considered here are written as

$$\mathsf{A}^{\varepsilon}_{\text{DEM}} = \left[\mathsf{I} - \mathsf{T}_1(\mathsf{C}^{\text{eff}}) : \left(\mathsf{C}^{\text{I}} - \mathsf{C}^{\text{eff}}\right)\right]^{-1}, \tag{5.34a}$$

$$\mathcal{A}^{\varepsilon v}_{\text{DEM}} = 0, \tag{5.34b}$$

$$\mathcal{A}^{v\varepsilon}_{\text{DEM}} = \mathcal{T}_3(\mathsf{C}^{\text{eff}}) : \left(\mathsf{C}^{\text{I}} - \mathsf{C}^{\text{eff}}\right) : \left[\mathsf{I} - \mathsf{T}_1(\mathsf{C}^{\text{eff}}) : \left(\mathsf{C}^{\text{I}} - \mathsf{C}^{\text{eff}}\right)\right]^{-1}, \tag{5.34c}$$

$$\boldsymbol{A}^{v}_{\text{DEM}} = \boldsymbol{\delta}. \tag{5.34d}$$

These equations may be solved using numerical methods. The results shown in Section 5.2 are found using this DEM theory with a fourth-order Runge-Kutta method. As discussed above, the fact that $\mathcal{A}^{\varepsilon v}_{\text{DEM}} = 0$ comes from the fact that we neglecting terms $O(k^{\text{M}}a)$ (or $O(k^{\text{eff}}a)$), and the macroscopic velocity does not generate a microscopic strain. This leads to an estimate of the WIllis coupling parameters where $(\tilde{\mathcal{S}}^{\text{eff}})^{\mathsf{T}} \neq \mathcal{S}^{\text{eff}}$. This inequality, which violates reciprocity [86, 50], is a consequence of the long-wavelength approximation.

Despite this fact, the prediction of $\tilde{S}^{\text{eff}}$ provided by this model captures the predominant microscale physics that lead to the macroscale properties of interest and is therefore used as the estimate of macroscopic coupling. This is the case because the model accurately localises strain, but not velocity, and assumes that dynamic density, stiffness and Willis coupling exists on the microscale (matrix and heterogeneity). Therefore, the macroscale strain and velocity will localise to generate the approximate microscale momentum that depends on both the microscale strain and velocity. Specifically, Eqns. (5.23) and the constitutive relations yield the following expression for the momentum in the heterogeneities

$$\vec{\mu}^{\text{I}} = \left(\tilde{\mathcal{S}}^{\text{I}} : \boldsymbol{A}^{\varepsilon} + \boldsymbol{\rho}^{\text{I}} : \mathcal{A}^{v\varepsilon}\right) : \varepsilon^{\text{g}} + \rho^{\text{I}} : \dot{u}^{\text{g}}. \tag{5.35}$$

This momentum density is clearly dependent on both the macroscopic strain and velocity, despite the long-wavelength approximation. This localised momentum will, in turn, give rise to macroscopic momentum that depends on the volume fraction, geometry, and anisotropy of the coupled inclusions along with the material properties of the matrix through the evaluation of the relations in Eq. (5.33). It therefore provides a good approximation of $\tilde{S}^{\text{eff}}$, which is used as the effective Willis coupling parameter from this point forward. Despite these obvious simplifications, it is important to note that the model provides an estimate of the effective Willis coupling for a class of materials that has not yet been accurately modeled: random heterogeneous media demonstrating Willis coupling.

In addition to higher volume fractions, the present approach can also be extended to multiple inhomogeneity types through iterative methods. The basic idea is that each type or orientation of an inhomogeneity has a certain volume fraction (the sum of which are ≤ 1) which may be successively homogenized until all of the full composite is modeled [91]. While this method is straightforward and of interest in the design of metamaterials such as double negative materials, it will not be covered in detail in this thesis in the interest of brevity.

5.2 Examples of Elastic Homogenization

The advantage of the homogenization scheme outlined in Section 5.1 is that the localization tensors may be predicted using an analytical model that only requires the evaluation of a simple numerical integral. It is thus an efficient model to explore the effective properties of a heterogeneous material displaying Willis coupling. In this section we present and briefly discuss four different examples that implement the above homogenization method. In all cases, the heterogeneities are assumed to be ellipsoidal and embedded in a conventional elastic matrix material. The case of isotropic spherical heterogeneities is first presented as a benchmark case, followed by an anisotropic spherical heterogeneity, an isotropic ellipsoidal heterogeneity, and finally an isotropic spherical heterogeneity displaying frequency-dependent mass density and stiffness due to assumed dynamic microstructure. Whenever possible, the predictions from the present model will be compared with other, well-

established models, notably, a self-consistent (SC) homogenization scheme based on the work of Hill [37], and the Hashin-Shtrikman (HS) bounds for isotropic, spherical inclusions. Since there are no published models, analytical or numerical, which account for Willis coupling in random media, the predictions for the coupling tensors will be presented alone.

5.2.1 Isotropic Spherical Inhomogeneities

Since there are numerous homogenization techniques which can account for isotropic spherical inhomogeneities in an isotropic matrix, this case may be treated as a benchmark for the present homogenization method. We consider a matrix with shear modulus $\mu^{\mathrm{M}} = 1$ GPa, bulk modulus $K^{\mathrm{M}} = 3$ GPa, and density $\rho^{\mathrm{M}} = 700$ kg/m^3 containing 0.1 mm radius spherical inhomogeneities with shear modulus $\mu^{\mathrm{I}} = 10$ GPa, bulk modulus $K^{\mathrm{I}} = 30$ GPa, and density $\rho^{\mathrm{I}} = 2000$ kg/m^3 (heavy and stiff inhomogeneities). Neither the matrix nor the inhomogeneity has any Willis coupling, because the only isotropic third-order tensor is the null third-order tensor. The frequency is assumed to be 50 Hz.

Figure 5.2 shows the effective plane wave modulus as a function of inhomogeneity volume fraction using the Willis differential effective medium approach (W-DEM), Eqs. (5.33) with Eqs. (5.34), with the associated Hashin-Shtrikman (HS) bounds and a self-consistent prediction (SC) [92, 93] based on the work of Hill [37], shown for comparison. The relative error of the W-DEM prediction relative to the SC prediction is 0.3% at 10% volume fraction, and is 1.7% at 20% volume fraction. Since SC and W-DEM are different

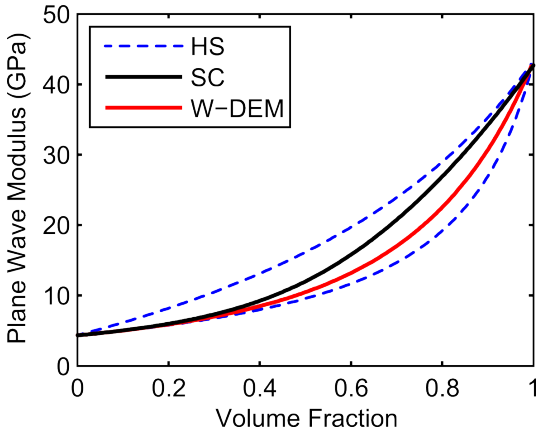

Figure 5.2: Predicted effective plane wave modulus (C_{1111}) for an isotropic matrix with spherical isotropic inhomogeneities using the Willis differential effective medium approach (W-DEM) extended to higher volume fractions using a differential effective medium theory. The Hashin-Shtrikman bounds (HS) and the predicted plane wave modulus using a self consistent approach (SC) are shown for comparison.

homogenization models, it is not expected that they would predict the same effective properties. What is expected is that the two predictions should be similar and to fall within the HS bounds, as is seen in this case.

Since both matrix and inhomogeneity materials are isotropic and the geometry is also isotropic, we expect the effective material properties to also be isotropic and therefore uncoupled. Indeed, this is the case, as seen by the effective material properties summarized in Table 5.1, which gives the matrix, inhomogeneity, W-DEM and SC predicted effective properties, along with the HS bounds for comparison at 5% volume fraction.

Table 5.1: List of material properties for an isotropic matrix containing isotropic spherical inhomogeneities (Inh) with a 5% volume fraction. The the predicted material properties using a self-consistent (SC) prediction and the upper and lower Hashin-Shtrikman (HS) bounds are shown for comparison. Stiffnesses are given in GPa and densities are given in kg/m^3. Moduli not listed are either determined by the symmetry of the material properties or are zero.

Modulus	**Matrix**	**Inh**	**W-DEM**	**SC**	**HS Lower**	**HS Upper**
C_{1111}, C_{2222}, C_{3333}	4.33	43.3	4.65	4.66	4.65	5.22
C_{1122}, C_{1133}, C_{2233}	2.33	23.3	2.47	2.47	2.47	2.68
C_{1212}, C_{1313}, C_{2323}	1	10	1.09	1.09	1.09	1.27
ρ_{11}, ρ_{22}, ρ_{33}	700	2000	765	765	–	–

5.2.2 Anisotropic Spherical Inhomogeneities

Consider a spherical inhomogeneity with anisotropic material properties. For convenience, only transverse isotropy (symmetric about the 1 axis), which allows for 10 independent material constants (5 stiffnesses + 2 densities + 3 couplings), will be considered. The matrix and inhomogeneity properties are summarized in Table 5.2, along with the effective properties predicted by the W-DEM. The matrix properties are the same as those presented in Table 5.1, the frequency is 50 Hz, the inhomogeneity radius is 0.1 mm, and the inhomogeneity volume fraction is 5%. Figure 5.3 shows the W-DEM and SC predictions for the stiffness moduli C_{1111} and C_{2222} (left) and the W-DEM prediction for the independent coupling moduli S_{111}, S_{221}, and S_{122}.

As expected, the effective material properties are also transversely isotropic and symmetric about the x_1 axis. All of the predicted material stiffnesses are closer to the Reuss average (lower bound) than the Voigt average

Table 5.2: List of material properties for an isotropic matrix containing spherical inhomogeneities (Inh) with transversely isotropic material properties. The volume fraction of heterogeneity is 5%. The material properties predicted using the Reuss and Voigt averages and a self-consistent (SC) prediction that cannot consider coupling effects are included for comparison with standard homogenization models. Stiffnesses are given in GPa, coupling moduli are given in kPa/(m/s), and densities are given in kg/m^3. Moduli not listed are either determined by the symmetry of the material properties or are zero. *The shear stress C_{2323} is not independent, but is calculated from the other values.

Modulus	**Matrix**	**Inh**	**W-DEM**	**Reuss Average**	**Voigt Average**	**SC**
C_{1111}	4.33	43.3	4.6	4.5	6.3	4.6
C_{2222}, C_{3333}	4.33	21.6	4.5	4.5	5.2	4.5
C_{1122}, C_{1133}	2.33	23.3	2.5	2.4	3.4	2.5
C_{2233}	2.33	11.6	2.4	2.4	2.8	2.4
C_{1212}, C_{1313}	1	10	1.1	1.0	1.5	1.1
$(C_{2323})^*$	1	5	1.1	1.0	1.2	1.1
S_{111}	0	$i24$	$i0.14$	0	$i1.2$	–
S_{221}, S_{331}	0	$i20$	$i0.18$	0	$i1.0$	–
S_{122}, S_{133}	0	$i18$	$i0.31$	0	$i0.9$	–
ρ_{11}	700	2000	765	724	765	–
ρ_{22}, ρ_{33}	700	1000	715	711	715	–

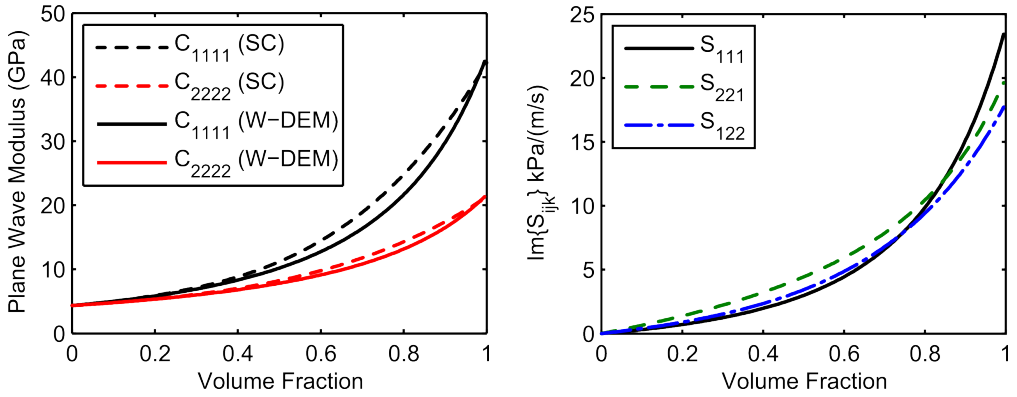

Figure 5.3: (Left) Effective plane wave moduli (C_{1111} and C_{2222}) for an isotropic matrix with identically oriented spherical transversely isotropic inhomogeneities using the Willis differential effective medium approach (W-DEM) and the generalized self-consistent (SC) methods. (Right) Effective coupling modulus S_{111} of the same system as predicted by the W-DEM.

(upper bound), which is similar to the isotropic case considered in Section 5.2.1 using the Hashin-Shtrikman bounds. The W-DEM and SC predictions for the stiffness moduli in Table 5.2, but follow different paths in Fig. 5.3, which means that the W-DEM and SC models are nearly the same for small volume fractions and close to one, but diverge somewhat at intermediate volume fractions. The W-DEM prediction of the coupling moduli are much smaller than the Voigt averages, following the pattern of the predicted stiffness moduli. The similarity of the evolution of the coupling moduli to the stiffness moduli is seen at all volume fractions in Fig. 5.3.

5.2.3 Isotropic Ellipsoidal Inhomogeneities

In addition to material anisotropy, the present homogenization technique can account for geometric anisotropy due to ellipsoidal inhomogeneities.

Table 5.3: List of material properties for an isotropic matrix with isotropic prolate or isotropic oblate spheroidal inhomogeneities (Inh). The axis of symmetry is the x_1, and the ratio of the long to short radius is 10. A volume fraction of 5% is assumed. *This quantity is not independent, but is calculated from the other values.

Modulus	**Matrix**	**Inh**	**W-DEM Estimate**	
			Oblate	**Prolate**
C_{1111}	4.33	43.3	4.5	5.4
C_{2222}, C_{3333}	4.33	43.3	5.0	4.6
C_{1122}, C_{1133}	2.33	23.3	2.5	2.5
C_{2233}	2.33	23.3	2.5	2.6
C_{1212}, C_{1313}	1	10	1.1	1.1
$(C_{2323})^*$	1	10	1.2	1.1
S_{111}	0	0	0	0
S_{221}, S_{331}	0	0	0	0
S_{122}, S_{133}	0	0	0	0
ρ_{11}	700	2000	765	765
ρ_{22}, ρ_{33}	700	2000	765	765

For convenience only spheroids, which are ellipsoids with two equal radii, are considered. This form of inhomogeneity will lead to transversely isotropic effective material properties. In particular, the cases of prolate spheroidal (needle-like) inhomogeneities and oblate spheroidal (penny-like) inhomogeneities will be considered. For both cases, the matrix and inhomogeneity material properties are assumed to be isotropic and the same as those in Section 5.2.1, and again the frequency is 50 Hz.

The predicted material properties for these two cases are given in Table 5.3. The numerical values are rounded to two digits, as the numerical error associated with the W-DEM prediction precluded any greater accuracy given the symmetry requirements on the material properties. Using an oblate

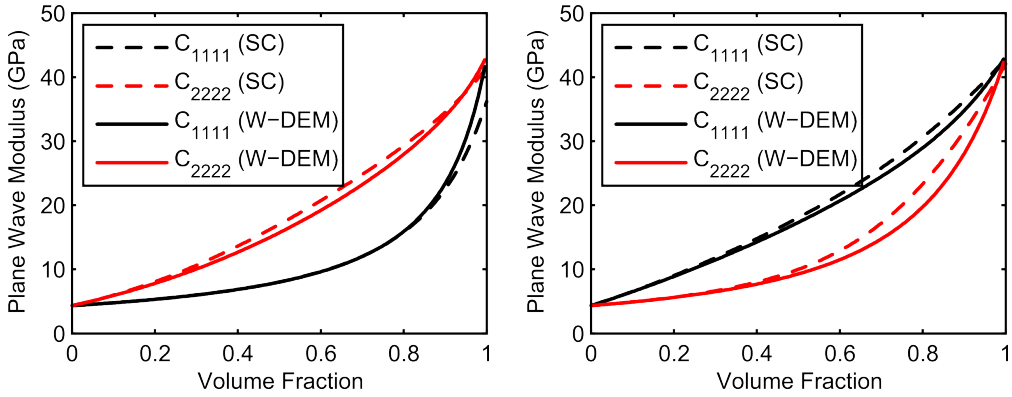

Figure 5.4: Effective plane wave moduli (C_{1111} and C_{2222}) for an isotropic matrix with (left) prolate spheroidal (needle-like) or (right) oblate spheroidal (penny-like) isotropic inhomogeneities using the Willis differential effective medium approach (W-DEM) and the generalized self-consistent (SC) methods.

spheroidal inhomogeneity causes the material to be more compliant in the 1 direction than using a prolate spheroidal inhomogeneity, though the stiffness of the inhomogeneity material causes both to be stiffer than the matrix material. Conversely, the stiffness in the 2 and 3 directions is greater for the oblate case than for the prolate case. Interestingly, no coupling was generated in either the prolate or oblate cases, and the density in both cases is simply the Voigt average.

The W-DEM predictions for the spheroidal inhomogeneities are compared with the SC predictions in Fig. 5.4. Again, the two predictions follow very similar trends for all volume fractions.

5.2.4 Dynamic Mass and Stiffness

In addition to dealing with material or geometric anisotropy, the W-DEM approach can account for dynamic inhomogeneities by homogenising frequency by frequency as long as the long-wavelength limit holds in the effective and constitutive media. For example, consider the isotropic spherical inhomogeneities in Section 5.2.1 with 20% volume fraction where the material properties of the heterogeneities are frequency dependent. This can be simply modeled by multiplying the property of interest by a frequency dependent factor $F(\omega)$ representing dispersion. For illustrative purposes, consider the case where $F(\omega)$ is chosen to be a Lorentzian distribution defined as

$$F(\omega) = 3\left[1 - \frac{2}{(\omega/\omega_0)^2 - 1 + i\Gamma(\omega/\omega_0)}\right]^{-1}, \tag{5.36}$$

where ω_0 is some (very small) characteristic frequency and Γ is a damping factor. The function $F(\omega)$ has the properties $F(0) = 1$ and $F(\infty) = 3$, and for $\Gamma = 0$, $F(\omega_0) = 0$ (see Fig. 5.5 for a plot of $F(\omega)$ with $\Gamma = 10^{-2}$, 10^{-1}, and 10^{0}). The maximum of the real part of $F(\omega)$ occurs at $\omega = \omega_0\sqrt{3 + \Gamma\sqrt{3}}$. The choice of $F(\omega)$ follows the form given by Fang *et al* [11]. which represents the effective stiffness in a one-dimensional periodic array of Helmholtz resonators.

For this example, the stiffness and mass density tensors of the inhomogeneity are both multiplied by $F(\omega)$. Varying C^{I} in this manner is equivalent to holding the Poisson's ratio constant and varying the shear or bulk modulus. Evaluation of the W-DEM with uncoupled constitutive materials yields an effective stiffness tensor that is insensitive to the constitutive mass densities,

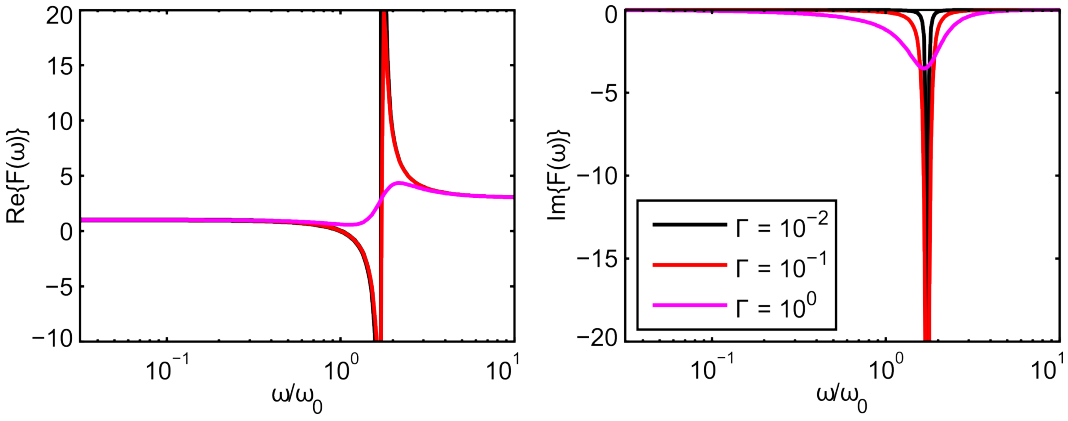

Figure 5.5: Plot of the characteristic dispersion relation $F(\omega)$ as a function of normalized frequency.

and the effective mass density tensor is insensitive to the constitutive stiffness tensors. Therefore, both the effects of frequency dependent stiffness and mass density may be analyzed at the same time, which is done here. Note that $\Im\{F(\omega)\} \leq 0$. Using the results of Chapter 2, imposing this dispersion relation on the inhomogeneity mass density implies that the inhomogeneities are not passive but active elements, and therefore the resultant effective material properties may also break passivity.

The W-DEM prediction of the dispersion curves for μ^{eff} and ρ^{eff} is shown in Fig. 5.6. The imaginary part of ρ^{eff} is negative-definite, implying that the homogenized effective material is active due to the influence of the inhomogeneities. It is interesting to note the strong dispersion of μ^{eff} occurs at $\omega/\omega_0 \approx 1$, while the frequency range of strong dispersion of ρ^{eff} occurs at $\omega/\omega_0 \approx 1.7$. This is due to the natures of the localization tensors A^{ε} and $\boldsymbol{A}^{v}$ in the W-DEM. Since $\boldsymbol{A}^{v} \approx \boldsymbol{\delta}$ (Eq. (5.34d)) and $\Delta\tilde{\mathcal{S}} = 0$, the effective density

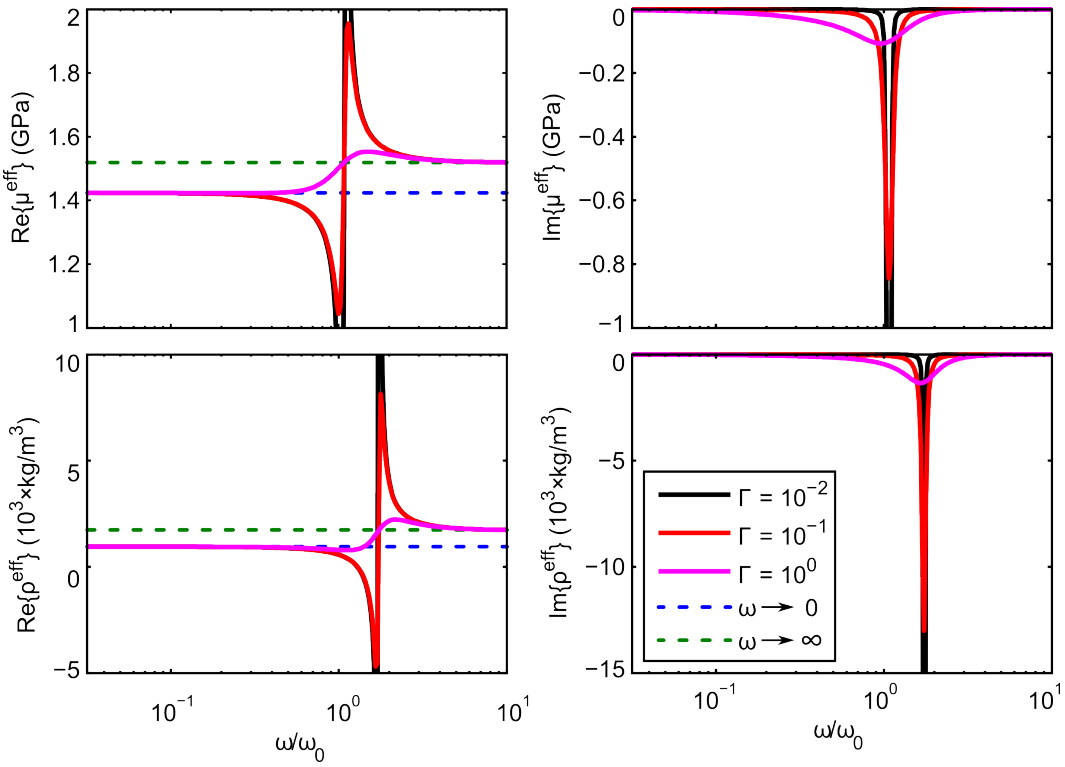

Figure 5.6: Real (left plots) and imaginary (right plots) parts of the W-DEM prediction of the effective shear modulus (μ^{eff}, top plots) and mass density (ρ^{eff}, bottom plots) for an isotropic matrix with dynamic isotropic spherical inhomogeneities as a function of frequency for three values of the damping constant Γ.

given in Eq. (5.32d) is approximately just a mixture law, and so the strong dispersion of the density will occur at the resonance of $F(\omega)$ (which is at $\omega = 1.73\omega_0$ in the undamped case). However, $\mathsf{A}^{\varepsilon} \approx [\mathsf{I} - \mathsf{T} : \Delta\mathsf{C}]^{-1}$ (Eq. (5.34a)), so the strongly dispersive response of the effective stiffness given in Eq. (5.32a) will occur when $\mathsf{T} : \Delta\mathsf{C} \approx \mathsf{I}$. It should be noted that since the resonance condition depends upon C^{M} in the dilute approximation, the implicit nature of the W-DEM method makes explicit analysis of this phenomenon difficult for significant volume fractions.

5.3 Summary

A homogenization technique for arbitrarily anisotropic elastic heterogeneous materials with no long-range order which exhibit Willis coupling has been derived and demonstrated. Explicit prediction of the effective material properties required using a micromechanical approximation ($k^{\mathrm{M}}a \ll 1$ where a is the characteristic dimension of the inhomogeneity) to turn the integral equations of Willis into algebraic equations that are presented for a biphase heterogeneous material with non-interacting inhomogeneities (inhomogeneity volume fraction $\phi \ll 1$). Using a standard micromechanical homogenization approach to approximate the macroscopic stress, strain, momentum, and velocity fields, the effective material properties may be approximated using localization tensors. Since the approximation neglects effects $O(k^{\mathrm{M}}a)$, only the strain localization is accurately predicted, and so only one of the Willis coupling tensors, $\tilde{\mathcal{S}}^{\mathrm{eff}}$, is likely to be well approximated by the homogenization

scheme. Extension of the present method to higher orders of $k^{\mathrm{M}}a$ is left as future work.

The homogenization technique was used to predict the effective material properties of various systems using a differential effective medium approach to extend the results to all $0 \leq \phi \leq 1$. The results are very similar in magnitude and volume fraction dependence to an established self-consistent homogenization scheme and falls within the well-established Hashin-Shtrickman bounds when Willis coupling is neglected. It was also found in the cases shown here that the presence of Willis coupling in the inhomogeneities does not significantly affect the effective stiffness. It was demonstrated that Willis coupling is not the result of anisotropy emerging from the presence of non-spherical inhomogeneities, as isotropic ellipsoidal inhomogeneities embedded in an isotropic matrix do not generate any coupling. However, the presence of Willis coupling in an inhomogeneity does generate Willis coupling in the effective material properties. These findings are consistent with recent work suggesting that Willis coupling is the result of long range order and a lack of "reflective symmetry" on the microscale [50, 86]. Finally, the ability to calculate effective dynamic stiffness and density when dynamic inhomogeneities having known, frequency-dependent, material properties are present has been shown. The behavior of the effective dynamic stiffness is shown to behave differently than the effective density, even when the inhomogeneity stiffness and density have similar microscale dynamics. This homogenization technique may be used to design acoustic and elastic metamaterials with random microstructure in cases

where the matrix material and/or heterogeneities display frequency-dependent stiffness, mass density, and Willis coupling as a result of microscopic inclusion structure. This model may be expanded to investigate the influence of multiple types of heterogeneities as well as the affects of orientation distribution in a random heterogeneous medium.

Chapter 6

Conclusions and Future Work

The purpose of this dissertation is to increase fundamental understanding of Willis materials through mathematical and physical descriptions of Willis coupling. This chapter presents a summary of the models and conclusions derived in this dissertation, along with descriptions of how these results assist in the stated purpose of the dissertation. This summary is followed by a succinct and itemized list of the major contributions derived in this dissertation. Finally, with an eye toward future research, some topics associated with Willis materials that have not been fully explored will be discussed.

6.1 Summary of Dissertation Conclusions

The original motivation for the present study of Willis materials was the presence of material properties with seemingly non-physical dispersion relations in the acoustic metamaterials literature based on standard constitutive equations, e.g. Fokin *et al.*, Fig. 6 [78]. In particular, the imaginary parts of the effective mass density and/or the effective bulk modulus changed sign. Similar results were found in the electromagnetic metamaterials literature with the conclusion that the more generalized constitutive equations of

bianisotropic materials were needed to accurately describe the effective material behavior [94]. The constitutive equations for Willis materials are similar in form to the constitutive equations for bianisotropic materials, and so the Willis constitutive equations were considered as an alternative representation of metamaterials with seemingly non-physical dispersion relations.

In order to determine what dispersion relations are physically meaningful, restrictions on the range of Willis material properties imposed by assuming reciprocal, passive, and causal behavior was derived in Chapter 2. Reciprocity was shown to impose symmetry conditions on the stiffness tensor, mass density tensor, and Willis coupling tensors. Passivity was shown relate the material properties to their complex conjugates. If a Willis material is both reciprocal and passive, the imaginary part of the stiffness tensor must be less than or equal to zero (assuming $e^{-i\omega t}$ time dependence), the imaginary part of the mass density tensor must be greater than or equal to zero, and the real part of the Willis coupling tensors (in the standard form) must be bounded. The restrictions on the imaginary parts of the stiffness and mass density tensors are independent of the presence of Willis coupling. Therefore, passivity is violated if the sign of the imaginary parts of standard material properties (i.e., bulk modulus and scalar mass density) change as a function of frequency.

The restrictions imposed by causality are of a more subtle nature, since causality is inherently a time-domain restriction but most applications are carried out in the frequency domain. Converting the restrictions of causality to the frequency-domain yields Kramers-Krönig relations, which relate the dis-

persion of the real and imaginary parts of each individual material property. In the special case of reciprocal, passive, and lossless media, the restrictions derived in Chapter 2 dictate that the Willis coupling tensors as defined by the standard set of Willis constitutive equations must be identically zero at all frequencies, which is contrary to published model predictions [48, 50]. However, as argued in Chapter 2 and derived in Chapter 3, the standard form of the Willis constitutive equations are only appropriate in the frequency domain, where a time derivative on the field quantities has been incorporated into the material properties. In an alternative form of the Willis constitutive equations where this time derivative is again applied to the field quantities, the Willis coupling tensors may be non-zero in the special limiting case described above. Furthermore, this alternative formulation is shown in Chapter 3 to be valid in the time domain. It should be noted that the restrictions of reciprocity and passivity places bounds on the imaginary part of the alternative Willis coupling tensors, rather than the real part.

The work of Chapters 3 and 4 is focused on identifying sources of Willis coupling in one-dimensional systems and determining the effects of Willis coupling on material behavior and what impact neglecting Willis coupling has on estimating material properties. A simple model of an effective material element as two unequal masses connected by a spring is shown to exhibit Willis coupling. This coupling is local, as there is only a single material element, and is generated by the fact that the geometric center of the element is not aligned with its center of mass. It is further shown using a transmission line-based

model and using general expansions of the volume averages of the momentum density and volumetric strain that, in general, asymmetry of mass density or stiffness within an effective material element will lead to a misalignment of its centroid and center of mass. Thus, asymmetric material elements will exhibit local Willis coupling, as was determined formally in the literature but never explained from the standpoint of microscale inclusion response [48, 50, 51].

These principles of Willis materials were then used in Chapter 4 to design a material element which exhibits Willis coupling. It consists of a membrane, air cavity, and perforated sheet of paper. A plane wave tube was used to measure scattering coefficients of the element in order to experimentally determine the effective material properties of the element. Then, using the extraction procedure developed by Fokin, *et al.* generalized to account for Willis coupling, the scattering coefficients were used to extract the effective material properties of the element. These extracted properties were compared with theoretical predictions based on the work in Chapter 3 with very good agreement. In addition, scattering coefficients were also used with the approach of Fokin, *et al.* without accounting for Willis coupling, resulting in inconsistent and non-physical material properties, similar to the non-physical material properties published in the literature. The agreement of the methods accounting for Willis coupling and the failure of the method that does not account for Willis coupling strongly suggests that Willis coupling is present and important to consider in the effective material element described and measured.

The effective material element described in Chapter 4 may not be con-

sidered a true material, since it is only an isolated element rather than a large array of elements. However, the effective material properties of such a large array are directly related to the properties of the individual element. For a one-dimensional periodic array of effective material elements, the work of Nemat-Nasser and Srivastava[48] or of Sieck, *et al* [51]. may be used to determine the effective Willis material properties. In three-dimensional periodic systems, the work of Srivastava and Nemat-Nasser[49] or of Norris, *et al* [50]. may be used to determine the effective Willis material properties. However, there are no published methods by which to determine the effective Willis material properties of a random distribution of inhomogeneities. Developing such a homogenization method is the work of Chapter 5.

Chapter 5 presents a method for determining the effective material properties of a uniform elastic matrix material with a dilute concentration of embedded ellipsoidal elastic inhomogeneities under quasi-static loading. The matrix and inhomogeneity materials may be themselves effective materials (similar to the effective material element described in Chapter 4), Willis coupled, arbitrarily anisotropic, and dynamic. The inhomogeneities are treated as source regions for the scattered field, and a Green's function-based analysis leads to integral equations for the displacement fields and its derivatives. Assuming the inhomogeneities do not interact with each other (dilute concentration) and using the mean-field approximation (quasi-static loading), these integral equations become algebraic equations relating the velocity and strain fields within the inhomogeneity to the imposed velocity and strain fields through

what are known as localization tensors. The localization tensors along with the constitutive equations of the matrix and inhomogeneities may be used to determine the volume-averaged stress, strain, momentum density, and velocity fields from knowledge of only the imposed fields. Finally, the coefficients relating the stress and momentum density fields to the strain and velocity fields may be identified as the effective material properties. The effects associated with the complexity of the geometry and constituent material properties are taken into account through the localization tensors. While the quasi-static loading is of fundamental importance to this homogenization method, the assumption of a dilute concentration of inhomogeneities may be relaxed using conventional methods. As an example, a differential effective medium approach, modeled after the work by Norris, *et al.* [33], was presented and demonstrated. This analysis demonstrates two important points: (1) microscopic Willis coupling may lead to macroscopic Willis coupling, and (2) the effects of the microscopic Willis coupling on the macroscopic material are dependent on geometry, microstructural properties, and orientation, and may be calculated using this method.

6.2 Contributions

Each of the main chapters of this dissertation present contributions to the body of effective medium theory and the work on Willis materials. These contributions are reiterated here succinctly and in an itemized list by chapter.

Chapter 2: Physical Restrictions on Material Properties

- Determined bounds on effective Willis coupling tensors/coefficients assuming reciprocal, passive, and causal behavior.
- Deduced and derived a form of the Willis constitutive equations that are valid for time-domain analyses in addition to frequency-domain analyses based on the principles of causality.

Chapter 3: Physical Interpretation of Willis Coupling

- Showed that Willis coupling arises from the misalignment of the centroid and center of mass of an effective material element.

Chapter 4: Experimental Evidence of One-Dimensional Willis Coupling

- Showed that Willis coupling modifies the specific acoustic impedance as a function of propagation direction.
- Demonstrated that neglecting Willis coupling when it is present leads to inconsistent and potentially non-physical material property estimates.

Chapter 5: Prediction of Macroscopic Willis Coupling

- Demonstrated that microscopic Willis coupling may generate macroscopic Willis coupling in disordered media.
- Derived a homogenization scheme which accounts for a random distribution of Willis coupled elastic inhomogeneities within an elastic matrix.

6.3 Future Work

As expected for a relatively unexplored phenomenon, there is a great amount of study necessary to fully understand and utilize Willis coupling. Below are some ideas on how the work presented in this dissertation may be extended to continue developing the understanding of Willis materials and then to use this behavior for applications that are based on acoustic and elastic wave phenomena.

In Chapter 2 restrictions on the range of the effective material properties were derived by assuming reciprocal, passive, and causal behavior. These behaviors are very general and apply to a wide class of materials and situations. However, additional insight into the structure of the Willis coupling tensors and coefficients by considering further restricted cases. For example, chiral elastic media, which may be formally considered a subset of Willis materials, has a net handedness or rotational symmetry [55, 95]. One approach to finding the mathematical connection between chiral elastic media and Willis materials would be to require the Willis materials to be rotationally invariant, but not reflection invariant. While there are likely to be other, more efficient methods of determining the relationship between Willis materials and elastic chiral media, it is also possible that other symmetry groups might yield additional interesting forms of Willis coupling. It should be noted that this method of determining forms of Willis coupling is purely mathematical, and the resultant forms of Willis coupling may not be related to physical mechanisms.

The principle contribution of the analysis of causality for Willis materi-

als in Chapter 2 was the development a representation of the Willis equations that are valid for time-domain analyses. Since there is nothing published on the subject of time-domain Willis coupling, this is a ripe field of study. Some examples of potentially interesting time-domain Willis coupling research are reflection and transmission problems for pulses, scattering of pulses from isolated Willis objects, and nonlinear Willis coupling.

The homogenization methods described in Chapter 3 provides an excellent backdrop for further research. The mass-spring-mass system demonstrated that the misalignment of an effective material element's centroid and center of mass leads to local Willis coupling, and the transmission line-based homogenization model showed that in one dimensions this misalignment is the only source of local Willis coupling. However, this conclusion does not preclude the possibility of different sources of local coupling that are unique to two- or three-dimensional materials, like chiral media [95]. As with the concept that Willis coupling is generated from the misalignment of centroid and center of mass, understanding the physical mechanism behind additional sources of local Willis coupling will lead to greater intuition for designing structures to maximize these effects.

Complementary to the work to determine additional sources of Willis coupling is the work to develop homogenization methods for two- and three-dimensional effective material elements accounting for Willis coupling. It is likely that only very simple and idealized cases, such as spheres and circular cylinders, will have analytic expressions for their homogenization schemes,

and so developing numerical homogenization schemes will become important as research in Willis materials continues. One possible route to numerical homogenization is to extend the principles that led to Eqs. (3.72) to higher-dimensional objects.

Chapter 5 was concerned with determining the macroscopic Willis coupling due to microscopic Willis coupling, but was confined to three-dimensional systems and ellipsoidal inhomogeneities. In order to determine the effective Willis material properties of layered one-dimensional media and fibrous two-dimensional media, additional homogenization methods are required. Examples of homogenization methods that do not include Willis coupling, but provide useful approaches to the problem of one- and two-dimensional random media, may be found in Refs. [96] and [97]. Another important problem is associated with homogenization of quasi-periodic[98] and low-disorder random structures [99].

The ideas for future research described above are surely only the tip of the iceberg that is the subject of Willis materials and their applications.

Appendix

Appendix A

Relations Between Forms of the One-Dimensional Willis Constitutive Equations

Due to the coupled nature of the Willis constitutive equations, the relationship between, e.g., stiffness and compliance forms of the constitutive equations are not as simple as for standard constitutive equations. In this appendix, the Willis equations as they appear in Eqs. (3.9) and (3.10) will be treated as the baseline. For convenience, all constitutive equations will be written in the frequency domain, such that the baseline equations may be written

$$\mu = \rho v - i\omega\tilde{\psi}\varepsilon, \tag{A.1}$$

$$-p = -i\omega\psi v + \kappa\varepsilon. \tag{A.2}$$

Since these are linear equations, any two of the field variables, μ, p, v, and ε, may be treated as the dependent variables. Deriving the form of any of these equations is not difficult, but we will only consider the case where μ and ε are the dependent variables. The Willis constitutive equations in this case are

written

$$\mu = \left[\rho + \frac{\omega^2 \psi \tilde{\psi}}{\kappa}\right] v + \frac{i\omega\tilde{\psi}}{\kappa} p, \tag{A.3}$$

$$\varepsilon = \frac{i\omega\psi}{\kappa} v - \frac{1}{\kappa} p. \tag{A.4}$$

Then, the compressibility may be identified as $1/\kappa$, the mass density as $\rho + \omega^2\psi\tilde{\psi}/\kappa$, and the coupling terms as $i\omega\psi/\kappa$ (assuming $\tilde{\psi} = \psi$). It is interesting to note that the expression for the mass density depends on the form of the constitutive equations, though only for $\omega \neq 0$. This suggests that the static definition of mass density is not necessarily the most appropriate definition for the dynamic mass density. Instead, the appropriate definition of the mass density for linear Willis materials is the variation of the momentum density with respect to the velocity while the other independent variable is held still. If the momentum density is an independent variable or if velocity is a dependent variable, the notion of mass density does not apply. Similar statements may be made with respect to the stiffness.

Appendix B

Expansion of Smooth Field Variables by Averages

In this appendix an expansion for smooth field variables with respect to their volume average and the volume averages of their gradients is derived. Let $u(\vec{x})$ be a field variable that is analytic (it is equal to its Taylor series) in the domain Ω. Then the average of $u(\vec{x})$ may be written as

$$\langle u \rangle = \frac{1}{\Omega} \int_{\Omega} u(\vec{x}') d\vec{x}'. \tag{B.1}$$

Expanding the integrand in a Taylor series about $\vec{x}'' \in \Omega$ and simplifying yields

$$\langle u \rangle = \frac{1}{\Omega} \int_{\Omega} \left[u(\vec{x}'') + \nabla u(\vec{x}'') \cdot (\vec{x}' - \vec{x}') + \cdots \right] d\vec{x}' \tag{B.2}$$

$$= u(\vec{x}'') + \nabla u(\vec{x}'') \cdot \frac{1}{\Omega} \int_{\Omega} (\vec{x}' - \vec{x}'') d\vec{x} + \cdots \tag{B.3}$$

$$= u(\vec{x}'') + \nabla u(\vec{x}'') \cdot \langle \vec{x}' - \vec{x}'' \rangle + \cdots . \tag{B.4}$$

A diagram of the geometry associated with this expansion is given in Fig. B.1. Since $u(\vec{x})$ is arbitrary and analytic in Ω, the volume average of its gradient may be written

$$\langle \nabla u \rangle = \nabla u + \nabla \nabla u \cdot \frac{1}{\Omega} \int_{\Omega} (\vec{x}' - \vec{x}'') d\vec{x} + \cdots , \tag{B.5}$$

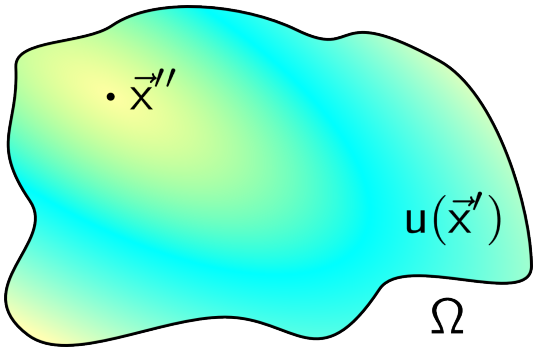

Figure B.1: Geometry of field expansion by averages.

where the functional dependence on $\vec{x}''$ has been suppressed for convenience. Similar expressions may be written for arbitrarily high order of gradients.

For this derivation, suppose there is a characteristic length scale d and "wavelength" $\lambda = 2\pi/k$ such that $\vec{x} \to O(d)$ and $\nabla \to O(k)$, and assume $kd \ll 1$. This assumption restricts the system to the long wavelength limit. While the method outlined below does not require long wavelengths, it is significantly simplified by them. Furthermore, the long-wavelength limit is often the case for situations of interest. Then,

$$\underbrace{\langle u \rangle}_{O(1)} = \underbrace{u(\vec{x}'')}_{O(1)} + \underbrace{\nabla u(\vec{x}'') \cdot \langle \vec{x}' - \vec{x}'' \rangle}_{O(kd)} + O[(kd)^2]. \tag{B.6}$$

Then, $u(\vec{x}'')$ to $O(kd)$ is just the average:

$$u(\vec{x}'') = \langle u \rangle + O(kd), \tag{B.7}$$

and to $O[(kd)^2]$ may be written

$$u(\vec{x}'') = \langle u \rangle - \nabla u(\vec{x}'') \cdot \langle \vec{x}' - \vec{x}'' \rangle + O[(kd)^2]. \tag{B.8}$$

Since u is arbitrary, it may be replaced by its gradient:

$$\nabla u(\vec{x}'') = \langle \nabla u \rangle + O(kd). \tag{B.9}$$

Thus, $u(\vec{x}'')$ to $O[(kd)^2]$ may be written in terms of its volume average and its gradient's volume average:

$$u(\vec{x}'') = \langle u \rangle - \langle \nabla u \rangle \cdot \langle \vec{x}' - \vec{x}'' \rangle + O[(kd)^2]. \tag{B.10}$$

This expansion method may be continued to higher orders of kd. For example, the variable u (as a function of $\vec{x}''$) may also be written

$$\begin{aligned} u = \langle u \rangle &- \langle \nabla u \rangle \cdot \langle \vec{x}' - \vec{x}'' \rangle \\ &+ \langle \nabla \nabla u \rangle : \left(\langle \vec{x}' - \vec{x}'' \rangle^2 - \frac{1}{2} \langle (\vec{x}' - \vec{x}'')^2 \rangle \right) + O[(kd)^3], \end{aligned} \tag{B.11}$$

where $\langle \vec{x}' - \vec{x}'' \rangle^2 \equiv \langle \vec{x}' - \vec{x}'' \rangle \otimes \langle \vec{x}' - \vec{x}'' \rangle$ and $(\vec{x}' - \vec{x}'')^2 \equiv (\vec{x}' - \vec{x}'') \otimes (\vec{x}' - \vec{x}'')$.

In one-dimensional systems the averages over the field positions may be explicitly calculated in general. If the domain Ω is the interval (a, b), then

$$\begin{aligned} \langle (x' - x'')^n \rangle &= \frac{1}{b-a} \int_a^b (x' - x'')^n dx' \\ &= \frac{1}{n+1} \frac{(b - x'')^{n+1} - (a - x'')^{n+1}}{b-a}. \end{aligned} \tag{B.12}$$

If $a = x - \Delta x$ and $b = x + \Delta x$, the variable u and its average may be written

$$\begin{aligned} u(x'') = \langle u \rangle &+ \left\langle \frac{\partial u}{\partial x} \right\rangle (x'' - x) \\ &+ \frac{1}{2} \left\langle \frac{\partial^2 u}{\partial x} \right\rangle \left((x'' - x)^2 - \frac{\Delta x^2}{3} \right) + O[(k\Delta x)^3], \end{aligned} \tag{B.13}$$

$$\begin{aligned} \langle u \rangle = u(x'') &+ \frac{\partial u(x'')}{\partial x''} (x - x'') \\ &+ \frac{1}{2} \frac{\partial^2 u(x'')}{\partial x''^2} \left((x - x'')^2 + \frac{\Delta x^2}{3} \right) + O[(k\Delta x)^3]. \end{aligned} \tag{B.14}$$

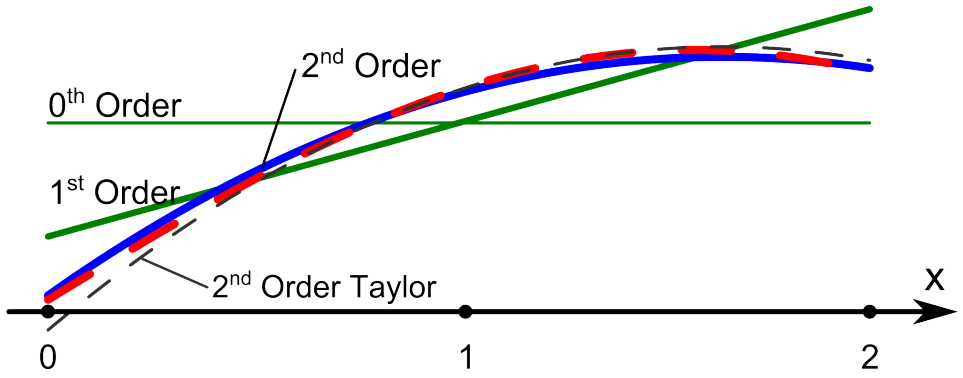

Figure B.2: Demonstration of field expansion by averages in one dimension. The original function (dashed line) is $u(x) = \sin(x)$ for $x \in (0, 2)$, and the zeroth, first, and second order expansion by averages are shown as the solid lines. The thin dashed line is the second-order Taylor series expansion about $x = 1$.

Another special case of interest to applications is the case of a sphere of radius $d/2$. In this case, setting $\vec{x} = 0$ (the center is the origin) yields

$$u(\vec{x}'') = \langle u \rangle + \langle \nabla u \rangle \cdot \vec{x}'' + \frac{1}{2} \langle \nabla^2 u \rangle : \left(\vec{x}'' \otimes \vec{x}'' - \frac{d^2}{20} \right) + O\left[(kd)^3 \right], \quad \text{(B.15)}$$

$$\langle u \rangle = u(\vec{x}'') - \nabla u(\vec{x}'') \cdot \vec{x}'' + \frac{1}{2} \nabla^2 u(\vec{x}'') : \left(\vec{x}'' \otimes \vec{x}'' + \frac{d^2}{20} \right) + O\left[(kd)^3 \right]. \quad \text{(B.16)}$$

An explicit example of this expansion may be useful. Consider $u(x) = \sin(x)$ over the domain $\Omega = (0, 2)$ (see Fig. B.2). In this case $kd = 2$. The

averages of $u(x)$ and its gradients are

$$\begin{aligned}
\langle u \rangle &= \frac{1}{2}\int_0^2 \sin(x')dx' \approx 0.708, \\
\langle \nabla u \rangle &= \frac{1}{2}\int_0^2 \cos(x')dx' \approx 0.455, \\
\langle \nabla^2 u \rangle &= -\frac{1}{2}\int_0^2 \sin(x')dx' \approx -0.708,
\end{aligned}$$

and $d^2/12 = 4/12 \approx 0.333$. Then, the second-order (neglecting terms $O[(kd)^3]$) expansion by averages of $u(x)$ about $x = 1$ may be written

$$\begin{aligned}
u(x) &\approx 0.708 + 0.455(x-1) - 0.354\left((x-1)^2 - 0.333\right) \\
&= 0.826 + 0.455(x-1) - 0.354(x-1)^2. \qquad \text{(B.17)}
\end{aligned}$$

For comparison, the second order Taylor series expansion of $u(x)$ about $x = 1$ is given by

$$u(x) \approx 0.841 + 0.540(x-1) - 0.421(x-1)^2. \qquad \text{(B.18)}$$

The expansion of $u(x)$ by averages about $x = 1$ at zeroth, first, and second order are plotted in Fig. B.2 along with the second order Taylor series expansion. As can be seen, both second order expansions predict the original function fairly well, but the series by averages approximation appears to stay closer to the original function near the boundaries than the Taylor series. This may be seen more explicitly by comparing the error of the two approximations, as shown in Fig. B.3. Near $x = 1$ the Taylor series does significantly better than the series by averages. However, near the boundaries $x = 0$ and $x = 2$

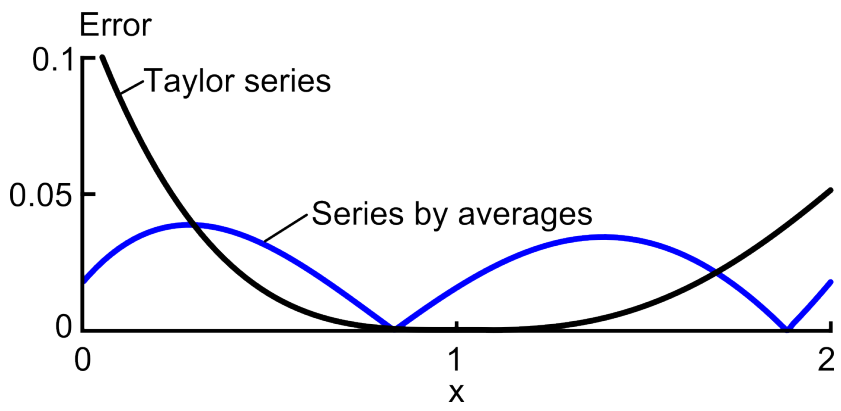

Figure B.3: Error of the second order expansion of the Taylor series and the series by averages of the function $u(x) = \sin(x)$.

the error of the series by averages remain within 0.05, which the Taylor series does not. In fact, the error of the Taylor series exceeds 0.10 near $x = 0$.

In addition to expanding a function with respect to its averages, the analysis above has provided a means to use the value of a function and its derivatives at a single point to estimate the average field. Using the same example as above, $u(x) = \sin(x)$ with $\Omega = (0, 2)$, the average value of $u(x)$ based on the field at x'' is estimated at second order as

$$\langle u \rangle \approx \sin(x'') + \cos(x'')(1 - x'') + \frac{1}{2}\sin(x'')\left([1 - x'']^2 + \frac{1}{3}\right). \qquad \text{(B.19)}$$

The actual value of $\langle u \rangle = 0.708$. The zeroth, first, and second order predictions of the average are shown in Fig. B.4 as a function of x''. As seen in the figure, the zeroth and first order predictions do very poorly, while the second order prediction does better, especially for $x > 0.5$.

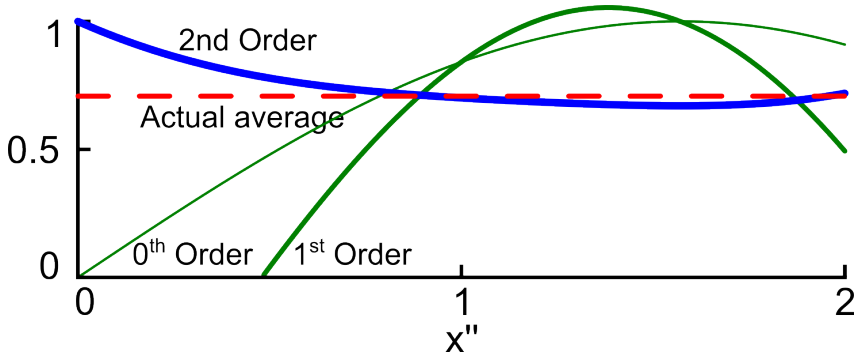

Figure B.4: Predictions of the average of $u(x) = \sin(x)$ using the zeroth, first, and second order predictions as a function of the averaging point x''. The actual average is represented by the dashed line.

Appendix C

Determination of Scattering Coefficients from an Imperfect Plane-Wave Tube Experiment

Consider a plane wave tube with a material sample of length L, as shown in Fig. C.1, with the associated lengths summarized in Table C.1. Our goal is to determine the scattering matrix for the material sample. Four microphone positions are available, as shown in the schematic above. Let the wavenumber in the tube be k, and let the specific acoustic impedance in the tube be Z_0. We will assume the time convention $e^{-i\omega t}$. Suppose there is an incident wave with amplitude A_L. Then the pressure and particle velocity fields may be written on the left-hand side as

$$p_L = A_L e^{ikx} + B_L e^{-ikx}, \tag{C.1}$$

$$Z_0 u_L = A_L e^{ikx} - B_L e^{-ikx}, \tag{C.2}$$

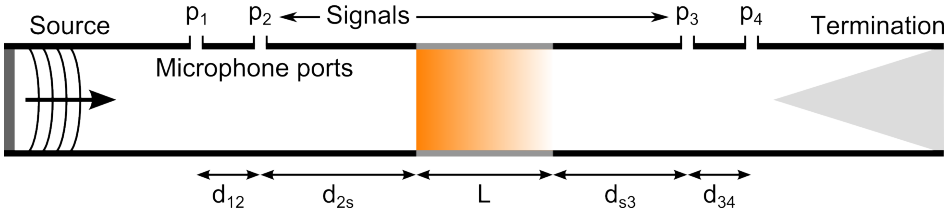

Figure C.1: Schematic of a three-medium reflection-transmission problem.

Table C.1: Summary of the lengths associated with the plane-wave tube experiment depicted in Fig. C.1.

Symbol	Value	Description
d_{12}	22.5 mm	Distance between microphone ports 1 and 2
d_{2s}	18.2 mm	Distance between microphone port 2 and the source-side sample edge
d_{s3}	103.2 mm	Distance between the termination-side sample edge and microphone port 3
d_{34}	22.5 mm	Distance between microphone ports 3 and 4
L	6.0 mm	Length of the sample

where we have assumed that $x = 0$ is the left-hand side of the material sample. Similarly, on the right-hand side we may write

$$p_R = A_R e^{ik(x-L)} + B_R e^{-ik(x-L)}, \tag{C.3}$$

$$Z_0 u_R = A_R e^{ik(x-L)} - B_R e^{-ik(x-L)}, \tag{C.4}$$

Given these definitions, the four measured pressure signals may be decomposed as

$$p_1 = A_L e^{ik(-d_{12}-d_{2s})} + B_L e^{-ik(-d_{12}-d_{2s})}, \tag{C.5}$$

$$p_2 = A_L e^{ik(-d_{2s})} + B_L e^{-ik(-d_{2s})}, \tag{C.6}$$

$$p_3 = A_R e^{ikd_{s3}} + B_R e^{-ikd_{s3}}, \tag{C.7}$$

$$p_4 = A_R e^{ik(d_{s3}+d_{34})} + B_R e^{-ik(d_{s3}+d_{34})}. \tag{C.8}$$

Using a single-microphone technique only yields the pressure at a single port relative to some unknown source: e.g., p_1/V_0 where V_0 is the complex magnitude of the source. In order to remove the unknown source from

the equations, only ratios of the measured signals are used: e.g., $H_{12} = (p_2/V_0)/(p_1/V_0) = p_2/p_1$, where H_{12} is the transfer function from port 1 to port 2. The transfer functions needed for this analysis may then be written as

$$H_{12} = \frac{A_L e^{ik(-d_{2s})} + B_L e^{-ik(-d_{2s})}}{A_L e^{ik(-d_{12}-d_{2s})} + B_L e^{-ik(-d_{12}-d_{2s})}}, \tag{C.9}$$

$$H_{13} = \frac{A_R e^{ikd_{s3}} + B_R e^{-ikd_{s3}}}{A_L e^{-ik(d_{12}+d_{2s})} + B_L e^{ik(d_{12}+d_{2s})}}, \tag{C.10}$$

$$H_{14} = \frac{A_R e^{ik(d_{s3}+d_{34})} + B_R e^{-ik(d_{s3}+d_{34})}}{A_L e^{-ik(d_{12}+d_{2s})} + B_L e^{ik(d_{12}+d_{2s})}}. \tag{C.11}$$

These three equations may be solved for the system (not sample) reflection coefficient $R = B_L/A_L$, transmission coefficient $T = A_R/A_L$, and termination scattering coefficient $V = B_R/A_L$:

$$R = -\frac{1 - H_{12}e^{-ikd_{12}}}{1 - H_{12}e^{ikd_{12}}} e^{-2ikd_{2s}}, \tag{C.12}$$

$$\begin{aligned} T = e^{-ikd_{2s}} &\left[e^{-ikd_{12}} - \frac{1 - H_{12}e^{-ikd_{12}}}{1 - H_{12}e^{ikd_{12}}} e^{ikd_{12}} \right] \\ &\times \frac{\csc(kd_{34})}{2i} e^{-ikd_{s3}} \left(H_{14} - H_{13}e^{-ikd_{34}} \right), \end{aligned} \tag{C.13}$$

$$\begin{aligned} V = e^{-ikd_{2s}} &\left[e^{-ikd_{12}} - \frac{1 - H_{12}e^{-ikd_{12}}}{1 - H_{12}e^{ikd_{12}}} e^{ikd_{12}} \right] \\ &\times \frac{\csc(kd_{34})}{-2i} e^{ikd_{s3}} \left(H_{14} - H_{13}e^{ikd_{34}} \right). \end{aligned} \tag{C.14}$$

The reflection and transmission coefficients are related to the scattering coefficients through the matrix equation

$$\begin{bmatrix} R \\ T \end{bmatrix} = \begin{bmatrix} S_{11} & S_{12} \\ S_{21} & S_{22} \end{bmatrix} \begin{bmatrix} 1 \\ V \end{bmatrix}. \tag{C.15}$$

Equations (C.12) – (C.14) provide a means to determine R, T, and V from measured quantities, so Eq. (C.15) results in two equations for four unknowns. Thus, additional information in the form of another experiment is necessary to fully determine the scattering matrix. There are basically two possibilities for the second experiment: (1) leave the sample as it is and modify the termination impedance, or (2) turn the sample around. In principle, if the sample is turned around it doesn't matter if the termination impedance has been changed or not. Both cases will be considered below.

For the following sections, the subscript 1 denotes the first experiment and the subscript 2 denotes the second experiment.

Consistent Sample Orientation

The two experiments may be summarized by the following set of equations:

$$R_1 = S_{11} + S_{12}V_1, \qquad T_1 = S_{21} + S_{22}V_1,$$
$$R_2 = S_{11} + S_{12}V_2, \qquad T_2 = S_{21} + S_{22}V_2.$$

These may be rearranged to solve for the scattering coefficients, yielding

$$S_{11} = \frac{R_2V_1 - R_1V_2}{V_1 - V_2}, \qquad S_{12} = \frac{R_1 - R_2}{V_1 - V_2}, \tag{C.16}$$
$$S_{21} = \frac{T_2V_1 - T_1V_2}{V_1 - V_2}, \qquad S_{22} = \frac{T_1 - T_2}{V_1 - V_2}. \tag{C.17}$$

The presence of $V_1 - V_2$ in the denominators of these expressions means error may be significant for V_2 close to V_1, and so having as different a termination condition as possible is important for this case.

Inverted Sample Orientation

In this case the experiments may be summarized as

$$R_1 = S_{11} + S_{12}V_1, \qquad T_1 = S_{21} + S_{22}V_1,$$
$$R_2 = S_{22} + S_{21}V_2, \qquad T_2 = S_{12} + S_{11}V_2.$$

Again, these equations may be solved for the scattering coefficients, yielding

$$S_{11} = \frac{R_1 - T_2V_1}{1 - V_1V_2}, \qquad S_{12} = \frac{T_2 - R_1V_2}{1 - V_1V_2}, \tag{C.18}$$
$$S_{21} = \frac{T_1 - R_2V_1}{1 - V_1V_2}, \qquad S_{22} = \frac{R_2 - T_1V_2}{1 - V_1V_2}. \tag{C.19}$$

The denominators for this case go to zero if $V_1V_2 \to 1$. However, the greatest V_1 and V_2 can be is $|T_1|$ and $|T_2|$, respectively, corresponding to perfect reflection at the termination. Thus, as long as the reflection coefficients are non-negligible, error associated with this determination method is not likely to be a concern.

As a final note, if the termination is anechoic for both experiments, the inverted sample orientation method reduces to simply

$$\begin{bmatrix} S_{11} & S_{12} \\ S_{21} & S_{22} \end{bmatrix} = \begin{bmatrix} R_1 & T_2 \\ T_1 & R_2 \end{bmatrix}. \tag{C.20}$$

Appendix D

Evaluation of T_1 and $\mathcal{T}_3$ tensors for ellipsoidal inhomogeneities

Throughout these derivations, extensive use of index notation will be made for the sake of clarity. Also, all material properties will be assumed to be matrix properties unless otherwise specified. In preparation to use spectral methods to analyze the tensors T_1 and $\mathcal{T}_3$, define the three-dimensional spatial Fourier transform (at a single frequency) with the pair

$$\widetilde{G}_{ij} = \iiint_{-\infty}^{\infty} G_{ij} e^{-ik_p x_p} d\vec{x} \qquad \text{and} \qquad G_{ij} = \frac{1}{(2\pi)^3} \iiint_{-\infty}^{\infty} \widetilde{G}_{ij} e^{ik_p x_p} d\vec{k}, \tag{D.1}$$

where $k_i = k\chi_i$ is the wave vector, k is the wave number, and χ_i is the unit direction-cosine vector. Note the transforms have the property $\widetilde{G}_{ij,l} = ik_l \widetilde{G}_{ij} = ik\chi_l \widetilde{G}_{ij}$. For later use, note

$$\iiint_{-\infty}^{\infty} G_{ij}(\vec{x} - \vec{x}') e^{-ik_p x_p} d\vec{x} = \iiint_{-\infty}^{\infty} G_{ij}(\vec{x}) e^{-ik_p (x_p + x'_p)} d\vec{x} = e^{-ik_p x'_p} \widetilde{G}_{ij}. \tag{D.2}$$

D.1 Derivation of $\mathcal{T}_1$ for Spherical Inhomogeneities

The Fourier transform of the quasistatic Green's function equation given in Eq. (5.16) yields $-k^2 \chi_l \chi_j C^0_{ijkl} \widetilde{G}_{km} + \delta_{im} = 0$, which may be solved for

the Green's function as $\widetilde{G}_{ij} = k^{-2}P_{ij}^{-1}$, where $P_{ik} = \chi_l\chi_j C_{ijkl}$.

The tensor T_1 as defined in Eq. (5.19a) may be expanded as $(\mathsf{T}_1)_{ijkl} = T^{(1)}_{ijkl} + T^{(1)}_{jikl}$ where

$$T^{(1)}_{ijkl} = -\frac{1}{2\Omega_{\mathrm{I}}}(2\pi)^{-3}\int_0^{\pi}\int_0^{2\pi}\sin\theta\chi_l\chi_j P^{-1}_{ki}d\theta d\phi \times \int_0^{\infty}k^2dk\int_{\Omega_{\mathrm{I}}}e^{-i\vec{k}\cdot\vec{x}'}d\vec{x}'\int_{\Omega_{\mathrm{I}}}e^{i\vec{k}\cdot\vec{x}}d\vec{x}, \tag{D.3}$$

Ω_{I} is the inhomogeneity volume and Ω_k is the k-space volume. The integrals over physical space may be performed exactly, as can the resulting integral over k. However, the remaining integrals over θ and ϕ cannot be readily integrated analytically. If we define

$$K^{(4)}_{ijkl} \equiv \int_0^{\pi}\int_0^{2\pi}\chi_l\chi_j\sin\theta P^{-1}_{ki}d\theta d\phi, \tag{D.4}$$

which must be integrated numerically, the tensor $T^{(1)}_{ijkl}$ may be written as

$$T^{(1)}_{ijkl} = -\frac{3}{4\pi a^3}\frac{(2\pi)^{-3}}{2}\left(\frac{8}{3}\pi^3a^3\right)K^{(4)}_{ijkl} = -\frac{1}{8\pi}K^{(4)}_{ijkl}. \tag{D.5}$$

Therefore, the full tensor $(\mathsf{T}_1)_{ijkl}$ may be written $T_{ijkl} = -(K^{(4)}_{ijkl} + K^{(4)}_{jikl})/8\pi$. This form is equivalent to previously published forms [100, 101]. Since $|P_{ij}| \sim |C_{ijkl}|$, $|T_{ijkl}| \sim |C_{ijkl}|^{-1}$ and is independent of inhomogeneity scale.

D.2 Derivation of $\mathcal{T}_3$ for Spherical Inhomogeneities

The tensor $\mathcal{T}_3$ as defined in Eq. (5.19b) may be written in index notation as

$$(\mathcal{T}_3)_{ijk} \equiv \frac{i\omega}{2\Omega_{\mathrm{I}}}\int_{\Omega_{\mathrm{I}}}\int_{\Omega_{\mathrm{I}}}G_{ik,j}(\vec{x}-\vec{x}')d\vec{x}d\vec{x}'. \tag{D.6}$$

Substituting $G_{ik,j}$ for its Fourier transform and performing similar integrals as in the analysis of $T^{(1)}_{ijkl}$, we may write $(\mathcal{T}_3)_{ijk} = -3a\omega K^{(3)}_{ijk}/16\pi^2$, where

$$K^{(3)}_{ijk} \equiv \int_0^{\pi} \int_0^{2\pi} \chi_j \sin\theta P^{-1}_{ki} d\theta d\phi. \tag{D.7}$$

Thus $|\mathcal{T}_3| \sim a\omega/|C_{ijkl}|$. Note that since $G_{ij,k}(\vec{x} - \vec{x}') = -G_{ij,k}(\vec{x}' - \vec{x})$, the value of $\mathcal{T}_3$ must be zero for center-symmetric geometries, and so $K^{(3)}_{ijk} = 0$. This argument also holds for $\mathcal{T}_2$, even though it is not needed because of the order analysis.

D.3 Extension to Ellipsoidal Inhomogeneities

Consider an ellipsoidal inhomogeneity defined such that the outer boundary of the inhomogeneity is expressed as

$$\frac{x_1^2}{a_1^2} + \frac{x_2^2}{a_2^2} + \frac{x_3^2}{a_3^2} = 1. \tag{D.8}$$

Define a new coordinate system X_i such that $x_i = \Phi_{ij} X_j$, where

$$\Phi_{ij} \rightarrow \begin{bmatrix} 1 & 0 & 0 \\ 0 & a_2/a_1 & 0 \\ 0 & 0 & a_3/a_1 \end{bmatrix}. \tag{D.9}$$

This suggests K_i should be defined such that $k_i = \Phi^{-1}_{ij} K_j$. In this coordinate system the inhomogeneity is a sphere of radius a_1 and $x_i k_i = X_i K_i$. The Jacobian determinant of the spatial transformation is $|\Phi_{ij}| = a_2 a_3/a_1^2$, and the Jacobian determinant of the wave-vector transformation is $|\Phi^{-1}_{ij}| = a_1^2/a_2 a_3$. Then $T^{(1)}_{ijkl}$ may be written as

$$T^{(1)}_{ijkl} = -\frac{1}{\pi\Omega_{\mathrm{I}}} \left(\frac{a_2 a_3}{a_1^2}\right)^2 \int_{\Omega_k} \chi_l \chi_j P^{-1}_{ki} K^{-6} \left[\sin(Ka_1) - Ka_1 \cos(Ka_1)\right]^2 d\vec{k}. \tag{D.10}$$

Recall χ_i is the vector of direction cosines of k_i. Thus, $\chi_i = k^{-1}k_i = k^{-1}\Phi_{ij}^{-1}K_j = (K/k)\Phi_{ij}^{-1}\chi'_j$, where χ'_i is the vector of direction cosines of K_i. Defining $P'_{ik} \equiv \chi'_l\chi'_j C'_{ijkl}$ where $C'_{ijkl} \equiv \Phi_{mi}^{-1}\Phi_{nj}^{-1}\Phi_{pk}^{-1}\Phi_{ql}^{-1}C_{mnpq}$, such that $P'_{ik} = (k/K)^2\Phi_{pi}^{-1}\Phi_{qk}^{-1}P_{pq}$, results in

$$T_{ijkl}^{(1)} = -\frac{1}{\pi\Omega_{\mathrm{I}}}\frac{a_2a_3}{a_1^2}\Phi_{i\beta}^{-1}\Phi_{lp}^{-1}\Phi_{jq}^{-1}\Phi_{k\alpha}^{-1} \times \int_{\Omega_K}\chi'_p\chi'_q(P'_{\alpha\beta})^{-1}\frac{\left[\sin(Ka_1) - Ka_1\cos(Ka_1)\right]^2}{K^6}d\vec{K}, \tag{D.11}$$

which becomes $T_{ijkl}^{(1)} = -\Phi_{i\alpha}^{-1}\Phi_{j\beta}^{-1}\Phi_{k\gamma}^{-1}\Phi_{l\delta}^{-1}K_{\alpha\beta\gamma\delta}^{'(4)}/8\pi$, where

$$K_{ijkl}^{'(4)} \equiv \int_0^{2\pi}\int_0^{\pi}\sin\theta'\chi'_l\chi'_j(P'_{ki})^{-1}d\theta'd\phi'. \tag{D.12}$$

Following similar steps, $(\mathcal{T}_3)_{ijk} = -3a_1\omega\Phi_{i\alpha}^{-1}\Phi_{j\beta}^{-1}\Phi_{k\gamma}^{-1}K_{\alpha\beta\gamma}^{'(3)}/16\pi^2$, where

$$K_{ijk}^{'(3)} \equiv \int_0^{2\pi}\int_0^{\pi}\sin\theta'\chi'_j(P'_{ki})^{-1}d\theta'd\phi'. \tag{D.13}$$

D.4 Analytical forms of the tensors for an isotropic matrix with spherical inhomogeneities

An important case to consider is an isotropic matrix with spherical inhomogeneities. In this simple case, analytical solutions may be found for $K_{ijkl}^{(4)}$ and $K_{ijk}^{(3)}$. The stiffness tensor for an isotropic material may be written as $C_{ijkl} = \lambda\delta_{ij}\delta_{kl} + \mu\left(\delta_{ik}\delta_{jl} + \delta_{il}\delta_{jk}\right)$. For this case, the tensor P_{ik} may be written as

$$P_{ik} = \chi_l\chi_j C_{ijkl} = \lambda\chi_i\chi_k + \mu\delta_{ik}\chi_\alpha\chi_\alpha + \mu\chi_k\chi_i = (\lambda+\mu)\chi_i\chi_k + \mu\delta_{ik} \tag{D.14}$$

and the inverse may be written as $P_{ij}^{-1} = \delta_{ij}/\mu - \chi_i\chi_j/2\mu(1-\nu)$. Notice $P_{ji}^{-1} = P_{ij}^{-1}$ is a symmetric tensor. The needed integrals are then written

$$K_{ijk}^{(3)} = \frac{1}{\mu}\int_0^{2\pi}\int_0^{\pi} \chi_j \left[\delta_{ik} - \frac{\chi_i\chi_k}{2(1-\nu)}\right] \sin\theta d\theta d\phi = 0, \tag{D.15}$$

$$\begin{aligned} K_{ijkl}^{(4)} &= \frac{1}{\mu}\int_0^{2\pi}\int_0^{\pi} \chi_l\chi_j \left[\delta_{ki} - \frac{\chi_k\chi_i}{2(1-\nu)}\right] \sin\theta d\theta d\phi \\ &= \frac{4\pi}{3\mu}\delta_{ik}\delta_{jl} - \frac{4\pi}{30\mu(1-\nu)}(\delta_{ij}\delta_{kl} + \delta_{ik}\delta_{jl} + \delta_{il}\delta_{jk}). \end{aligned} \tag{D.16}$$

Then for an isotropic matrix with spherical inhomogeneities $\mathcal{T}_3 = 0$ and

$$T_{ijkl} = -\frac{1}{8\pi}\left(K_{ijkl}^{(4)} + K_{jikl}^{(4)}\right) = \frac{\delta_{ij}\delta_{kl} + (5\nu-4)(\delta_{ik}\delta_{jl} + \delta_{jk}\delta_{il})}{30\mu(1-\nu)}. \tag{D.17}$$

Bibliography

[1] M. Ostoja-Starzewski, *Microstructural Randomness and Scaling in Mechanics of Materials*. Boca Raton, FL: CRC Press, 2007, pp. xvii–xxi.

[2] F. Sharipov, W. Marques, and G. M. Kremer, "Free molecular sound propagation," *J. Acoust. Soc. Am.*, vol. 112, pp. 395–401, 2002.

[3] B.-Y. Cao, J. Sun, M. Chen, and Z.-Y. Guo, "Molecular momentum transport at fluid-solid interfaces in mems/nems: A review," *Int. J. Mol. Sci.*, vol. 10, pp. 4638–4706, 2009.

[4] H. E. Bass, L. C. Sutherland, A. J. Zuckerwar, D. T. Blackstock, and D. M. Hester, "Atmospheric absorption of sound: Further developments," *J. Acoust. Soc. Am.*, vol. 97, pp. 680–683, 1995.

[5] D. T. Blackstock, *Fundamentals of Physical Acoustics*. Hoboken, NJ: John Wiley & Sons, Inc., 2000.

[6] M. Wegener and S. Linden, "Shaping optical space with metamaterials," *Phys. Today*, vol. 63, p. 32, 2010.

[7] J. N. A. Matthews, "Mechanical metamaterials roll off the 3d printing press," *Phys. Today*, vol. 68, p. 26, 2015.

[8] X. Zhou, X. Liu, and G. Hu, "Elastic metamaterials with local resonances: an overview," *Theor. Appl. Mech. Lett.*, vol. 2, pp. 1–12, 2012.

[9] X. Zhou, X. Liu, G. Hu, and G. Huang, "Micromechanics of elastic metamaterials," in *Handbook of Micromechanics and Nanomechanics*, S. Li and X.-L. Gao, Eds. Singapore: Pan Stanford Publishing Pte. Ltd., 2013, pp. 29–71.

[10] Z. Liu, X. Zhang, Y. Mao, Y. Y. Zhu, Z. Yang, C. T. Chan, and P. Sheng, "Locally resonant sonic materials," *Science*, vol. 289, pp. 1734–1736, 2000.

[11] N. Fang, D. Xi, J. Xu, M. Ambati, W. Srituravanich, C. Sun, and X. Zhang, "Ultrasonic metamaterials with negative modulus," *Nature Mat. Lett.*, vol. 5, pp. 452–456, 2006.

[12] Y. M. Seo, J. J. Park, S. H. Lee, C. M. Park, C. K. Kim, and S. H. Lee, "Acoustic metamaterial exhibiting four different sign combinations of density and modulus," *J. Appl. Phys.*, vol. 111, pp. 1–6, 2012.

[13] Y. Li, B. Liang, Z. ming Gu, X. ye Zou, and J. chun Cheng, "Reflected wavefront manipulation based on ultrathin planar acoustic metasurfaces," *Sci. Rep.*, vol. 3, pp. 1–6, 2013.

[14] P. Li, S. Yao, X. Zhou, G. Huang, and G. Hu, "Effective medium theory of thin-plate acoustic metamaterials," *J. Acoust. Soc. Am.*, vol. 135, pp. 1844–1852, 2014.

[15] Y. Xie, W. Wang, H. Chen, A. Konneker, B.-I. Popa, and S. A. Cummer, "Wavefront modulation and subwavelength diffractive acoustics with an acoustic metasurface," *Nat. Comm.*, vol. 5, pp. 1–5, 2014.

[16] A. J. Ward and J. B. Pendry, "Refraction and geometry in maxwell's equations," *J. Mod. Optics*, vol. 43, pp. 773–793, 1996.

[17] A. N. Norris, "Acoustic cloaking theory," *Proc. Roy. Soc. Lond. A*, vol. 464, pp. 2411–2434, 2008.

[18] U. Leonhardt, "Optical conformal mapping," *Science*, vol. 312, pp. 1777–1780, 2006.

[19] J. B. Pendry, D. Schurig, and D. R. Smith, "Controlling electromagnetic fields," *Science*, vol. 312, pp. 1780–1782, 2006.

[20] D. Schurig, J. J. Mock, B. J. Justice, S. A. Cummer, J. B. Pendry, A. F. Starr, and D. R. Smith, "Metamaterial electromagnetic cloak at microwave frequencies," *Science*, vol. 314, pp. 977–980, 2006.

[21] M. D. Guild, M. R. Haberman, and A. Alù, "Plasmonic cloaking and scattering cancelation for electromagnetic and acoustic waves," *Wave Motion*, vol. 48, pp. 468–482, 2011.

[22] X. Ao and C. T. Chan, "Far-field image magnification for acoustic waves using anisotropic acoustic metamaterials," *Phys. Rev. E*, vol. 77, pp. 1–4, 2008.

[23] G. Ma and P. Sheng, "Acoustic metamaterials: From local resonances to broad horizons," *Sci. Adv.*, vol. 2, pp. 1–16, 2016.

[24] L. Zigoneanu, B.-I. Popa, and S. A. Cummer, "Design and measurements of a broadband two-dimensional acoustic lens," *Phys. Rev. B*, vol. 84, pp. 1–5, 2011.

[25] Y. Xie, B.-I. Popa, L. Zigoneanu, and S. A. Cummer, "Measurement of a broadband negative index with space-coiling acoustic metamaterials," *Phys. Rev. Lett.*, vol. 110, pp. 1–4, 2013.

[26] S. Koo, C. Cho, J. ho Jeong, and N. Park, "Acoustic omni meta-atom for decoupled access to all octants of a wave parameter space," *Nat. Comm.*, vol. 7, pp. 1–7, 2016.

[27] D. V. Schroeder, *An Introduction to Thermal Physics.* New York, NY: Addison Wesley, 2000, pp. 6–13.

[28] M. Kardar, *Statistical Physics of Fields.* Cambridge, MA: Cambridge University Press, 2007, pp. 156–161.

[29] J. W. Strutt, "Investigation of the disturbance produced by a spherical obstacle on the waves of sound," *Proc. Lond. Math. Soc.*, vol. 1, pp. 253–283, 1871.

[30] C. J. T. Sewell, "The extinction of sound in a viscous atmosphere by small obstacles of cylindrical and spherical form," *Phil. Trans. Roy. Soc. Lond. A*, vol. 210, pp. 239–270, 1911.

[31] C. F. Ying and R. Truell, "Scattering of a plane longitudinal wave by a spherical obstacle in an isotropically elastic solid," *J. Appl. Phys.*, vol. 27, pp. 1086–1097, 1956.

[32] I. A. Chaban, "Self-consistent field approach to calculation of the effective parameters of microinhomogeneous media," *Sov. Phys. Acoust*, vol. 10, pp. 298–304, 1965.

[33] A. N. Norris, "A differential scheme for the effective moduli of composites," *Mech. Mat.*, vol. 4, pp. 1–16, 1985.

[34] J. D. Eshelby, "The determination of the elastic field of an ellipsoidal inclusion, and related problems," *Proc. Roy. Soc. Lond. A*, vol. 241, pp. 376–396, 1957.

[35] J. Qu and M. Cherkaoui, *Fundamentals of Micromechanics of Solids*. Hoboken, NJ: John Wiley & Sons, Inc., 2006, pp. 158–163.

[36] T. M. Michelitsch, H. Gao, and V. M. Levin, "Dynamic eshelby tensor and potentials for ellipsoidal inclusions," *Proc. R. Soc. Lond. A*, vol. 459, pp. 863–890, 2003.

[37] R. Hill, "A self-consistent mechanics of composite materials," *J. Mech. Phys. Solids*, vol. 13, pp. 213–222, 1965.

[38] L. L. Foldy, "The multiple scattering of waves. I. General theory of isotropic scattering by randomly distributed scatterers," *Phys. Rev.*, vol. 67, pp. 107–119, 1945.

[39] M. Lax, "Multiple scattering of waves," *Rev. Mod. Phys.*, vol. 23, pp. 287–310, 1951.

[40] P. C. Waterman and R. Truell, "Multiple scattering of waves," *J. Math. Phys.*, vol. 2, pp. 513–537, 1961.

[41] I. Newton, *Principia–Book II.* London: Imprimatur S. Pepys, Reg. Soc. Praeses, 1686.

[42] J. W. S. Rayleigh, *The Theory of Sound.* New York, NY: Dover Publications, Inc., 1945, vol. 1.

[43] F. Bloch, "Über die quantenmechanik der elektronen in kristallgittern," *Z. Physik*, vol. 52, pp. 555–600, 1929.

[44] G. Floquet, "Sur les équations différentielles linéaires à coefficients périodiques," in *Annales Scientifiques de l'École Normale Supérieure*, vol. 12, 1883, pp. 47–88.

[45] L. Brillouin, *Wave Propagation in Periodic Structures Electric Filters and Crystal Lattices.* New York, NY: Dover Publications, Inc., 1946.

[46] J. R. Willis, "Variational principles for dynamic problems for inhomogeneous elastic media," *Wave Motion*, vol. 3, pp. 1–11, 1981.

[47] ——, "Dynamics of composites," in *Continuum Micromechanics: CISM Lecture Notes.* New York, NY: Springer, 1997, no. 377, pp. 265–290.

[48] S. Nemat-Nasser and A. Srivastava, "Overall dynamic constitutive relations of layered elastic composites," *J. Mech. Phys. Solids*, vol. 59, pp. 1953–1965, 2011.

[49] A. Srivastava and S. Nemat-Nasser, "Overall dynamic properties of three-dimensional periodic elastic composites," *Proc. R. Soc. A*, vol. 468, pp. 269–287, 2011.

[50] A. N. Norris, A. L. Shuvalov, and A. A. Kutsenko, "Analytical formulation of three-dimensional dynamic homogenization for periodic elastic systems," *Proc. R. Soc. A*, vol. 468, pp. 1629–1651, 2012.

[51] C. F. Sieck, A. Alù, and M. R. Haberman, "Dynamic homogenization of acoustic metamaterials with coupled field response," *Phys. Procedia*, vol. 70, pp. 275–278, 2015.

[52] A. Alù, "First-principles homogenization theory for periodic metamaterials," *Phys. Rev. B*, vol. 84, pp. 1–18, 2011.

[53] A. A. Kutsenko, A. L. Shuvalov, O. Poncelet, and A. N. Darinskii, "Tunable effective constants of the one-dimensional piezoelectric phononic crystal with internal connected electrodes," *J. Acoust. Soc. Am.*, vol. 137, pp. 606–616, 2015.

[54] J. D. Achenbach, *Wave Propagation in Elastic Solids*. Amsterdam: Elsevier Science Publishers B.V., 1975, pp. 59–61.

[55] V. V. Varadan, A. Lakhtakia, and V. K. Varadan, "Geometry can be the basis for acoustic activity (a la optical activity) in composite media," *J. Wave Mater. Interact.*, vol. 1, pp. 315–323, 1986.

[56] O. B. Wilson, *Introduction to Theory and Design of Sonar Transducers*, 3rd ed. Los Altos, CA: Peninsula Publishing, 1988.

[57] D. Del Vescovo and I. Giorgio, "Dynamic problems for metamaterials: Review of existing models and ideas for further research," *Int'l. J. Eng. Sci.*, vol. 80, 2014.

[58] R. Lakes, "On the torsional properties of single osteons," *J. Biomech.*, vol. 28, pp. 1409–1410, 1995.

[59] G. W. Militon and J. R. Willis, "On modifications of newton's second law and linear continuum elastodynamics," *Proc. R. Soc. A*, vol. 463, 2007.

[60] J. D. Achenbach, *Reciprocity in Elastodynamics*. Cambridge, MA: University of Cambridge, 2003, pp. 91–92.

[61] R. Fleury, D. L. Sounas, M. R. Haberman, and A. Alù, "Nonreciprocal acoustics," *Acoust. Today*, vol. 11, pp. 14–21, 2015.

[62] R. Fleury, D. L. Sounas, C. F. Sieck, M. R. Haberman, and A. Alù, "Sound isolation and giant linear nonreciprocity in a compact acoustic circulator," *Science*, vol. 343, pp. 516–519, 2014.

[63] J. Mei, G. Ma, M. Yang, Z. Yang, W. Wen, and P. Sheng, "Dark acoustic metamaterials as super absorbers for low-frequency sound," *Nat. Comm.*, vol. 3, 2012.

[64] A. Srivastava, "Causality and passivity in elastodynamics," *Proc. Roy. Soc. A*, vol. 471, pp. 1–12, 2015.

[65] H. Nassar, Q.-C. He, and N. Auffray, "Willis elastodynamic homogenization theory revisited for periodic media," *J. Mech. Phys. Solids*, vol. 77, pp. 158–178, 2015.

[66] L.-Q. Shui, Z.-F. Yue, Y.-S. Liu, Q.-C. Liu, J.-J. Guo, and X.-D. He, "Novel composites with asymmetrical elastic wave properties," *Comp. Sci. Tech.*, vol. 113, pp. 19–30, 2015.

[67] Y. C. Fung and P. Tong, *Classical and Computational Solid Mechanics*. Singapore: World Scientific, 2001.

[68] N. N. Bojarski, "Generalized reaction principles and reciprocity theorems for the wave equations, and the relationship between the time-advanced and time-retarded fields," *J. Acoust. Soc. Am.*, vol. 74, pp. 281–285, 1983.

[69] B. Banerjee, *An Introduction to Metamaterials and Waves in Composites*, 1st ed. Boca Raton, FL: Taylor & Francis Group, LLC, 2011.

[70] L. D. Landau and E. M. Lifshitz, *Electrodynamics of Continuous Media*. New York, NY: Pergamon Press, 1960, pp. 266–268.

[71] R. M. Christensen, *Theory of Viscoelasticity*, 2nd ed. Mineola, NY: Dover Publications, Inc., 1982, pp. 1–8.

[72] M. O'Donnell, E. T. Jaynes, and J. G. Miller, "Kramers-krönig relationship between ultrasonic attenuation and phase velocity," *J. Acoust. Soc. Am.*, vol. 69, pp. 696–701, 1980.

[73] T. L. Szabo, "Time domain wave equations for lossy media obeying a frequency power law," *J. Acoust. Soc. Am.*, vol. 96, pp. 491–500, 1994.

[74] K. R. Waters, M. S. Hughes, J. Mobley, and J. G. Miller, "Differential forms of the kramers-krönig dispersion relations," *IEEE Trans. Ultr. Ferr. Freq. Cont.*, vol. 50, pp. 68–76, 2003.

[75] E. B. Saff and A. D. Snider, *Fundamentals of Complex Analysis*. Upper Saddle River, NJ: Prentice Hall, 2003.

[76] G. W. Milton, "New metamaterials with macroscopic behavior outside that of continuum elastodynamics," *New J. Phys.*, vol. 9, pp. 1–13, 2007.

[77] T. L. Szabo, *Diagnostic Ultrasound Imaging: Inside Out*. Cambridge, MA: Academic Press, 2004.

[78] V. Fokin, M. Ambati, C. Sun, and X. Zhang, "Method for retrieving effective properties of locally resonant acoustic metamaterials," *Phys. Rev. B*, vol. 76, pp. 1–5, 2007.

[79] W. T. Chu, "Transfer function technique for impedance and absorption measurements in an impedance tube using a single microphone," *J. Acoust. Soc. Am.*, vol. 80, pp. 555–560, 1986.

[80] F. Bongard, H. Lissek, and J. R. Mosig, "Acoustic transmission line metamaterial with negative/zero/positive refractive index," *Phys. Rev. B*, vol. 82, pp. 1–11, 2010.

[81] P. M. Morse and K. U. Ingard, *Theoretical Acoustics*. New York, NY: McGraw-Hill, Inc., 1968.

[82] C. E. Bradley, "Time harmonic acoustic Bloch wave propagation in periodic waveguides. Part I. Theory," *J. Acoust. Soc. Am.*, vol. 96, pp. 1844–1853, 1994.

[83] J. H. Park, H. J. Lee, and Y. Y. Kim, "Characterization of anisotropic acoustic metamaterial slabs," *J. App. Phys.*, vol. 119, pp. 1–10, 2016.

[84] H.-C. Zeng, C.-R. Luo, H.-J. Chen, S.-L. Zhai, C.-L. Ding, and X.-P. Zhao, "Flute-model acoustic metamaterials with simultaneously negative bulk modulus and mass density," *Solid State Comm.*, vol. 173, pp. 14–18, 2013.

[85] J. Dubois, C. Ariségui, and O. Poncelet, "Spaces of electromagnetic and mechanical constitutive parameters for dissipative media with either positive or negative index," *J. Appl. Phys.*, vol. 115, pp. 1–7, 2014.

[86] A. Srivastava and S. Nemat-Nasser, "Overall dynamic properties of three-dimensional periodic elastic composites," *Proc. R. Soc. A*, vol. 468, pp. 269–287, 2012.

[87] F. J. Sabina and J. R. Willis, "A simple self-consistent analysis of wave propagation in particulate composites," *Wave Motion*, vol. 10, pp. 127–142, 1988.

[88] M. R. Haberman, Y. H. Berthelot, J. Jarzynki, and M. Cherkaoui, "Micromechanical modeling of viscoelastic voided composites in the low-frequency approximation," *J. Acoust. Soc. Am.*, vol. 112, pp. 1937–1943, 2002.

[89] R. M. Christensen, *Theory of Viscoelasticity*, 2nd ed. Mineola, NY: Dover Publications, Inc., 1982, pp. 1–14.

[90] G. Dvorak, *Micromechanics of Composite Materials*. New York, NY: Springer, 2013, pp. 145–176.

[91] M. R. Haberman, Y. H. Berthelot, and M. Cherkaoui, "Micromechanical modeling of particulate composites for damping of acoustic waves," *J. Eng. Mat. Tech.*, vol. 128, pp. 320–329, 2006.

[92] A. V. Hershey, "The elasticity of an isotropic aggregate of anisotropic cubic crystals," *ASME J. Appl. Mech.*, vol. 21, pp. 236–240, 1954.

[93] E. Kröner, "Berechnung der elastishen konstanten des vielkristalles aus den konstanten des einkristalls," *Z. Physik*, vol. 151, pp. 504–518, 1958.

[94] A. Alù, "Restoring the physical meaning of metamaterial constitutive parameters," *Phys. Rev. B*, vol. 83, pp. 1–4, 2011.

[95] A. Lakhtakia, V. V. Varadan, and V. K. Varadan, "Elastic wave propagation in noncentrosymmetric, isotropic media: Dispersion and field equations," *J. Appl. Phys.*, vol. 63, pp. 5246–5250, 1988.

[96] M. van der Baan, "Acoustic wave propagation in one-dimension random media: the wave localization approach," *Geophys. J. Int.*, vol. 145, pp. 631–646, 2001.

[97] J. Garnier and K. S. lna, "Effective fractional acoustic wave equations in one-dimensional random multiscale media," *J. Acoust. Soc. Am.*, vol. 127, pp. 62–72, 2010.

[98] S. He and J. D. Maynard, "Eigenvalue spectrum, density of states, and eigenfunctions in a two-dimensional quasicrystal," *Phys. Rev. Lett.*, vol. 62, pp. 1888–1891, 1989.

[99] D. Sornette, "Acoustic waves in random media. I. Weak disorder regime," *Acustica*, vol. 67, pp. 199–215, 1989.

[100] O. Fassi-Fehri, "Le problème de la paire d'inclusions plastiques et hétérogènes dans une matrice anisotrope," Ph.D. dissertation, Universite de Metz, 1985.

[101] M. R. Haberman, "Design of high loss viscoelastic composites through micromechanical modeling and decision based materials design," Ph.D. dissertation, Georgia Institute of Technology, 2007.